



UNIVERSITÀ
DEGLI STUDI
DI FERRARA

- EX LABORE FRUCTUS -

THE ELECTRONIC STRUCTURE OF MOLECULES: NEW
INSIGHTS FROM ORTHOGONAL VALENCE BOND

Candidate

Lorenzo Tenti

Supervisor

Prof. Celestino Angeli

A dissertation for the degree of
Philosophiae Doctor in Chemistry

XXIX cycle – years 2014/2016

Coordinator: Prof. Carlo Alberto Bignozzi

Scientific Disciplinary Sector: CHIM/02

Lorenzo Tenti: *The electronic structure of molecules: new insights from orthogonal valence bond*, A PhD thesis, © January 2017

PUBLICATIONS

- M. El Khatib, G. L. Bendazzoli, S. Evangelisti, W. Helal, T. Leininger, L. Tenti, C. Angeli, "Beryllium dimer: a bond based on non-dynamical correlation", *The Journal of Physical Chemistry A* **118**, 6664– 6673 (2014).
- E. Giner, L. Tenti, C. Angeli, J.-P. Malrieu, "The Fermi hole and the correlation introduced by the symmetrization or the anti-symmetrization of the wave function", *The Journal of Chemical Physics* **145**, 124114 (2016).
- L. Tenti, D. Maynau, C. Angeli, C. J. Calzado, "Highly efficient perturbative+variational strategy based on orthogonal valence bond theory for the evaluation of magnetic coupling constants. Application to the trinuclear Cu (II) site of multicopper oxidases", *Physical Chemistry Chemical Physics* **18**, 18365-18380 (2016).
- L. Tenti, E. Giner, J.-P. Malrieu, C. Angeli, "Strongly localized approaches for delocalized systems. I. Ground state of linear polyenes", *Computational and Theoretical Chemistry*, DOI: 10.1016/j.comptc.2017.01.021, (2017).
- E. Giner, L. Tenti, C. Angeli, N. Ferré, "Computation of the isotropic hyperfine coupling constant: efficiency and insights from a new approach based on wave function theory", *Journal of Chemical Theory and Computation*, DOI: 10.1021/acs.jctc.6b00827, (2017).
- A manuscript concerning the OVB analysis of the excited states of polyenes (Chapter 5) is in preparation.
- A manuscript concerning the OVB analysis of the cations of polyenes (Chapter 5) is in preparation.
- A manuscript concerning the OVB analysis of benzene (Chapter 6) is in preparation.
- A manuscript concerning the dependence of entanglement properties on the choice of orbitals (Chapter 8) is in preparation.

CONTENTS

I	THEORY	1
1	INTRODUCTION	3
2	THEORETICAL METHODS	5
2.1	Time-independent Schrödinger equation	5
2.2	The Born-Oppenheimer approximation	5
2.3	Antisymmetry principle and Slater determinants	6
2.4	Slater's rules	8
2.5	Second quantization techniques	9
2.5.1	Annihilation and creation operators	9
2.5.2	Anticommutation properties	10
2.5.3	The representation of one- and two-electron operators	10
2.5.4	Unitary transformation of a spin orbital basis	11
2.6	The Hartree-Fock method	13
2.6.1	Brillouin's theorem	13
2.6.2	Hartree-Fock equations	14
2.6.3	Roothan's equations	16
2.6.4	Beyond Hartree-Fock	17
2.7	Configuration interaction: the variational methods	18
2.7.1	Truncated CI and size-consistency	19
2.7.2	Multiconfigurational SCF methods	20
2.7.3	Complete Active Space SCF	22
2.7.4	Difference Dedicated CI	23
2.8	Perturbation methods	24
2.8.1	Effective and intermediate Hamiltonian theory	26
2.9	Entanglement	29
3	THE ORTHOGONAL VALENCE BOND APPROACH	31
3.1	Traditional Valence Bond	32
3.2	Orthogonal Valence Bond	34
3.3	VB reading of a correlated (MO) wave function	36
II	APPLICATIONS	39
4	LINEAR CONJUGATED POLYENES: THE GROUND STATE	41
4.1	Introduction	41
4.2	Computational details	43
4.3	Strongly localized molecular orbitals	44
4.4	Short-range character of delocalization and correlation energies	51
4.5	Reduced CI model spaces	54
4.6	Rotation around a single bond: the butadiene case	60
4.7	Bond alternation dependence of the ground state energy	61

4.8	Conclusions	65	
5	LINEAR CONJUGATED POLYENES: CATIONS AND EXCITED STATES		67
5.1	Cations	67	
5.2	Excited states	71	
5.2.1	Computational details	73	
5.2.2	Orthogonal valence bond structures	73	
5.2.3	Truncated CI matrices	77	
5.2.4	Conclusions	79	
6	AROMATIC COMPOUNDS: BENZENE		83
6.1	Computational details	83	
6.2	Orbitals	84	
6.3	OVB structures	86	
6.4	Rumer structures	90	
6.5	Linear combinations of structures	97	
6.6	Order of ionicity	98	
6.7	Conclusions	99	
7	MAGNETIC SYSTEMS: STUDY OF BINUCLEAR COPPER COMPLEXES		101
7.1	Description of the systems and computational details	103	
7.2	The Lewis localization method	105	
7.3	Results and discussion	107	
7.3.1	Difference Dedicated CI results	107	
7.3.2	Orthogonal Valence-Bond analysis	113	
7.4	Conclusions	128	
8	ENTANGLEMENT PROPERTIES		131
8.1	The hydrogen molecule: two different approaches	131	
8.2	Analytic entanglement in H ₂	132	
8.2.1	Entanglement in the MO scheme	133	
8.2.2	Entanglement in the OVB scheme	135	
8.3	Entanglement for more complex wave functions	137	
8.3.1	Entanglement in H ₂ using Full-CI	137	
8.3.2	Entanglement in F ₂	138	
8.3.3	Entanglement in N ₂	140	
8.3.4	Entanglement in Cr ₂	142	
8.3.5	Entanglement in decapentaene	143	
9	IMPROVING THE DMRG EFFICIENCY WITH ORBITAL LOCALIZATION		145
9.1	Introduction	145	
9.2	The density matrix renormalization group	146	
9.3	Computational details	147	
9.4	Orbital localization	148	
9.5	Results and discussion	148	
9.6	Conclusions	156	
	BIBLIOGRAPHY		159

ACRONYMS

AO	Atomic Orbitals
CASSCF	Complete Active Space Self Consistent Field
CASCI	Complete Active Space Configuration Interaction
CC	Coupled Clusters
CI	Configuration Interaction
CID	Configuration Interaction of Doubles
CISD	Configuration Interaction of Singles and Doubles
DDCI	Difference Dedicated Configuration Interaction
DFT	Density Functional Theory
DMO	Delocalized Molecular Orbitals
DMRG	Density Matrix Renormalization Group
EA	Electron Affinity
FCI	Full Configuration Interaction
GS	Ground State
GDPT	Generalized Degenerate Perturbation Theory
HF	Hartree-Fock
IP	Ionization Potential
LMO	Localized Molecular Orbitals
MCSCF	Multiconfigurational Self Consistent Field
MO	Molecular Orbitals
MO-LCAO	Molecular Orbitals as Linear Combination of Atomic Orbitals
MPPT	Møller-Plesset Perturbation Theory
MPS	Matrix Product States
OAO	Orthogonal Atomic Orbitals
OVB	Orthogonal Valence Bond

OVB-S	Orthogonal Valence Bond Structures
QDPT	Quasi Degenerate Perturbation Theory
ROHF	Restricted Open-Shell Hartree-Fock
RS	Rumer Structures
RSPT	Rayleigh-Schrödinger Perturbation Theory
SA-RS	Symmetry Adapted Rumer Structures
SCF	Self Consistent Field
SCI	Super-CI
SLMO	Strongly Localized Molecular Orbitals
VB	Valence Bond

Part I

THEORY

In the following chapters, the main methods of quantum chemistry used in this work are briefly resumed, preceded by a general introduction in Chapter 1.

INTRODUCTION

The main topic of this thesis is to explore the possibilities offered by the orthogonal valence bond (OVV) approach in order to get new insights in the nature of the electronic structure of molecules. This approach constitutes a new and original way of thinking, which aims to re-establish the importance of quantum chemistry as a subject able to rationalize, interpret and modeling, and not only as a powerful computational spectroscopy producing accurate data (which is very important, as well). This target is truly ambitious, and what is reported here, together with a few recent other studies, represents a first pioneering exploration in this territory.

The idea behind the orthogonal valence bond method is to combine, in an efficient way, two of the main theories of quantum chemistry: molecular orbitals (MO) and valence bond (VB). In particular, the approach takes advantage of the high computational efficiency of molecular orbitals and of the interpretative potential of valence bond. This is made possible by the use of localized orbitals, which allows the interpretation of a correlated MO wave function using VB-like structures. In this way, a high quality wave function obtained using a MO method (CASSCF, for instance) may be “read” in terms of structures that are in agreement with the Lewis intuition, that is, the same structures that any chemist uses to draw molecules on paper.

In order to exploit diverse implications of orthogonal valence bond, this thesis reports on a series of applications to several molecular systems, ranging from simple homonuclear dimers to large metal complexes.

Following a short overview on the theoretical methods useful for a comprehensive understanding of the subject, the OVB approach is introduced starting from the simplest molecular system, the hydrogen dimer. This basic example allows one to highlight the peculiarities of the method.

Afterward, the focus is moved to the series of all-trans linear conjugated polyenes, and it is shown that the nature of the electronic structures of their ground, excited and ionized states may receive a clear explanation from the OVB point of view. Moreover, the correlation effects are shown to be local, allowing, in combination with an intermediate effective Hamiltonian scheme, the definition of a model Hamiltonian which makes possible to study the ground state of larger terms of the series.

The benzene molecule is then analyzed, using different kinds of contraction schemes offering different point of views on the electronic

structure. For this system, OVB is able to clarify not only the relative importance of the structures, but the reasons laying behind the observed hierarchy of the relevance of the structures. This is possible because, within the OVB scheme, the calculation of energies and interactions between local structures is straightforward.

Then, two binuclear magnetic copper complexes are approached with a perturbative+variational strategy allowing the evaluation of the magnetic coupling constant. The strategy includes the OVB reading of a DDCI wave function and the use an intermediate effective Hamiltonian. The coupling constants are estimated at low-cost and the main excitations contributing to the coupling are isolated and characterized.

A final topic concerns entanglement properties and mutual information of a series of dimers, such as H_2 , F_2 , N_2 and Cr_2 , and of more complex systems such as polyenes. In particular, the subject is analyzed highlighting its dependence on the choice of the orbitals, showing how entanglement patterns are affected by a unitary transformation of the orbitals. Entanglement maps are therefore proposed as a way to visually understand and interpret different orbital localizations and their consequences. Finally, the dependence of entanglement on orbital localization is shown to be the reason behind the improvement of the efficiency of a DMRG calculation when using localized molecular orbitals or orthogonal atomic orbitals.

THEORETICAL METHODS

2.1 TIME-INDEPENDENT SCHRÖDINGER EQUATION

One of the main goals of quantum chemistry is the resolution of the non-relativistic time-independent Schrödinger equation:

$$H\Psi_{\text{tot}}(\chi, Q) = E_{\text{tot}}\Psi_{\text{tot}}(\chi, Q) \quad (2.1)$$

where H is the total molecular Hamiltonian for a system of electrons and nuclei, represented by the coordinates χ and Q , respectively. $\Psi_{\text{tot}}(\chi, Q)$ is the total wave function, which contains all the possible information that can be known about the molecular system and depends on the coordinates of both electrons and nuclei.

The resolution of this equation provides the energies of the stationary states of the molecule. Given the complexity of such an equation, the research of approximate methods enabling its resolution is of fundamental importance.

2.2 THE BORN-OPPENHEIMER APPROXIMATION

The Born-Oppenheimer approximation plays a crucial role in the solution of the Schrödinger equation. The total molecular Hamiltonian, devoid of the magnetic and relativistic terms, may be written as

$$H = T_{\text{nuc}} + T_{\text{el}} + V_{\text{en}} + V_{\text{ee}} + V_{\text{nn}} \quad (2.2)$$

with each term defined as follow:

$$\begin{aligned} T_{\text{nuc}} &= \sum_{\alpha=1}^N \frac{p_{\alpha}^2}{2M_{\alpha}} && \text{nuclear kinetic energy} \\ T_{\text{el}} &= \sum_{i=1}^n \frac{p_i^2}{2m} && \text{electronic kinetic energy} \\ V_{\text{en}} &= - \sum_{\alpha=1}^N \sum_{i=1}^n \frac{Z_{\alpha}e^2}{r_{\alpha i}} && \text{electron-nuclei potential energy} \\ V_{\text{ee}} &= \frac{1}{2} \sum_{i \neq j}^n \frac{e^2}{r_{ij}} && \text{electronic repulsion} \\ V_{\text{nn}} &= \frac{1}{2} \sum_{\alpha \neq \beta}^N \frac{Z_{\alpha}Z_{\beta}e^2}{r_{\alpha\beta}} && \text{nuclear repulsion} \end{aligned}$$

Here, n is the number of electrons, labeled with i and j , N is the number of nuclei, labeled with α and β , and Z_{α} is the atomic number

of atom α . Using the total Hamiltonian, the solution of Equation 2.1 is problematic, and the proposal of Born and Oppenheimer makes a huge step in facilitate this task. Indeed, they demonstrated that the motion of electrons and nuclei can be decoupled due to the large difference in their masses, and it is therefore possible to split the problem in two different equations.

First, one defines an electronic Hamiltonian as

$$H_{el} = T_{el} + V_{en} + V_{ee} + V_{nn} \quad (2.3)$$

and an electronic wave function, $\Psi_n(x; Q)$, obtained separating the motion of nuclei and electrons in the total wave function (for each electronic (n) and roto-vibrational (k) state):

$$\Psi_{tot,n,k}(x, Q) \approx \Psi_n(x; Q)\chi_{n,k}(Q) \quad (2.4)$$

Both H_{el} and $\Psi_n(x; Q)$ depends only parametrically on the nuclear coordinates, and it is straightforward to write a new Schrödinger equation regarding only the motion of the electrons in the field generated by the fixed nuclei:

$$H_{el}\Psi_n(x; Q) = E_n(Q)\Psi_n(x; Q) \quad (2.5)$$

where the electronic energy $E_n(Q)$ depends on the nuclear coordinates Q only as an external parameter and defines the so-called *potential energy surface*.

The so-obtained energy $E_n(Q)$ may be seen as the potential energy term in a Schrödinger equation regarding the motion of the nuclei:

$$[T_{nuc} + E_n(Q)]\chi_{n,k}(Q) = E_{tot,n,k}\chi_{n,k}(Q) \quad (2.6)$$

The Born-Oppenheimer approximation is of fundamental importance and most of the applications of quantum chemistry are based on it, given its reliability and the fact that, even in the cases when it breaks down, it often represents a good starting point for further improvements. In this work, the Born-Oppenheimer is always valid and given for granted even if not explicitly stated. Therefore, the generic Schrödinger equation to be solved is of the kind:

$$H_{el}\Psi_n(1, 2, \dots, n) = E_n\Psi_n(1, 2, \dots, n) \quad (2.7)$$

where $1, 2, \dots, n$ represent the spatial and spin coordinates of electrons, while the nuclei are considered fixed at a given molecular geometry.

2.3 ANTISYMMETRY PRINCIPLE AND SLATER DETERMINANTS

The antisymmetry principle states that a many-electron wave function, of the kind of the $\Psi_n(1, 2, \dots, n)$ solution of Equation 2.7, must

be antisymmetric with respect to the interchange of the total coordinates of two electrons:

$$\Psi_n(1, 2, \dots, i, \dots, j, \dots, n) = -\Psi_n(1, 2, \dots, j, \dots, i, \dots, n) \quad (2.8)$$

A convenient way to express an n -electron wave function would be to write it as a product of n spin orbitals, known as an Hartree product:

$$\Psi_n^{\text{hp}}(1, 2, \dots, n) = \psi_1 \psi_2 \dots \psi_n \quad (2.9)$$

where each spin orbital is a wave function for one electron describing its spatial and spin distributions. Unfortunately, such a product does not satisfy the antisymmetry principle and an alternative form is desirable. A simple strategy to obtain an antisymmetrized product is to build a Slater determinant as:

$$\Phi_K = \frac{1}{\sqrt{(n!)}} \begin{vmatrix} \psi_{k_1}(1) & \psi_{k_2}(1) & \dots & \psi_{k_n}(1) \\ \psi_{k_1}(2) & \psi_{k_2}(2) & \dots & \psi_{k_n}(2) \\ \vdots & \vdots & \ddots & \vdots \\ \psi_{k_1}(n) & \psi_{k_2}(n) & \dots & \psi_{k_n}(n) \end{vmatrix} \quad (2.10)$$

This determinant is usually referred to indicating only its diagonal, $\Phi_K = \|\psi_{k_1} \psi_{k_2} \dots \psi_{k_n}\|$. One should note that a Slater determinant is simply a very smart way to build all the possible permutations of an ensemble of spin orbitals, with the right phase to ensure the antisymmetry principle. In addition to that, the Pauli exclusion principle appears naturally considering that the determinant of a matrix with two identical columns is always vanishing.

Moreover, considering a complete basis of orthonormal spin orbitals one obtains a complete set of antisymmetric functions, which allows to expand any wave function as:

$$\Psi_n = \sum_K \Phi_K c_K \quad (2.11)$$

and substituting it in Equation 2.7 one obtains:

$$\sum_K H_{eL} \Phi_K c_K = E \sum_K \Phi_K c_K \quad (2.12)$$

Applying to both sides of the above equation the *bra* vector $\langle \Phi_L |$ (that corresponds to multiplying by Φ_L^* and integrating over the coordinates) leads to

$$\sum_K \langle \Phi_L | H_{eL} | \Phi_K \rangle c_K = E c_L \quad (2.13)$$

which may be rewritten in a more flexible matrix formalism as:

$$\mathbf{Hc} = E\mathbf{c} \quad (2.14)$$

where the elements of the matrix \mathbf{H} are defined as $H_{LK} = \langle \Phi_L | H_{el} | \Phi_K \rangle$ and \mathbf{c} is a vector containing the coefficients c_K .

Equation 2.14 is the algebraic version of the Schrödinger equation and it is of central importance; its solution consists in the diagonalization of the Hamiltonian matrix \mathbf{H} . If a complete basis set of one-electron wave function is used and considering all the possible Slater determinants one obtains the exact solution to the Schrödinger equation. However, even without a complete basis set (that would have an infinite dimension), this method, known as full configuration interaction (FCI), is not approachable apart for very small molecules and an approximation is therefore needed. The research for these approximations is a crucial point in the field of quantum chemistry and a few of them are described and applied in this work.

2.4 SLATER'S RULES

For the calculation of the matrix elements $H_{LK} = \langle \Phi_L | H_{el} | \Phi_K \rangle$ built using orthonormal spin orbitals, one may use the well-known Slater's rules for one- and two-electron operators (1).

Given a one-electron operator as $H_M = \sum_{i=1}^n h(i)$, the elements $\langle \Phi_L | H_M | \Phi_K \rangle$ are non zero only if:

1. $\Phi_L = \Phi_K$, with $H_{KK} = \sum_{i=1}^n \langle \psi_{k_i} | h | \psi_{k_i} \rangle$
2. $\Phi_L \neq \Phi_K$ for only one spin orbital difference, ($\psi_{l_i} \neq \psi_{k_i}$), with $H_{LK} = \langle \psi_{l_i} | h | \psi_{k_i} \rangle$

Similarly, for a two-electron operator of the type $G = \frac{1}{2} \sum_{i \neq j} g(i, j)$, the elements $\langle \Phi_L | G | \Phi_K \rangle$ differ from zero only if:

1. $\Phi_L = \Phi_K$,
with $G_{KK} = \frac{1}{2} \sum_{i,j=1}^n (\langle \psi_{k_i} \psi_{k_j} | g | \psi_{k_i} \psi_{k_j} \rangle - \langle \psi_{k_i} \psi_{k_j} | g | \psi_{k_j} \psi_{k_i} \rangle)$
2. $\Phi_L \neq \Phi_K$ for only one spin orbital difference ($\psi_{l_i} \neq \psi_{k_i}$),
with $G_{LK} = \sum_{j=1}^n (\langle \psi_{l_i} \psi_{k_j} | g | \psi_{k_i} \psi_{k_j} \rangle - \langle \psi_{l_i} \psi_{k_j} | g | \psi_{k_j} \psi_{k_i} \rangle)$
3. $\Phi_L \neq \Phi_K$ for two spin orbital differences ($\psi_{l_i} \neq \psi_{k_i}, \psi_{l_j} \neq \psi_{k_j}$),
with $G_{LK} = \langle \psi_{l_i} \psi_{l_j} | g | \psi_{k_i} \psi_{k_j} \rangle - \langle \psi_{l_i} \psi_{l_j} | g | \psi_{k_j} \psi_{k_i} \rangle$

If the spin orbital differences are more than one in the case of one-electron operators and more than two in the case of two-electron operators, the matrix element is always zero. It should be noted that the different spin orbitals must be in the same position of each determinant, or a phase factor has to be taken into account for each permutation needed to bring them in the same position.

At this point, it is possible to use these rules to write the energy of a Slater determinant, that is, $E = \langle \Phi | H_{el} | \Phi \rangle$. Indeed, the electronic Hamiltonian operator can be rewritten as:

$$H_{el} = \sum_{i=1}^n h(i) + \frac{1}{2} \sum_{i=1}^n \sum_{j=1}^n g(i, j) + V_{nn} \quad (2.15)$$

where $h(i) = \frac{p_i^2}{2m} - \sum_{\alpha=1}^N \frac{Z_{\alpha} e^2}{r_{\alpha i}}$ and $g(i, j) = \frac{e^2}{r_{ij}}$, thus the energy results

$$\begin{aligned} E &= \langle \Phi | H_{el} | \Phi \rangle = \\ &= \sum_{i=1}^n \langle \psi_i | h | \psi_i \rangle + \frac{1}{2} \sum_{i=1}^n \sum_{j=1}^n (\langle \psi_i \psi_j | g | \psi_i \psi_j \rangle - \langle \psi_i \psi_j | g | \psi_j \psi_i \rangle) + V_{nn} \end{aligned} \quad (2.16)$$

2.5 SECOND QUANTIZATION TECHNIQUES

Second quantization techniques are nowadays commonly used in every field of quantum chemistry. Although this is not the place for a comprehensive overview on these techniques, a quick summary of its main features is essential to better understand the rest of this work.

2.5.1 Annihilation and creation operators

Second quantization techniques are based on the definition of two new operators, namely the *annihilation* (or destruction) operator, a_k , and the *creation* operator, a_k^+ . These two operators are defined starting from an orthonormal spin orbital basis $\{\psi_1, \psi_2, \dots\}$ and an arbitrary n -electron Slater's determinant $|M\rangle = \|\psi_k \psi_a \psi_b \dots\|$.

The annihilation operator is defined by its action on the $|M\rangle$ determinant:

$$a_k \|\psi_k \psi_a \psi_b \dots\| = \|\psi_a \psi_b \dots\| \quad (2.17)$$

$$a_k |M\rangle = |N\rangle \quad (2.18)$$

that produces a new $(n-1)$ -electron Slater's determinant, $|N\rangle$, from which the electron occupying the spin orbital ψ_k has been removed. If ψ_k is not in the first position, one must consider the proper permutations and the consequent possible change of sign. If $|M\rangle$ does not contain the spin orbital ψ_k , the action of a_k produces zero: $a_k |M\rangle = 0$.

The creation operator is defined as the adjoint of the annihilation operator, $a_k^+ = a_k^\dagger$. Starting from the consideration that $\langle N | a_k | M \rangle = 1$, one takes the adjoint and gets $\langle M | a_k^+ | N \rangle = 1$, which trivially leads to:

$$a_k^+ |N\rangle = |M\rangle \quad (2.19)$$

$$a_k^+ \|\psi_a \psi_b \dots\| = \|\psi_k \psi_a \psi_b \dots\| \quad (2.20)$$

Therefore, the application of a_k^+ on a $(n - 1)$ -electron determinant produce a new n -electron determinant with an additional electron in the spin orbital ψ_k , positioned in first position. If the spin orbital ψ_k is already present, the application of the creator operator leads to zero: the Pauli exclusion principle is built-in in this kind of formalism.

2.5.2 Anticommutation properties

It is interesting, and useful for the following chapters, to analyze how the second quantization operators behave when applied in sequence. It is easy to demonstrate that creation operators, as well as annihilation operators, anticommute among themselves.

$$\left[a_i, a_j \right]_+ = a_i a_j + a_j a_i = 0 \quad (2.21)$$

$$\left[a_i^+, a_j^+ \right]_+ = a_i^+ a_j^+ + a_j^+ a_i^+ = 0 \quad (2.22)$$

Instead, a creation operator a_i^+ and an annihilation operator a_j anticommute only if $i \neq j$ and the following relations holds:

$$\left[a_i^+, a_j \right]_+ = a_i^+ a_j + a_j^+ a_i = \delta_{ij} \quad (2.23)$$

The operator $a_i^+ a_j$ is referred to as an *excitation* operator, because it excites an electron from the spin orbital ψ_j to spin orbital ψ_i . $a_i^+ a_i$ is instead a *counting* operator, due to the fact that it simply verifies the presence of an electron on spin orbital ψ_i in a given determinant.

Finally, it should be noted that every Slater's determinant could be seen as the result of the application of a sequence of creation operators to the *vacuum* state, $|vac\rangle$, which represents a completely ionized system depleted of all its electrons:

$$|M\rangle = a_{i_1}^+ a_{i_2}^+ \dots a_{i_n}^+ |vac\rangle \quad (2.24)$$

Conversely, one may obtain the vacuum state starting from the $|M\rangle$ determinant:

$$|vac\rangle = a_{i_n} a_{i_{n-1}} \dots a_{i_1} |M\rangle \quad (2.25)$$

2.5.3 The representation of one- and two-electron operators

One- and two-electron operators can be rewritten in the formalism of second quantization in a way that ensures that the same matrix elements, and therefore the same expectation values, are obtained.

In first quantization, a generic one-electron operator is represented as

$$t^c = \sum_{i=1}^N t^c(x_i) \quad (2.26)$$

and its second quantization analogue is

$$T = \sum_{r,s} t_{rs} a_r^+ a_s \quad (2.27)$$

where $t_{rs} = \int \psi_r^*(\mathbf{x}) t^c \psi_s(\mathbf{x}) d\mathbf{x}$. It can be demonstrated that the so-defined T operator automatically satisfies Slater's rules for one-electron operators, that is, the matrix element $\langle N | T | M \rangle$ is different from zero only if determinants N and M are equal or differ only for a single spin orbital.

The same may be obtained for two-electron operators, represented in first quantization as

$$g^c = \frac{1}{2} \sum_{i \neq j}^N g^c(\mathbf{x}_i, \mathbf{x}_j) \quad (2.28)$$

and in second quantization as

$$G = \frac{1}{2} \sum_{rs,tu} g_{rs,tu} a_r^+ a_s^+ a_u a_t \quad (2.29)$$

where $g_{rs,tu} = \int \psi_r^*(\mathbf{x}_1) \psi_s^*(\mathbf{x}_2) g^c \psi_t(\mathbf{x}_1) \psi_u(\mathbf{x}_2) d\mathbf{x}_1 d\mathbf{x}_2$ and again one may demonstrate that G obeys Slater's rules for a two electron operator.

Equations 2.27 and 2.29 represent the most general form for one- and two-electron operators in second quantization. Starting from them, one may express all operators of first quantization or create new ones. For instance, the electronic Hamiltonian may be written as

$$H_{el_{sq}} = \sum_{rs} \langle \psi_r | h | \psi_s \rangle a_r^+ a_s + \frac{1}{2} \sum_{rstu} \langle \psi_r \psi_s | g | \psi_t \psi_u \rangle a_r^+ a_s^+ a_u a_t \quad (2.30)$$

Finally, it should be noted that, unlike the first quantization operators, the second quantization operators are independent of the number of electrons, but they depend on the used spin orbital basis.

2.5.4 Unitary transformation of a spin orbital basis

The change of spin orbital basis is of fundamental importance in quantum chemistry, being an essential steps in methods like Hartree-Fock and others. It is therefore useful to analyze how the second quantization operators transform when the spin orbital basis changes:

$$|\psi\rangle \rightarrow |\psi'\rangle \quad (2.31)$$

where $|\psi\rangle = \{|\psi_1\rangle, |\psi_2\rangle, \dots\}$ and $|\psi'\rangle$ is analogous. The basis transformation is made by means of a unitary operator U

$$|\psi'\rangle = U |\psi\rangle = |\psi\rangle U \quad (2.32)$$

where \mathbf{U} is a unitary matrix. A generic one-electron operator may be written in the same form for both basis:

$$\mathbb{T} = \sum_{r,s} t_{rs} a_r^+ a_s = \sum_{r,s} t'_{rs} a_r'^+ a_s' \quad (2.33)$$

or, introducing the matrix notation

$$\mathbf{a} = \begin{bmatrix} a_1 \\ a_2 \\ \vdots \end{bmatrix} \quad \mathbf{a}^+ = [a_1^+ \quad a_2^+ \quad \dots] \quad (2.34)$$

it may be rewritten as

$$\mathbb{T} = \mathbf{a}^+ \mathbb{T} \mathbf{a} = \mathbf{a}'^+ \mathbb{T}' \mathbf{a}' \quad (2.35)$$

where the matrix \mathbb{T} is

$$\mathbb{T} = \langle \psi | t | \psi \rangle = \mathbf{U} \langle \psi' | t | \psi' \rangle \mathbf{U}^+ \quad (2.36)$$

Therefore, one obtains:

$$\mathbb{T} = \mathbf{a}^+ \mathbf{U} \mathbb{T}' \mathbf{U}^+ \mathbf{a} \quad (2.37)$$

and the representation of creation and annihilation operators in the new basis results:

$$\mathbf{a}' = \mathbf{U}^+ \mathbf{a} \quad \mathbf{a}'^+ = \mathbf{a}^+ \mathbf{U} \quad (2.38)$$

$$a_r' = \sum_s U_{sr}^* a_s \quad a_r'^+ = \sum_s a_s^+ U_{sr} \quad (2.39)$$

Finally, it is interesting to see the effect of \mathbf{U} on a generic determinant $|\mathbf{K}\rangle = \|\psi_1 \psi_2 \dots \psi_n\| = a_1^+ a_2^+ \dots a_n^+ |\text{vac}\rangle$ (remembering that the unitary transformation of a generic operator is $A' = \mathbf{U} A \mathbf{U}^+$):

$$\mathbf{U} |\mathbf{K}\rangle = \mathbf{U} a_1^+ a_2^+ \dots a_n^+ |\text{vac}\rangle \quad (2.40)$$

$$= \mathbf{U} a_1^+ \mathbf{U}^+ \mathbf{U} a_2^+ \mathbf{U}^+ \mathbf{U} a_3^+ \dots \mathbf{U} a_n^+ \mathbf{U}^+ \mathbf{U} |\text{vac}\rangle \quad (2.41)$$

$$= a_1'^+ a_2'^+ \dots a_n'^+ |\text{vac}\rangle \quad (2.42)$$

$$= \|\psi_1' \psi_2' \dots \psi_n'\| \quad (2.43)$$

Therefore, one obtains a new determinant expanded on the new spin orbital basis. In conclusion, the unitary operator \mathbf{U} may be expressed as $\mathbf{U} = e^{i\Lambda}$, where Λ is just a simple one-electron operator:

$$\Lambda = \sum_{r,s} \lambda_{rs} a_r^+ a_s \quad (2.44)$$

Λ is a hermitian matrix with elements λ_{rs} and one may demonstrate that it is associated with \mathbf{U} by the relation $\mathbf{U} = e^{i\Lambda}$.

Finally, often one sets $\mathbb{T} = i\Lambda$, where \mathbb{T} is an anti-hermitian operator ($\mathbb{T}^\dagger = -\mathbb{T}$). Therefore, the unitary operator performing the unitary transformation is usually written as $\mathbf{U} = e^{\mathbb{T}}$.

2.6 THE HARTREE-FOCK METHOD

The Hartree-Fock method (HF) plays a crucial role in chemistry, being the basis of the chemists' common idea of electrons occupying molecular orbitals. The aim of this approach is to obtain the best approximation to the wave function of the electronic ground state (GS) as a single Slater's determinant $\Psi = \|\psi_1\psi_2\dots\psi_n\|$. This method allows to optimize the spin orbital in such a way that the energy functional $E = \langle\Psi|H|\Psi\rangle$ is variationally minimized.

It must be highlighted that the term "best approximation" refers to the general variational idea that the lower the energy the better the wave function (the better the description of the system). This idea is often valid but it shouldn't be taken as a fundamental rule.

2.6.1 Brillouin's theorem

At the point of minimum, any infinitesimal variation of the spin orbitals, $\psi_i \rightarrow \psi_i + \delta\psi_i$, leads to a vanishing variation of the energy, $\delta E = 0$. As described in the above section, the change of spin orbital basis is done using the unitary operator $U = e^T$, where $T = -T^\dagger = \sum_{r,s} t_{rs} a_r^\dagger a_s$ ($t_{rs} = -t_{sr}^*$).

The energy of the new spin orbital set is defined trivially as $E' = \langle\Psi'|H|\Psi'\rangle$, where $|\Psi'\rangle = e^T|\Psi\rangle$. Therefore, one may write

$$E' = \langle e^T\Psi|H|e^T\Psi\rangle = \langle\Psi|e^{-T}He^T|\Psi\rangle \quad (2.45)$$

and the energy variation appears to be

$$\delta E = E' - E = \langle\Psi|e^{-T}He^T - H|\Psi\rangle \quad (2.46)$$

One may express the term $e^{-T}He^T$ using the Baker-Campbell-Hausdorff relation:

$$e^{-T}He^T = H - [T, H] + \frac{1}{2}[T, [T, H]] + \dots \quad (2.47)$$

and truncate it to the first order due to the infinitesimal size of t_{rs} :

$$\delta E = \langle\Psi|H + [H, T] - H|\Psi\rangle = \langle\Psi|[H, T]|\Psi\rangle \quad (2.48)$$

The above relation may be rewritten making use of the replacement operators $E_{rs} = E_{sr}^\dagger = a_r^\dagger a_s$:

$$\delta E = \sum_{r,s} t_{rs} \langle\Psi|H|E_{rs}\Psi\rangle - \sum_{r,s} t_{sr} \langle E_{sr}\Psi|H|\Psi\rangle \quad (2.49)$$

It can be noted that, in the first term, to have a non vanishing element s must denote an occupied spin orbital and r a virtual one, while in the second term the situation is reversed. Introducing the

notation in which $i, j \dots$ refer to occupied spin orbitals and a, b, \dots to virtual spin orbital, the last equation may be expressed as

$$\delta E = \sum_{i=1}^n \sum_{a>n} t_{ai} \langle \Psi | H | \Psi_i^a \rangle + \text{c.c.} \quad (2.50)$$

where c.c. stands for complex conjugate and $\Psi_i^a = E_{ai}\Psi$ is a singly excited determinant. Given that the t_{ai} can be arbitrarily chosen, one may see that δE vanishes if

$$\langle \Psi | H | \Psi_i^a \rangle = 0 \quad (2.51)$$

The above equation is a very important achievement and it is known as Brillouin's theorem (2). This theorem states that the variational energy E of a wave function Ψ constituted by a single Slater's determinant is minimized with respect to the spin orbital basis if the interactions between Ψ and any singly excited determinant $E_{ai}\Psi = \Psi_i^a$ is zero.

2.6.2 Hartree-Fock equations

Using the Brillouin's theorem it is possible to obtain the Hartree-Fock equations that produce the spin orbitals minimizing the variational energy.

If $\Psi = \|\psi_1\psi_2 \dots \psi_i \dots \psi_n\|$ and $\Psi_i^a = \|\psi_1\psi_2 \dots \psi_a \dots \psi_n\|$, one may rewrite the Brillouin's theorem making use of the Slater's rules:

$$\begin{aligned} \langle \Psi_i^a | H | \Psi \rangle = \\ \langle \psi_a | h | \psi_i \rangle + \sum_{j=1}^n \left(\left\langle \psi_a \psi_j \left| \frac{1}{r_{12}} \right| \psi_i \psi_j \right\rangle - \left\langle \psi_a \psi_j \left| \frac{1}{r_{12}} \right| \psi_j \psi_i \right\rangle \right) = 0 \end{aligned} \quad (2.52)$$

Here, it is convenient to introduce two new operators:

$$\langle \psi_r | J | \psi_s \rangle = \sum_{j=1}^n \left\langle \psi_r \psi_j \left| \frac{1}{r_{12}} \right| \psi_s \psi_j \right\rangle \quad (2.53)$$

$$\langle \psi_r | K | \psi_s \rangle = \sum_{j=1}^n \left\langle \psi_r \psi_j \left| \frac{1}{r_{12}} \right| \psi_j \psi_s \right\rangle \quad (2.54)$$

J is known as the *Coulomb operator* and it represents the average Coulomb potential generated by the electronic distribution, while K is the *exchange operator* and it represents the exchange interaction that appears between electrons of the same spin and it is a pure quantum contribution.

Putting together these operators in Equation 2.52, one obtains

$$\langle \psi_a | h + J - K | \psi_i \rangle = 0 \quad (2.55)$$

and, introducing a new operator, the *Fock operator* $F = h + J - K$, leads to

$$\langle \psi_\alpha | F | \psi_i \rangle = 0 \quad (2.56)$$

The last equation states that each vector $F\psi_i$ has to be orthogonal to each vector ψ_α (or, in other words, ψ_α and ψ_i do not interact via the Fock operator). This means that the generic vector $F\psi_i$ should belong to the subspace of the occupied spin orbitals, and it can be expressed as a generic linear combination of these vectors, obtaining the *generalized Hartree-Fock equations*:

$$F|\psi_i\rangle = \sum_{j=1}^n |\psi_j\rangle \varepsilon_{ji} \quad (2.57)$$

where ε_{ji} are the elements of the hermitian matrix ε .

Then, it is possible to find a unitary matrix \mathbf{U} that diagonalizes ε , and write the so-called *canonical Hartree-Fock equations*:

$$F\psi'_i = \varepsilon_i \psi'_i \quad (2.58)$$

where the spin orbitals ψ'_i , known as *canonical spin orbitals*, are obtained from the unitary transformation

$$\psi'_i = \sum_{j=1}^n \psi_j U_{ji} \quad (2.59)$$

These are the equations that the spin orbitals must satisfy in order to minimize the variational energy. Equation 2.58 may resemble a simple eigenvalue equation, however, the Fock operator itself depends on the spin orbitals. This means that it is necessary to use an iterative procedure, namely the *self consistent field* method (SCF). One starts from guess spin orbitals, $\{\psi_1^{(0)}, \psi_2^{(0)}, \dots\}$, and builds a first approximation of the Fock operator, $F^{(0)}$; then, diagonalizing the Fock matrix, that is, solving the eigenvalue equation $F^{(0)}\psi_i^{(1)} = \varepsilon_i^{(0)}\psi_i^{(1)}$, one obtains a new set of spin orbitals, $\{\psi_1^{(1)}, \psi_2^{(1)}, \dots\}$, required to restart the iterative procedure until convergence, the so-called *self consistence*.

The eigenvalues ε_i obtained from the solution of the canonical Hartree-Fock equations are often referred to as *orbital energies* and bear a clear physical meaning. Indeed, the so-called *Koopmans theorem* (3) states that

$$E_i^+ - E = \langle \Psi | [a_i^+, H] a_i | \Psi \rangle = -h_{ii} - (J_{ii} - K_{ii}) = -\varepsilon_i \quad (2.60)$$

where $E_i^+ = \langle a_i \Psi | H | a_i \Psi \rangle$ is the energy associated to the ionized state $\Psi_i^+ = a_i \Psi$. Therefore, the energy needed to remove an electron from spin orbital ψ_i , the ionization potential (IP), is approximated by the orbital energy ε_i changed of sign. Similarly, it can be demonstrated

that an approximation to the electronic affinity (EA) may be obtained as $E - E_v^- = -\varepsilon_v$, where v is a virtual orbital.

The ionization potentials obtained with the Koopmans theorem is a good approximation to the experimental value, while the electronic affinity is usually not very accurate.

Finally, to simplify the use of Hartree-Fock equations, it is common to consider only spatial functions. Indeed, a generic spin orbital may be written as $\psi_i(x_1, y_1, z_1, s_1) = \varphi_i(x_1, y_1, z_1)\eta_m(s_1)$, where φ_i is a spatial orbital and $\eta_m(s_1)$ is a spin function. For a closed-shell system with the same number of α and β electrons, the canonical Hartree-Fock equations may be rewritten as

$$f\varphi_i = \varepsilon_i\varphi_i \quad (2.61)$$

where $f = h + 2J - K$ is a new Fock operator and the Coulomb and exchange operators are defined, without spin coordinates, as

$$\langle \varphi_r | J | \varphi_s \rangle = \sum_{j=1}^{n/2} \left\langle \varphi_r \varphi_j \left| \frac{1}{r_{12}} \right| \varphi_s \varphi_j \right\rangle \quad (2.62)$$

$$\langle \varphi_r | K | \varphi_s \rangle = \sum_{j=1}^{n/2} \left\langle \varphi_r \varphi_j \left| \frac{1}{r_{12}} \right| \varphi_j \varphi_s \right\rangle \quad (2.63)$$

Of course, similar equations exist even for open-shell systems (restricted open-shell Hartree-Fock, ROHF) and can be found elsewhere.

2.6.3 Roothan's equations

Using the Hartree-Fock equations described above, one may obtain the optimized orbitals that minimize the variational energy of a single Slater's determinant. Unfortunately, these are very complicated integro-differential equations whose analytical solution is not practical. Therefore, one usually prefers to expand the orbital φ_i in a chosen atomic basis set $\{\chi_1, \chi_2, \dots\}$:

$$\varphi_i = \sum_r \chi_r c_{ri} \quad (2.64)$$

that is, the molecular orbitals are written as linear combination of atomic orbitals (MO-LCAO).

This expansion allows to move from an integro-differential problem to an algebraic one, where the expansion coefficients c_{ri} have to be determined. Of course, this is an approximation depending on the size of the basis set: only using a complete basis set would yield the true solutions of the Hartree-Fock equations.

Inserting Equation 2.64 in Equation 2.61, one obtains

$$\sum_r f\chi_r c_{ri} = \varepsilon_i \sum_r \chi_r c_{ri} \quad (2.65)$$

Multiplying by χ_s^* and integrating on the whole space leads to

$$\sum_r \langle \chi_s | f | \chi_r \rangle c_{ri} = \varepsilon_i \sum_r \langle \chi_s | \chi_r \rangle c_{ri} \quad (2.66)$$

that may be rewritten in algebraic notation to obtain what is known as the *Roothan's SCF* equations:

$$\mathbf{F} \mathbf{c}_i = \varepsilon_i \mathbf{S} \mathbf{c}_i \quad (2.67)$$

where \mathbf{c}_i is a vector containing the coefficients, \mathbf{S} is the overlap matrix ($S_{sr} = \langle \chi_s | \chi_r \rangle$) and \mathbf{F} is the Fock matrix written in the atomic basis, whose elements are

$$F_{sr} = \langle \chi_s | f | \chi_r \rangle = \langle \chi_s | h | \chi_r \rangle + \sum_{t,u} \left(2 \left\langle \chi_s \chi_t \left| \frac{1}{r_{12}} \right| \chi_r \chi_u \right\rangle - \left\langle \chi_s \chi_t \left| \frac{1}{r_{12}} \right| \chi_u \chi_r \right\rangle \right) R_{ut} \quad (2.68)$$

where R_{ur} are the elements of the *density matrix* \mathbf{R}

$$R_{ut} = \sum_{j=1}^n c_{uj}^* c_{tj} \quad \mathbf{R} = \mathbf{C} \mathbf{C}^\dagger \quad (2.69)$$

and \mathbf{C} is the matrix collecting all the coefficients c_j .

The Roothan's equations are *pseudoeigenvalue* equations, because the matrix \mathbf{F} depends on the solutions c_j . Thus, one may solve this equations using an iterative scheme, starting from a guess matrix of coefficients $\mathbf{C}^{(0)}$ to build a first approximation to the matrices \mathbf{R} and \mathbf{F} , then one diagonalizes \mathbf{F} and obtains a new matrix $\mathbf{C}^{(1)}$, from which it is possible to restart the iterative scheme and continue until self-consistence is reached.

2.6.4 Beyond Hartree-Fock

The Hartree-Fock method occupies a central role in chemistry and often the results obtained are in good agreement with the experimental data. This happens especially for the study of the ground state of closed-shell molecule at geometries close to equilibrium. For more complex systems, such as open-shells, excited states or non-equilibrium geometries (very common in the study of reaction paths and bond breaking), the Hartree-Fock method fails. For this kind of problems, one need to go beyond Hartree-Fock and its approximation, introducing the so-called electron correlation. This can be done in several ways and some of them are discussed in the following.

2.7 CONFIGURATION INTERACTION: THE VARIATIONAL METHODS

The *correlation energy*, E_{corr} , is defined as the difference between the exact non-relativistic energy \mathcal{E}_0 and the Hartree-Fock limit energy (when the basis is complete):

$$E_{\text{corr}} = \mathcal{E}_0 - E_0 \quad (2.70)$$

This is due to the fact that in the Hartree-Fock approximation the motion of the electrons with the same spin is only partially correlated (thanks to the antisymmetry of the wave function) and those with different spin are not correlated. Thus, one may start from the Hartree-Fock method and add the electron correlation effects.

The configuration interaction (CI) method is conceptually the most simple method used to introduce the electron correlation. Unfortunately, it is also one of the most computationally expensive. It consists in building a wave function as a linear combination of different Slater's determinants and then diagonalize the Hamiltonian matrix built on the basis of these functions. If the basis is complete, one obtains the exact energy both for the ground state (GS) and for all excited states (ES), and the method is called full configuration interaction (FCI).

Indicating the Hartree-Fock determinant with $|\Phi_0\rangle$, the other determinants may be seen as different excitations made on top of it and the total wave function may be written as

$$\Psi = c_0 |\Phi_0\rangle + \sum_{i,a} c_i^a |\Phi_i^a\rangle + \sum_{\substack{i<j \\ a<b}} c_{ij}^{ab} |\Phi_{ij}^{ab}\rangle + \sum_{\substack{i<j<k \\ a<b<c}} c_{ijk}^{abc} |\Phi_{ijk}^{abc}\rangle + \dots \quad (2.71)$$

where $|\Phi_i^a\rangle$ are single excitations, $|\Phi_{ij}^{ab}\rangle$ are double and so on. They may be contracted as

$$\Psi = c_0 |\Phi_0\rangle + c_S |S\rangle + c_D |D\rangle + c_T |T\rangle + \dots \quad (2.72)$$

Therefore, the CI matrix would appear as

$$\begin{bmatrix} \langle \Phi_0 | H | \Phi_0 \rangle & 0 & \langle \Phi_0 | H | D \rangle & 0 & 0 & \dots \\ & \langle S | H | S \rangle & \langle S | H | D \rangle & \langle S | H | T \rangle & 0 & \dots \\ & & \langle D | H | D \rangle & \langle D | H | T \rangle & \langle D | H | Q \rangle & \dots \\ & & & \langle T | H | T \rangle & \langle T | H | Q \rangle & \dots \\ & & & & \langle Q | H | Q \rangle & \dots \\ & & & & & \dots \end{bmatrix} \quad (2.73)$$

where one may note that the single excitations do not interact with the Hartree-Fock determinant due to Brillouin's theorem and, moreover, determinants with more than two spin orbital differences do not interact, according to Slater's rules.

Using the so-called *intermediate normalization*, one can divide Equation 2.71 by c_0 and write

$$\Psi = |\Phi_0\rangle + \sum_{i,a} c_i^a |\Phi_i^a\rangle + \sum_{\substack{i<j \\ a<b}} c_{ij}^{ab} |\Phi_{ij}^{ab}\rangle + \sum_{\substack{i<j<k \\ a<b<c}} c_{ijk}^{abc} |\Phi_{ijk}^{abc}\rangle + \dots \quad (2.74)$$

so that $\langle\Psi|\Phi_0\rangle = 1$.

Considering now the Schrödinger equation

$$H|\Psi\rangle = \varepsilon_0 |\Psi\rangle \quad (2.75)$$

and inserting in the left term expansion 2.74, one gets

$$H\Phi_0 + \sum_{i,a} c_i^a H|\Phi_i^a\rangle + \sum_{\substack{i<j \\ a<b}} c_{ij}^{ab} H|\Phi_{ij}^{ab}\rangle + \dots = \varepsilon_0 |\Psi\rangle \quad (2.76)$$

Multiplying by $\langle\Phi_0|$ and considering Slater's rules and Brillouin's theorem, leads to

$$\langle\Phi_0|H|\Phi_0\rangle + \sum_{\substack{i<j \\ a<b}} c_{ij}^{ab} \langle\Phi_0|H|\Phi_{ij}^{ab}\rangle = \varepsilon_0 \quad (2.77)$$

Finally, considering that $\langle\Phi_0|H|\Phi_0\rangle$ is the Hartree-Fock limit energy, the correlation energy can be expressed as

$$E_{\text{corr}} = \varepsilon_0 - E_0 = \sum_{\substack{i<j \\ a<b}} c_{ij}^{ab} \langle\Phi_0|H|\Phi_{ij}^{ab}\rangle \quad (2.78)$$

This demonstrates that the double excitations play a fundamental role for electron correlation. Nevertheless, one should note that the coefficients c_{ij}^{ab} are obtained from the diagonalization of the whole CI matrix and therefore they depend on all other determinants.

2.7.1 Truncated CI and size-consistency

As already stated, Full CI is computationally prohibitive for the large majority of molecular systems. A natural approximation to this expensive technique consists in lowering the number of determinants in expansion 2.71. Such an approach is usually referred to as truncated CI and often it can recover a large part of the correlation energy. This is due to the fact that the Full CI expansion considers many irrelevant determinants that, for instance, have very high energies and/or low interactions with other important determinants.

A common approach is to limit the Full CI expansion only to the singly and doubly excited determinants. This method is known as CISD and the wave function may be written as

$$\Psi = |\Phi_0\rangle + \sum_{i,a} c_i^a |\Phi_i^a\rangle + \sum_{\substack{i<j \\ a<b}} c_{ij}^{ab} |\Phi_{ij}^{ab}\rangle \quad (2.79)$$

The size of the Hamiltonian matrix built starting from this wave function is much smaller than the Full CI one and the diagonalization procedure is more computationally feasible.

The CISD works very well for molecular systems that have already received a good description at the Hartree-Fock level, but it may fail for bond breaking and reaction path descriptions. This problem, which affects (almost) all types of truncated CI, is known as *size-consistency problem* and may be better understood with an example.

Let's consider a system, AB, composed by two non-interacting subsystems, A and B. The total Hamiltonian for such a system is the sum of the Hamiltonian regarding the two subsystems. Therefore, the total energy is the sum of the energies of the two subsystems and the total wave function is the product:

$$H_{AB} = H_A + H_B \quad (2.80)$$

$$\Psi_{AB} = \Psi_A \Psi_B \quad (2.81)$$

$$E_{AB} = E_A + E_B \quad (2.82)$$

Applying the CID technique (configuration interaction of doubles), the wave functions of the two subsystems are

$$\Psi_A = \Psi_A^{\text{HF}} + \Psi_A^{\text{D}} \quad (2.83)$$

$$\Psi_B = \Psi_B^{\text{HF}} + \Psi_B^{\text{D}} \quad (2.84)$$

where HF indicates the Hartree-Fock determinant and D all possible doubly excitations made on top of it. The total wave function, obtained as the product of Ψ_A and Ψ_B , is therefore

$$\Psi_{AB} = \Psi_A \Psi_B = \Psi_A^{\text{HF}} \Psi_B^{\text{HF}} + \Psi_A^{\text{HF}} \Psi_B^{\text{D}} + \Psi_A^{\text{D}} \Psi_B^{\text{HF}} + \Psi_A^{\text{D}} \Psi_B^{\text{D}} \quad (2.85)$$

The lack of size-consistence of CID is due to the term $\Psi_A^{\text{D}} \Psi_B^{\text{D}}$ that, as one may note, is a quadrupole excitation with respect to the Hartree-Fock determinant of the total system AB and would not be present in the CID wave function of the total system. Thus, the energy of AB, E_{AB} , is not the sum of E_A and E_B , that is, applying the method to the two separate subsystems or to the total system leads to different results and the method is not size-consistent. This is a critical defect that can considerably limit the applicability of a computational technique. Among the size-consistent methods, one may find Hartree-Fock, many-body perturbation theory, coupled cluster (CC), Full CI and complete active space self consistent field (CASSCF), a method that plays a central role in this work and that will be analyzed in the following.

2.7.2 Multiconfigurational SCF methods

Truncated CI are commonly employed starting from the Hartree-Fock method. One starts from the Hartree-Fock determinant and considers

a set of excited determinants obtained exciting electrons from occupied orbitals to virtual ones. The molecular orbitals used are therefore the Hartree-Fock canonical orbitals, those that diagonalize the Fock matrix. The results of a Full CI calculation is independent from the chosen set of molecular orbitals. However, in a truncated scheme, the choice of orbitals plays a crucial role.

A technique that allows both the optimization of the CI coefficients and the optimization of the MOs is the multiconfigurational self consistent field method (MCSCF).

Considering a wave function as a generic combination of Slater's determinant

$$\Psi = \sum_{\mathbf{K}} \Phi_{\mathbf{K}} c_{\mathbf{K}} \quad (2.86)$$

where $\Phi_{\mathbf{K}} = \|\varphi_1 \varphi_2 \dots \varphi_n\|$ and $\varphi_i = \sum_r \chi_r c_{ri}$, the MCSCF method allows to optimize both $c_{\mathbf{K}}$ than c_{ri} . This means that the energy $E = \langle \Psi | H | \Psi \rangle$ has to be stationary with respect to an infinitesimal variation of these two sets of coefficients: $c'_{\mathbf{K}} \rightarrow c_{\mathbf{K}} + \delta c_{\mathbf{K}}$ and $\varphi'_i \rightarrow \varphi_i + \delta \varphi_i$ (which depends on c_{ri}). In both cases, the orthonormality constraints must be retained: $\sum_{\mathbf{K}} c_{\mathbf{K}}^* c_{\mathbf{K}} = 1$ and $\langle \varphi_i | \varphi_j \rangle = \delta_{ij}$.

The above request is obtained through an iterative procedure, consisting in two steps to be repeated until convergence:

1. One builds the Hamiltonian matrix with the determinants $\Phi_{\mathbf{K}}$ starting from a given set of orbitals and then obtains a set of coefficients $c_{\mathbf{K}}$.
2. Knowing the coefficients $c_{\mathbf{K}}$, one may look for a set of orbitals minimizing the energy $E = \langle \Psi | H | \Psi \rangle$.

Step 1 is realized solving the eigenvalue equation $\mathbf{H}\mathbf{c} = E\mathbf{c}$, where the elements of the \mathbf{H} matrix are $H_{\mathbf{KL}} = \langle \Phi_{\mathbf{K}} | H | \Phi_{\mathbf{L}} \rangle$ and the vector \mathbf{c} contains the coefficients $c_{\mathbf{K}}$. Step 2 is similar to the SCF procedure used in the Hartree-Fock method: the energy is minimized with respect to the set of molecular orbitals when the *extended Brillouin's theorem* (4) is fulfilled. This theorem, known also as *Brillouin-Levy-Berthier's theorem*, is the natural extension of the Brillouin's theorem (see Section 2.6.1) for the case of a multiconfigurational wave function and it is satisfied when

$$\langle \Psi | H | (E_{rs} - E_{sr}) \Psi \rangle = 0 \quad (2.87)$$

where E_{rs} and E_{sr} are replacement operators. Therefore, the function $(E_{rs} - E_{sr})\Psi$ does not interact with Ψ when the orbitals are optimized. The replacement operator E_{rs} replace the spin orbital φ_s with spin orbital φ_r in all Slater's determinants $\Phi_{\mathbf{K}}$ of the expansion 2.86, when the excitation is feasible. Defining $\Psi_s^r = (E_{rs} - E_{sr})\Psi$, the self consistency is achieved when $\langle \Psi | H | \Psi_s^r \rangle = 0$, that is, when the wave function

Ψ does not interact with any of its *contracted* single excitations. The terms “contracted” refers to the fact that the coefficients c_K are kept fixed in the expansion of Ψ .

Far from self consistency, at each iterative step the corrected wave function may be seen as $\Psi' = \Psi + \sum_{s < r} c_{sr} \Psi_{sr}^r$, and the coefficients c_{sr} can be taken as the t_{rs} of the spin orbitals unitary transformation (see Section 2.5.4):

$$\psi' = \psi e^T \quad \text{with} \quad t_{sr} = c_{sr} \quad (2.88)$$

Then, the so-obtained spin orbital basis may be used to rebuild the CI wave function and continue the iterative procedure, until convergence is reached. This method is called Super-CI (SCI), and despite the existence of more sophisticated approaches it is still used due to its simplicity.

2.7.3 Complete Active Space SCF

Among the MCSCF methods, the one that surely requires more attention is the complete active space self consistent field method (CASSCF). Indeed, one of the major problem of MCSCF techniques is the choice of the configurations that must be considered in the CI wave function.

Within the CASSCF method, one partitions the spin orbitals in three different classes:

1. core spin orbitals, which are always occupied in all determinants;
2. active spin orbitals, having all the possible occupations between 0 and 1;
3. virtual spin orbitals, which are always unoccupied in all determinants.

The most important class is clearly the active one. One chooses a certain number of orbitals, which should be occupied or virtual in a previous Hartree-Fock calculation, and then considers all possible determinants that can be generated putting a certain (and fixed) number of electrons in these orbitals. The so-obtained calculations is usually referred to as CASSCF(*n* electrons, *n* orbitals), and, *de facto*, it is a Full CI calculation performed in the subspace spanned by the active orbitals. Therefore, the CASSCF has the same good properties of the Full CI, such as size consistency and invariance with respect to a unitary transformation of the active orbitals.

In addition to that, the CASSCF is more computationally efficient than a generic MCSCF, because extended Brillouin’s theorem assume a simplified form. Indeed, one may demonstrate that the theorem is automatically satisfied for any couple of indices belonging to the same set of orbitals.

2.7.4 *Difference Dedicated CI*

Performing a valence CASSCF calculation, that is, considering all valence orbitals as active orbitals, one covers the so-called *non-dynamical correlation*. Although the definition of different correlation effects is not always clear, generally one defines this kind of correlation as the one given by quasi-degenerate determinants needed to well describe a molecular system even at dissociation. Conversely, *dynamical correlation* takes into account the actual correlation of the motion of the electrons, such as, among other effects, the fluctuation of the core electrons in response to the valence electrons. To calculate this correlation, one may consider a CAS+SD approach, adding to the CASSCF configuration space all possible single and double excitations doable on the CASSCF determinants.

The CAS+SD approach falls in the category of truncated CI methods and it is not size consistent. Moreover, it is computationally expensive and not suitable for large systems.

The possible excitations are usually grouped in 8 different classes, named after the number of *holes* created in the occupied orbitals and *particles* promoted to virtual orbitals:

- 1h: single excitations from core to active orbitals;
- 2h: double excitations from core to active orbitals;
- 1p: single excitations from active to virtual orbitals;
- 2p: double excitations from active to virtual orbitals;
- 1h-1p: single excitations from core to virtual orbitals;
- 2h-1p: double excitations from core to active and virtual orbitals;
- 1h-2p: double excitations from core and active to virtual orbitals;
- 2h-2p: double excitations from core to active orbitals.

Using second order perturbation arguments, it has been demonstrated that the 2h-2p class has a small effect on the excitation energies and does not play a differential role in distinct electronic or spin states. In other words, the 2h-2p excitations have a large impact on the absolute energy of a certain state, but do not affect (markedly) the energy difference between two states. Considering that the 2h-2p class could represent the 90% of the total CI space, eliminating these excitations lead to a large improvement in the computational efficiency. The resulting method is known as difference dedicated configuration interaction (DDCI), and it is considered the reference method for molecular magnetism applications, where the fundamental property to be calculated is the energy difference between two spin states.

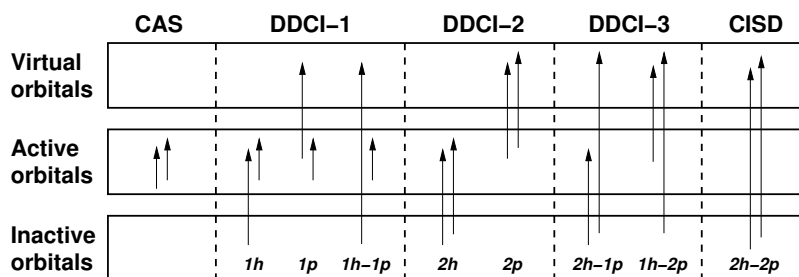


Figure 2.1: Different kinds of configuration interactions: from CAS to CAS+SD (CISD).

Sometime, DDCI is referred to as DDCI-3, to distinguish it from further approximations, namely DDCI-1 and DDCI-2, where other classes of excitations are eliminated. Figure 2.1 summarizes these different possible techniques.

2.8 PERTURBATION METHODS

Perturbation techniques may be applied to an approximate wave function to gradually improve its results by means of successive approximations. In quantum chemistry, the most important technique is the Rayleigh-Schrödinger perturbation theory (RSPT), which has been successfully applied both to single determinant wave function such as the Hartree-Fock one and to multiconfigurational wave function coming, for instance, from a MCSCF calculation.

In the most general case, the first step is to partition the Hamiltonian in two parts:

$$H = H_0 + \lambda V \quad (2.89)$$

where V is the *perturbation operator* and H_0 is the unperturbed zero-order Hamiltonian operator for which all eigenvalues ($E_n^{(0)}$) and all eigenvectors ($\Psi_n^{(0)}$) are known. That is, one knows how to solve the eigenvalue problem

$$H_0 \Psi_n^{(0)} = E_n^{(0)} \Psi_n^{(0)} \quad (2.90)$$

The total wave function and the total energy are consequently written as a sum of successive improvement on top of the zero-order (a series expansion):

$$\Psi_n = \Psi_n^{(0)} + \lambda \Psi_n^{(1)} + \lambda^2 \Psi_n^{(2)} + \dots \quad (2.91)$$

$$E_n = E_n^{(0)} + \lambda E_n^{(1)} + \lambda^2 E_n^{(2)} + \dots \quad (2.92)$$

where the k -th terms are referred to as the k -th order correction to the wave function and to the energy.

It is possible to demonstrate that the k -th order correction to the energy may be written as:

$$E_n^{(k)} = \langle \Psi_n^{(0)} | V | \Psi_n^{(k-1)} \rangle \quad (2.93)$$

and one should note that to know the k -th term of the energy expansion one only needs to know the 0-th and $(k-1)$ -th order of the wave function. Actually one can show that the knowledge of the k -th correction of the wave function allows to compute the energy up to the $2k+1$ -th term. The first order correction to the energy is simply:

$$E_n^{(1)} = \langle \Psi_n^{(0)} | V | \Psi_n^{(0)} \rangle \quad (2.94)$$

that is, the mean value of the perturbation operator in the unperturbed state $\Psi_n^{(0)}$.

The second order, however, depends on $\Psi_n^{(1)}$:

$$E_n^{(2)} = \langle \Psi_n^{(0)} | V | \Psi_n^{(1)} \rangle \quad (2.95)$$

where

$$\Psi_n^{(1)} = - \sum_{k \neq n} \frac{\langle \Psi_n^{(0)} | V | \Psi_k^{(0)} \rangle}{E_k^{(0)} - E_n^{(0)}} \Psi_k^{(0)} \quad (2.96)$$

that easily leads to

$$E_n^{(2)} = - \sum_{k \neq n} \frac{|\langle \Psi_n^{(0)} | V | \Psi_k^{(0)} \rangle|^2}{E_k^{(0)} - E_n^{(0)}} \quad (2.97)$$

The last equation is very important. Indeed, in the vast majority of the cases, a second order correction to the energy is more than enough to well describe the system under study. Moreover, higher order of perturbation are often very complex and computational expensive, especially in the case of multiconfigurational zero-order wave function.

The most important perturbation theory are the Møller-Plesset perturbation theory (MPPT), used on top of the Hartree-Fock method, and the CASPT (5-7) and NEVPT (8-11), used on top of CASSCF. Both are commonly used at the second order, MP2 and CASPT2/NEVPT2, although higher orders are available in computational chemistry program packages.

In this work, perturbation theory is only used as a tool for compressing the information of a large CI space into a smaller one, with an approach called effective, or intermediate, Hamiltonian theory; therefore, the above perturbation theories are not reported here, given the large amount of literature available.

2.8.1 Effective and intermediate Hamiltonian theory

In the following a brief summary of effective and intermediate Hamiltonians theories is presented. The aim of these theories is to select a small subspace of configurations from a CI space and *dress it*, through perturbation techniques, with the effect of the whole space. The idea behind this is that the small subspace should behave as if all the effects describing the system were taken into account by few but meaningful configurations. As one may imagine, it is a powerful tool, especially for getting insights on large and complex molecular systems.

The effective Hamiltonians theory starts with the partition of the vectorial space into a N_m -dimensional model subspace S_0 and its orthogonal complement S_0^\perp , called outer subspace. S_0 and S_0^\perp are defined, respectively, by the projectors P_0 and Q_0 :

$$P_0 = \sum_{m=1}^{N_m} |m\rangle \langle m| \quad (2.98)$$

$$Q_0 = \sum_{\alpha \notin S_0} |\alpha\rangle \langle \alpha| \quad (2.99)$$

$$P_0 + Q_0 = 1. \quad (2.100)$$

The first effective Hamiltonian, H_{eff} , defined by Bloch in 1958 (12), requires that the N_m roots of H_{eff} are the eigenvalues of the exact Hamiltonian H , while the corresponding eigenvectors are the projections on the model space of the exact eigenvectors of H :

$$H_{eff} = \sum_{m=1}^{N_m} E_m |\bar{\psi}_m\rangle \langle \bar{\psi}_m^\perp| \quad (2.101)$$

$$H |\psi_m\rangle = E_m |\psi_m\rangle \quad (2.102)$$

$$H_{eff} |\bar{\psi}_m\rangle = E_m |\bar{\psi}_m\rangle \quad (2.103)$$

$$|\bar{\psi}_m\rangle = P_0 |\psi_m\rangle \quad (2.104)$$

where the $|\bar{\psi}_m\rangle$ are the projections of $|\psi_m\rangle$ in the model space.

This effective Hamiltonian is defined as:

$$H_{eff} = P_0 H \Omega \quad (2.105)$$

where Ω is the wave-operator that transforms the projected states $|\bar{\psi}_m\rangle$ into the corresponding exact eigenstates $|\psi_m\rangle$:

$$\Omega |\bar{\psi}_m\rangle = \Omega P_0 |\psi_m\rangle = |\psi_m\rangle \quad (2.106)$$

Ω must obey the operator equation

$$Q_0 H \Omega = Q_0 \Omega H \Omega \quad (2.107)$$

that can be solved by the quasi degenerate perturbation theory (QDPT) splitting the exact Hamiltonian H into an unperturbed zeroth-order Hamiltonian H_0 and a perturbation V

$$H_0 = \sum_{m=1}^{N_m} E_m^0 |m\rangle \langle m| + \sum_{\alpha} E_{\alpha}^0 |\alpha\rangle \langle \alpha| \quad (2.108)$$

$$V = H - H_0 \quad (2.109)$$

Using the QDPT strategy leads to the second order perturbation terms:

$$H_{\text{eff}}^{(2)} = \sum_{i,j} \sum_{\alpha} \frac{|i\rangle \langle i| V |\alpha\rangle \langle \alpha| V |j\rangle \langle j|}{E_j^0 - E_{\alpha}^0} \quad (2.110)$$

$$\langle i| H_{\text{eff}}^{(2)} |j\rangle = \sum_{\alpha} \frac{\langle i| V |\alpha\rangle \langle \alpha| V |j\rangle}{E_j^0 - E_{\alpha}^0} \quad (2.111)$$

The intermediate Hamiltonians theory is based on these results. The main difference is that the intermediate Hamiltonian H_{int} provides only N_m exact energies and projected eigenstates in a model space that has dimension $N_m + N_i$, allowing N_i solutions to be an approximation to the exact ones. The full model space S_0 is partitioned into a main model space S_m and an intermediate space S_i , whose corresponding projectors follow the equations

$$P_m = \sum_{m=1}^{N_m} |m\rangle \langle m| \quad (2.112)$$

$$P_i = \sum_{i=1}^{N_i} |i\rangle \langle i| \quad (2.113)$$

$$P_0 = P_m + P_i \quad (2.114)$$

Therefore, it is possible to write:

$$H_{\text{int}} = \sum_{m=1}^{N_m} E_m |\tilde{\psi}_m\rangle \langle \tilde{\psi}_m^{\perp}| + \sum_{i=1}^{N_i} \tilde{E}_i |\tilde{\psi}_i\rangle \langle \tilde{\psi}_i^{\perp}| \quad (2.115)$$

where

$$H |\psi_m\rangle = E_m |\psi_m\rangle \quad (2.116)$$

$$H_{\text{int}} |\tilde{\psi}_m\rangle = E_m |\tilde{\psi}_m\rangle \quad (2.117)$$

$$|\tilde{\psi}_m\rangle = (P_m + P_i) |\psi_m\rangle \quad (2.118)$$

and the $|\tilde{\psi}_m\rangle$ are the projections of $|\psi_m\rangle$ in the model space.

Also in this case one can introduce an operator equation and solve it through the use of perturbation theory, specifically the generalized

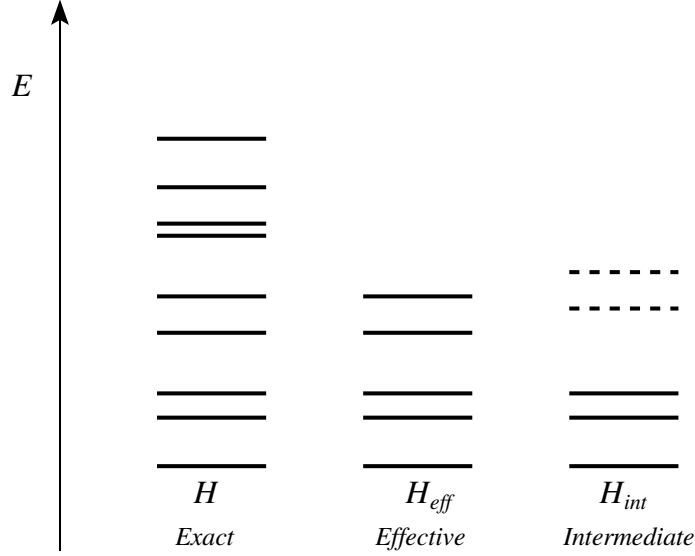


Figure 2.2: Energy spectra with different Hamiltonians.

degenerate perturbation theory (GDPT), splitting the exact Hamiltonian into an unperturbed zeroth-order Hamiltonian H_0 and a perturbation V :

$$H_0 = \sum_{m=1}^{N_m} E_0 |m\rangle \langle m| + \sum_{i=1}^{N_i} E_i^0 |i\rangle \langle i| + \sum_{\alpha} E_{\alpha}^0 |\alpha\rangle \langle \alpha| \quad (2.119)$$

$$V = H - H_0 \quad (2.120)$$

considering the main model space as degenerate with a common energy E_0 .

Using the GDPT leads to the second order perturbation terms

$$H_{\text{int}}^{(2)} = \sum_{i,j} \sum_{\alpha} \frac{|i\rangle \langle i| V |\alpha\rangle \langle \alpha| V |j\rangle \langle j|}{E_0 - E_{\alpha}^0} \quad (2.121)$$

$$\langle i| H_{\text{int}}^{(2)} |j\rangle = \sum_{\alpha} \frac{\langle i| V |\alpha\rangle \langle \alpha| V |j\rangle}{E_0 - E_{\alpha}^0} \quad (2.122)$$

widely used for the application of the intermediate Hamiltonians theory to the problems covered in this work. One may note that at the second order the only difference with the effective Hamiltonian terms (equations 2.110 and 2.111) stands in the denominator. Specifically, the E_j^0 terms are replaced by E_0 . Because the denominator is independent from the index j , the Hamiltonian matrix is now hermitian. Moreover, if the E_0 is well separated from the energies of the perturbers α the sum is finite, avoiding the intruder-state problems.

A comparison between the energy spectrum of the exact, effective and intermediate Hamiltonian is reported in Figure 2.2.

One last comment concerns the energy E_0 . In the original paper presenting the intermediate Hamiltonians theory, E_0 is introduced as

an arbitrary energy parameter coinciding with the degenerate zeroth-order energy of the model space. This arbitrariness allows a certain freedom in the definition of E_0 and consequently different versions of this method can be implemented.

2.9 ENTANGLEMENT

Entanglement has recently been introduced in quantum chemistry as a way to obtain a quantitative measure of orbital interaction (13). Using concepts from quantum information theory, one may quantify entanglement, and thus orbital interaction, through the von Neumann entropy s , a function of density-matrix eigenvalues. This has been done extensively in the last years, especially in the framework of Density Matrix Renormalization Group (DMRG), where these quantities are easily accessible (14–16).

For a given molecular system, the entanglement between one orbital i and the other orbitals can be calculated as the one-orbital von Neumann entropy:

$$s(1)_i = - \sum_{\alpha=1}^4 \omega_{\alpha,i} \ln \omega_{\alpha,i} \quad (2.123)$$

where $\omega_{\alpha,i}$ are the eigenvalues of the one-orbital Reduced Density Matrix (RDM) and the states indicated with α correspond to the 4 possible occupations of the spatial orbital i : 0, 1 (α or β spin) and 2 electrons, which can be referred to as $|-\rangle$, $|\uparrow\rangle$, $|\downarrow\rangle$, and $|\uparrow\downarrow\rangle$, respectively.

The eigenvalue spectrum of the one-orbital RDM depends on the environment in which the given orbital is embedded and thus it incorporates in some way a correlation effect (17). Therefore, even if two orbitals have similar occupation numbers, their one-orbital von Neumann entropies may largely differ. That is why $s(1)$ is a measure of the interaction between orbital i and the other orbitals of the system.

In a similar way, starting from the eigenvalues of the two-orbital RDM, $\omega_{\alpha,i,j}$, one may define the two-orbital entropy as:

$$s(2)_{i,j} = - \sum_{\alpha=1}^{16} \omega_{\alpha,i,j} \ln \omega_{\alpha,i,j} \quad (2.124)$$

In this case, the sum runs over the 16 possible occupations of orbital i and j : $|--\rangle$, $|\uparrow-\rangle$, $|\downarrow-\rangle$, $|\uparrow\downarrow-\rangle$, \dots , $|\uparrow\downarrow\uparrow\rangle$, $|\uparrow\downarrow\downarrow\rangle$. This value quantifies the entanglement between the pair of orbitals i, j and the rest of the environment.

If the orbitals i and j are not entangled with each other, one has that $s(1)_i + s(1)_j = s(2)_{i,j}$ and a measure of the entanglement between the two orbitals, $I_{i,j}$, can be defined as the deviation from this equality:

$$I_{i,j} = \frac{1}{2} [s(1)_i + s(1)_j - s(2)_{i,j}] (1 - \delta_{ij}) \quad (2.125)$$

where $(1 - \delta_{ij})$ ensures that $I_{i,i} = 0$. This quantity is usually referred to as *mutual information*, representing the amount of information orbital i has about orbital j , that is, how much i knows about j .

A simple interpretation is given by the fact that $s(1)_i$ and $s(1)_j$ represent the entanglement of i and j with the rest of the orbitals, respectively, while $s(2)_{i,j}$ represents the entanglement of the pair of i , j with the rest of the orbitals. Any interaction between i and j reduces the two-orbital entropy $s(2)_{i,j}$ with respect to the sum of the one-orbital entropies $s(1)_i$ and $s(1)_j$.

Entropy measures and mutual information have been used to obtain useful information on electron correlation effects and bond-formation processes (17, 18), as well as for the automated selection of active orbital spaces (19) and the identification of the model space for a perturbative + variational strategy to be applied to magnetic systems. (20)

THE ORTHOGONAL VALENCE BOND APPROACH

In 1916, with a paper entitled “The Atom and the Molecule” (21) Gilbert N. Lewis proposed a rationalization of the molecular structure based on the distribution of the valence electrons in bonds and lone pairs. After a century, this idea remains the everyday language of chemists, who still think and draw molecules using the so-called *Lewis’ structures*.

Then, in 1926, Erwin Schrödinger established the mathematical foundations of quantum chemistry with his famous equations and, shortly after, Walter Heitler and Fritz London applied them to the hydrogen molecule, obtaining results in full agreement with Lewis’ picture. Their approach, extended by John C. Slater and Linus Pauling, is still known as valence bond theory (VB). This first success has been rapidly eclipsed by the work of Robert Mulliken and Friedrich Hund, who proposed the molecular orbital theory (MO). This theory, through the use of Hartree-Fock method and Koopmans’ theorem, gives easy access to a large number of properties and readily explains several effects that are less clear in a valence bond picture, such as light-matter interaction, ionization potentials and excited states. In addition to that, the VB method met the problem of the explosion of the number of the structures, which made it inadequate for the study of large molecular systems, while MO based method are more computational efficient and suitable for more complex problems.

Nevertheless, valence bond theory has never died, being the method of choice for those topics where a delocalized picture is not suitable. Among these, one may cite molecular magnetism, diradical transition states and spin polarization in free radical. Moreover, the delocalized picture proposed by molecular orbitals contrasts with Lewis’ intuition: the electrons are no longer localized in bonds and lone pairs but they appear delocalized on the whole molecular space, being characterized mainly by the nodal properties and energy of the orbitals they occupy. The central advantage of valence bond is therefore conceptual: it allows an understanding of the electronic structure that would not be straightforward with molecular orbitals.

Actually, even if it has not received the deserved attention by quantum chemists’ community, a reconciliation between the MO theory and Lewis’ intuition has been proposed by Coulson, Lennard-Jones and others. Indeed, they showed that the Hartree-Fock determinant is invariant for a transformation of the delocalized molecular orbitals in bonds and lone pairs localized MOs, and this may be generalized to

more sophisticated and correlated wave function such as the CASSCF one.

The use of localized orbitals allows the interpretation of a MO-based correlated wave function in terms of VB-like structures. This is the case with orthogonal valence bond (OVB), an approach that aims to combine, in an efficient way, the computational performance of molecular orbitals methods and the interpretative potential of valence bond. As described in the following, a fundamental difference between OVB and VB is the orthogonality of the one-electron functions, which is intimately correlated not only to the computational efficiency (the non-orthogonality is perhaps the major issue in VB methods) but even to a new and different interpretation of bonds and electronic structures.

The rest of this chapter presents an introduction to the orthogonal valence bond approach by means of its application to one of the simplest molecular systems: the hydrogen molecule, H_2 .

3.1 TRADITIONAL VALENCE BOND

The traditional presentation of valence bond theory for the hydrogen molecule starts from the assumption that, for two non-interacting hydrogen atoms at infinite distance, the total Hamiltonian reduces to the sum of two separate Hamiltonians, one for each hydrogen atoms. Thus, the wave function representing the singlet ground state (GS) of the molecule is obtained as the product (properly antisymmetrized) of the two GS wave functions of the atoms (A and B):

$${}^1\Psi_N^n = \frac{1s_A 1s_B + 1s_B 1s_A}{\sqrt{2(1+S^2)}} \frac{\alpha\beta - \beta\alpha}{\sqrt{2}} \quad (3.1)$$

where N indicates that the state is neutral, that is, each atom bears an electron, n refers to the non orthogonality of the atomic orbitals used ($1s_A$ and $1s_B$) and S is their overlap $\langle 1s_A | 1s_B \rangle$. This wave function is exact for two non-interacting atoms, and the idea behind VB approach is to take it as a variational approximation at closer geometries.

One of the strengths of the valence bond approach is that the so-obtained neutral wave function is a really good approximation to the ground state wave function, as one may see in Figure 3.1. To improve this result, that is, to obtain the curve indicated with GS in the figure, one combines the neutral wave function ${}^1\Psi_N^n$ with the ionic wave function ${}^1\Psi_I^n$ (firstly introduced by Majorana in 1931 (22)), where a hydrogen atom bears two electrons and the other none (and vice versa):

$${}^1\Psi_I^n = \frac{1s_A 1s_A + 1s_B 1s_B}{\sqrt{2(1+S^2)}} \frac{\alpha\beta - \beta\alpha}{\sqrt{2}} \quad (3.2)$$

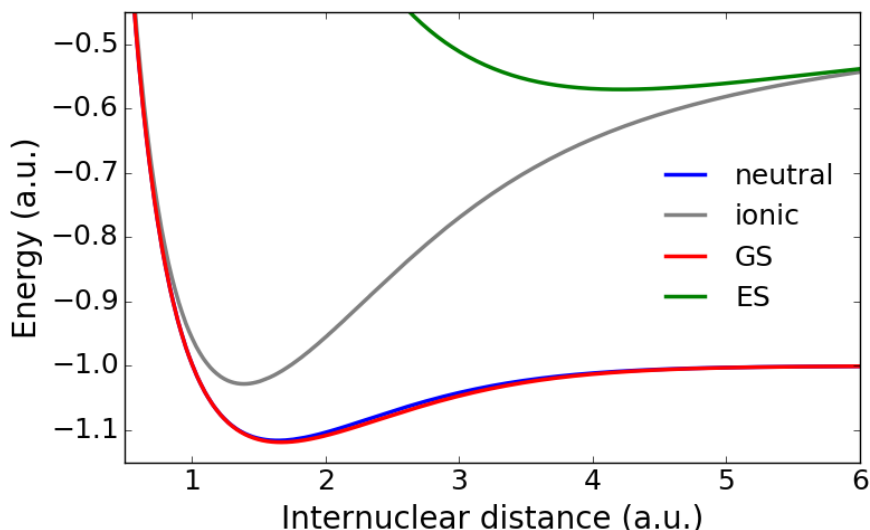


Figure 3.1: Valence bond energies for the hydrogen molecule.

The GS wave function is therefore obtained as

$${}^1\Psi_{\text{GS}} = c_{\text{N}} {}^1\Psi_{\text{N}}^{\text{n}} + c_{\text{I}} {}^1\Psi_{\text{I}}^{\text{n}} \quad (3.3)$$

where the coefficients c_{N} and c_{I} are variationally optimized from the diagonalization of the Hamiltonian matrix in the basis $\{{}^1\Psi_{\text{N}}^{\text{n}}, {}^1\Psi_{\text{I}}^{\text{n}}\}$, which furnishes also the energy and wave function of the first singlet *gerade* excited state (ES). Of course, these curves are only an approximation to the exact ones. For instance, the minimum of the “true” potential energy curve for the ground state is at a lower energy and shorter internuclear distance. However, the curves obtained here are able to well represent the formation of the bond, at least from a qualitative point of view.

From Figure 3.1 it appears clearly that the ground state is well approximated by ${}^1\Psi_{\text{N}}^{\text{n}}$ while the excited state is badly represented by ${}^1\Psi_{\text{I}}^{\text{n}}$. It is usually stated that the chemical bond between the two hydrogen atoms is given by the neutral function, while the ionic function has a negligible effect. However, it must be considered that the two atomic orbitals employed in the construction of the wave functions are non orthogonal and present a strong overlap integral, especially at the equilibrium geometry. The non orthogonality of the atomic orbitals reflects on the non orthogonality of neutral and ionic wave functions:

$$\langle {}^1\Psi_{\text{N}}^{\text{n}} | {}^1\Psi_{\text{I}}^{\text{n}} \rangle = \frac{2S}{1+S^2} \quad (3.4)$$

This means that the two functions are not independent and each one contains a non-negligible contribute from the other that is proportional to the atomic overlap S . In other words, the neutral function is not really neutral and describes a situation that is both neutral

and ionic. Of course, this is true also for the ionic function. The next section provides a solution to this problem, making use of orthogonal atomic orbitals which produce orthogonal wave functions with a clear and well-defined nature.

3.2 ORTHOGONAL VALENCE BOND

The main difference between traditional valence bond (VB) and orthogonal valence bond (OVB) is, as stated by the name, the orthogonality of the atomic orbitals used to build the wave functions. In the case of the hydrogen molecule in the minimal basis $\{1s_A, 1s_B\}$, the orthogonal atomic orbitals may be obtained using the *Löwdin orthogonalization*. Indeed, this technique is more “democratic” than the well-known Gram-Schmidt orthogonalization, in the sense that both starting vectors are transformed similarly (equally, for a symmetric problem) toward the orthogonalized vectors. By contrast, the Gram-Schmidt orthogonalization leaves one initial vector as it is and transforms only the other in accordance until the orthogonality is reached.

It can be shown that the orthogonalization process leads to the following expressions:

$$a = \frac{1}{2} \left(\frac{1}{\sqrt{1+S}} + \frac{1}{\sqrt{1-S}} \right) 1s_A + \frac{1}{2} \left(\frac{1}{\sqrt{1+S}} - \frac{1}{\sqrt{1-S}} \right) 1s_B \quad (3.5)$$

$$b = \frac{1}{2} \left(\frac{1}{\sqrt{1+S}} + \frac{1}{\sqrt{1-S}} \right) 1s_B + \frac{1}{2} \left(\frac{1}{\sqrt{1+S}} - \frac{1}{\sqrt{1-S}} \right) 1s_A \quad (3.6)$$

where a and b are orthogonal atomic orbitals centered on atom A and B, respectively. Moreover, these orbitals are transformed one into the other under the symmetry operations which move the nucleus A into the nucleus B. As one may see, each atom-centered orbital presents a *tail* on the other atom, required to ensure the orthogonality, usually referred to as “orthogonalization tail”.

Considering a small atomic overlap, $S \ll 1$, the above equations may be simplified as

$$a \approx 1s_A - \frac{1}{2}S 1s_B \quad (3.7)$$

$$b \approx 1s_B - \frac{1}{2}S 1s_A \quad (3.8)$$

where the orthogonalization tails become more evident.

Consequently, the neutral and ionic wave functions (Equations 3.1 and 3.2) may be written in an orthogonal valence bond formalism as

$${}^1\Psi_N^o = \frac{ab + ba}{\sqrt{2}} \frac{\alpha\beta - \beta\alpha}{\sqrt{2}} \quad (3.9)$$

$${}^1\Psi_I^o = \frac{aa + bb}{\sqrt{2}} \frac{\alpha\beta - \beta\alpha}{\sqrt{2}} \quad (3.10)$$

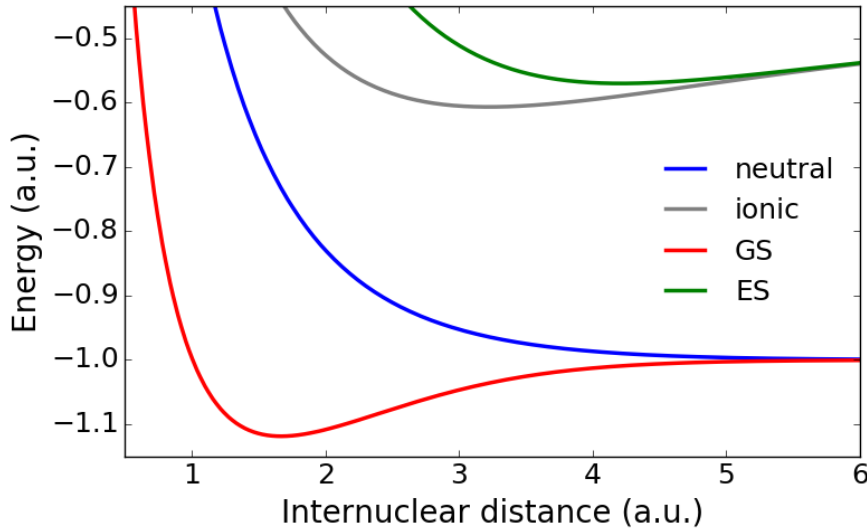


Figure 3.2: Orthogonal valence bond energies for the hydrogen molecule.

where o indicates that these functions are built starting from orthogonal orbitals. It is important to highlight the absence of the atomic overlap S ; moreover, one verifies that these two functions are orthogonal and their nature is univocally defined:

$$\langle {}^1\Psi_N^o | {}^1\Psi_I^o \rangle = 0 \quad (3.11)$$

In addition to that, it is interesting to see that these two orthogonal functions may be written as a combination of the two non orthogonal functions:

$${}^1\Psi_N^o = \frac{\sqrt{1+S^2}}{1-S^2} ({}^1\Psi_N^n - S {}^1\Psi_I^n) \quad (3.12)$$

$${}^1\Psi_I^o = \frac{\sqrt{1+S^2}}{1-S^2} ({}^1\Psi_I^n - S {}^1\Psi_N^n) \quad (3.13)$$

The clear nature of these wave functions has been demonstrated (23) showing that they represent diabatic states, that is, states for which the non adiabatic coupling is vanishing. The nature of the diabatic states does not change when the nuclear coordinates are modified, thus ${}^1\Psi_N^o$ and ${}^1\Psi_I^o$ keep their neutral and ionic nature (clear at infinite distance) for all values of the nuclear distance.

Considering that the neutral and ionic nature of the wave functions ${}^1\Psi_N^o$ and ${}^1\Psi_I^o$ is univocally defined, from the above equations one has another demonstration of the ambiguity of the non orthogonal functions: to obtain functions that are “truly” neutral and ionic one must consider a combination of the non orthogonal ones.

The energies obtained using the orthogonal valence bond approach are reported in Figure 3.2. The ground and excited states energies are strictly the same as in traditional valence bond, given the fact that

the orthogonal valence bond approach only performs a change of basis while the space spanned by the orthogonal and non orthogonal functions remains exactly the same. By contrast, the energy curves corresponding to the neutral and ionic OVB functions are substantially different from the ones obtained using traditional VB approach.

The most important and interesting difference lays in the neutral curve. Indeed, using orthogonal orbitals leads to a neutral curve that is no longer a good approximation to the GS curve as it happens with traditional valence bond. In addition, this curve is dissociative and therefore is not able to describe the bond between the two atoms. Thus, the combination with the ionic function is compulsory to obtain a bonding curve.

In such a way, orthogonal valence bond loses one of the strengths of traditional valence bond, that is, the ability to describe with a good approximation the ground state of H_2 using only the neutral function. Nevertheless, this demonstrates that the bond is due to the interaction between neutral and ionic functions: the situation in which two electrons stay in the same atom is crucial for the description of the chemical bond, and it is not just a small improvement to the energy curve.

In addition to that, orthogonal valence bond is intrinsically more efficient than traditional valence bond due to the orthonormality of the basis $\{^1\Psi_N^o, ^1\Psi_I^o\}$. Indeed, one has to solve a simple eigenvalue problem of the type

$$\mathbf{H}\mathbf{c} = E\mathbf{c} \quad (3.14)$$

instead of the more elaborated *generalized eigenvalue problems* in the non-orthonormal basis $\{^1\Psi_N^n, ^1\Psi_I^n\}$:

$$\mathbf{H}\mathbf{c} = E\mathbf{M}\mathbf{c} \quad (3.15)$$

where \mathbf{M} is the metric matrix depending on the atomic overlap:

$$\mathbf{M} = \begin{bmatrix} 1 & \frac{2S}{1+S^2} \\ \frac{2S}{1+S^2} & 1 \end{bmatrix} \quad (3.16)$$

In the case of orthogonal valence bond, this matrix coincides with the identity matrix and the diagonalization of the Hamiltonian matrix is more computational efficient. Obviously, this is not a crucial issue for a 2×2 problem (as is the case for H_2), but it can be a limit for larger molecules.

3.3 VB READING OF A CORRELATED (MO) WAVE FUNCTION

In the previous sections, the relations and differences between traditional valence bond and orthogonal valence bond have been analyzed for the study of the hydrogen dimer in the minimal basis set spanned

by the $1s$ H atomic orbitals. In order to broaden the range of possible applications of the orthogonal valence bond approach, an analysis of its relation with the molecular orbitals theory is required.

Starting from the atomic orbitals (both orthogonal or not) of the previous sections, it is always possible to define two molecular orbitals:

$$\sigma_g = \frac{1s_A + 1s_B}{\sqrt{2(1+S)}} = \frac{a+b}{\sqrt{2}} \quad (3.17)$$

$$\sigma_u = \frac{1s_A - 1s_B}{\sqrt{2(1-S)}} = \frac{a-b}{\sqrt{2}} \quad (3.18)$$

Using these molecular orbitals, it is possible to write two singlet Slater determinants of $^1\Sigma_g^+$ symmetry suited for the description of the ground state of the molecule. The first is

$$\Phi_g = \|\sigma_g \bar{\sigma}_g\| = \sigma_g \sigma_g \frac{\alpha\beta - \beta\alpha}{\sqrt{2}} \quad (3.19)$$

that coincides with the single-determinantal description used, for instance, within the Hartree-Fock method and represents by itself a good approximation for the ground state at geometries close to equilibrium. The second determinant represents a double excitation where the two electrons occupy the σ_u orbital:

$$\Phi_g^* = \|\sigma_u \bar{\sigma}_u\| = \sigma_u \sigma_u \frac{\alpha\beta - \beta\alpha}{\sqrt{2}} \quad (3.20)$$

It is interesting to see that these determinants may be expressed as in-phase and out-of-phase combinations of the ionic and neutral valence bond functions (both traditional and orthogonal):

$$\Phi_g = \frac{{}^1\Psi_I^o + {}^1\Psi_N^o}{\sqrt{2}} = \frac{1}{\sqrt{2}} \frac{\sqrt{1+S^2}}{1+S} ({}^1\Psi_I^n + {}^1\Psi_N^n) \quad (3.21)$$

$$\Phi_g^* = \frac{{}^1\Psi_I^o - {}^1\Psi_N^o}{\sqrt{2}} = \frac{1}{\sqrt{2}} \frac{\sqrt{1+S^2}}{1-S} ({}^1\Psi_I^n - {}^1\Psi_N^n) \quad (3.22)$$

Considering that the ground state wave function of H_2 is a linear combination of these determinants, one may write:

$${}^1\Psi_{GS} = \lambda\Phi_g - \mu\Phi_g^* \quad (3.23)$$

$$= \frac{(\lambda + \mu)}{\sqrt{2}} {}^1\Psi_N^o + \frac{(\lambda - \mu)}{\sqrt{2}} {}^1\Psi_I^o \quad (3.24)$$

$$= \frac{\sqrt{1+S^2}}{\sqrt{2}} \left[\left(\frac{\lambda}{1+S} + \frac{\mu}{1-S} \right) {}^1\Psi_N^n + \left(\frac{\lambda}{1+S} - \frac{\mu}{1-S} \right) {}^1\Psi_I^n \right] \quad (3.25)$$

and given that the basis employed is the same, these wave functions are strictly equivalent to the ones obtained with traditional and orthogonal valence bond.

The above relations demonstrate the tight relation between the VB and MO methods and allow one to perform a valence bond reading of molecular orbital wave functions. This means that one may express a wave function obtained from an MO procedure using valence bond structures, that is, with neutral and ionic structures in full accordance with Lewis' intuition.

In order to go a step further, it is possible to generalize this approach for a more general basis set of atomic orbitals, $\{\chi_r\}$, defining the molecular orbitals σ_g and σ_u as follow:

$$\sigma_g = \sum_r c_r \chi_r \quad (3.26)$$

$$\sigma_u = \sum_r c_r^* \chi_r \quad (3.27)$$

where, for instance, the coefficients can be optimized in a way that minimizes the energy of a two-electrons in two-orbitals wave function (together with the optimization of the ratio λ/μ , this would coincide with a CASSCF(2,2) treatment for H_2).

Starting from the so-obtained molecular orbitals, one may express the best valence orthogonal atomic orbitals a and b as

$$a = \frac{\sigma_g + \sigma_u}{\sqrt{2}} \quad (3.28)$$

$$b = \frac{\sigma_g - \sigma_u}{\sqrt{2}} \quad (3.29)$$

optimized at the CASSCF(2,2) level. Consequently, the OVB reading of this correlated wave function gives

$${}^1\Psi_N^o = \frac{\Phi_g - \Phi_g^*}{\sqrt{2}} \quad (3.30)$$

$${}^1\Psi_I^o = \frac{\Phi_g + \Phi_g^*}{\sqrt{2}} \quad (3.31)$$

which are neutral and ionic functions that represent all the effects (non-dynamical correlation and so on) contained in traditional CASSCF wave function.

Obviously, this approach may be generalized to different kinds of correlated wave functions, such as CASSCF, DDCI, CASSD and others, and to larger molecules with more than two orbitals. In order to do this, the localization of the delocalized molecular orbitals (like in Equations 3.28 and 3.29 but for more than two orbitals) is a crucial step, which can be achieved using different techniques as shown in the next chapters for several applications.

Part II

APPLICATIONS

In the following chapters, several applications of the previously analyzed techniques are reported. Among these, one may find the orthogonal valence bond reading of correlated wave functions of polyenes (ground state, excited states and ionized states) and a similar application to the benzene molecule; a more advanced application to molecular magnets leading to an highly-efficient variational+perturbation method; an analysis of the dependence of entanglement measures on orbital localization, both in a DMRG framework and in other multireference wave function methods.

LINEAR CONJUGATED POLYENES: THE GROUND STATE

Linear conjugated polyenes are poly-unsaturated organic compounds characterized by a variable number of alternating single and double carbon-carbon bonds.

Linear polyenes have received a huge consideration in the history of modern chemistry, both from theoretical and experimental point of view. They have played a crucial role in the development of molecular quantum theory as a model for conjugated systems and several tools have been created for their analysis since the dawn of modern quantum chemistry, when the use of empirical or semi-empirical methods was the only way to approach large systems. One may consider, for instance, the models of Hückel, Pariser-Parr-Pople, and Hubbard (24–27).

Moreover, these systems have been experimentally analyzed for the study of the cis-trans photoisomerization, of particular interest in photochemistry. Indeed, several chromophores found in nature present conjugated chains similar to those of linear polyenes, and they are involved in important biological processes such as eyesight and energy production in some bacteria.

In order to explain these effects and many others, a deep understanding of the electronic structures of linear conjugated polyenes is of paramount importance. In addition to that, it is interesting to analyze how the electronic structure is modified by excitation processes or changes of the geometrical parameters.

Despite the large number of studies focussed on these molecules, indeed, their description is not yet completed, especially for what concerns the excited states. In this chapter, an orthogonal valence bond reading of correlated wave functions for the ground state of these polyenes is reported, together with study of the rotation around a single bond, the analysis of the bond length alternation and the development of a model Hamiltonian that allows the study of very large chains.

4.1 INTRODUCTION

The conjugated hydrocarbons are usually presented as intrinsically strongly delocalized. In its early days, Quantum Chemistry started their study from the Hückel Hamiltonian, restricted to the π electrons, which concentrates on delocalization effects and totally omits the bi-electronic repulsion. This model provides symmetry-adapted,

and thus delocalized, mono-electronic functions. It also gives a first estimate of ionization potentials and possibly some crude description of the lowest excited states. Self-Consistent Field (SCF) methods using the exact Hamiltonian provided a stronger basis to these descriptions. Nevertheless, ionization and excitations are intrinsically delocalized phenomena, and Koopmans' theorem, which shows the relevance of the eigenvalues and eigenfunctions (the delocalized so-called canonical molecular orbitals, MOs) (3, 28, 29) of the Fock operators, does not give an indication on the strength of the electronic delocalization in the ground state. It was rapidly recognized by Lennard-Jones (30–33) and others that the SCF single determinant is invariant under rotations of the occupied MOs and that a localizing unitary transformation of the canonical MOs might produce SCF localized MOs, essentially localized on the bonds and lone pairs, where Lewis (21) in a bright intuition, had suggested to put electron pairs. The qualitative picture used by the chemists thus found support from quantum mechanics.

One can note that the SCF description takes into account the bi-electronic repulsion in a static manner, the electrons move in their mean field. The fluctuations of this field is responsible for the so-called electronic correlation, the electronic correlation energy being the difference between the exact energy and the SCF energy. Its evaluation requires to expand the wave function as a linear combination of the SCF determinant and of the excited determinants, promoting electrons from the occupied SCF MOs to virtual MOs.

It is worth noticing that the inter-site delocalization is taken into account in the SCF step and the SCF localized MOs (SCF-LMO), although concentrated in the space between adjacent atoms, have tails on other neighbour atoms, the shape of which minimize the SCF energy. These tails are required in order to satisfy the Brillouin theorem, (2, 34) that is, in order to make vanishing the interaction between the SCF determinant and its mono excitations, among which one counts the inter-bond charge transfer determinants. The SCF-LMOs are particularly interesting for the computation of the correlation energy, since the electron-electron repulsion is a local operator and one may expect that the double excitations from remote SCF-LMOs will not contribute significantly to the correlation energy. Many computational post-Hartree-Fock methods based on localized orbitals have been proposed for the treatment of large molecules, in search for a computation effort scaling linearly with the size of the molecule (or the number of electrons), see for instance Refs. (35–40).

Here, a return to a Lewis-type strongly localized zero-order wave function is presented, following a research line which has a long story (see, for instance, Refs. (41–43)). It is of particular relevance to cite the PCILO approach (44–46) (Perturbative Configuration Interaction using Localized Orbitals), a seminal idea in which one finds

the fundamentals of the interpretative and computational advantages brought by a multi-determinantal expansion based on strongly localized (bonding and antibonding) MOs. The first terms in the series of the all-trans linear polyenes, with regular bond alternations of different amplitudes, are taken as a typical model problem. We will define orthogonal strongly localized bond MOs (SLMOs). Their tails on atoms different from those involved in the double bond on which the SLMOs are localized are essentially orthogonalization tails, they do not optimize the energy. The corresponding single determinant, which we may call “Lewis determinant”, is of course of higher energy than the SCF determinant. One may as well define antibonding valence MOs, orthogonal to the bonding MOs and between themselves. One may start the expansion of the wave function, treating on an equal foot the delocalization effects, brought by the single excitations, and the correlation effects, brought by the double excitations. It will be shown that both effects are of very short-range character. This concentration of the most important excitation processes makes possible the definition of a very small model space collecting the determinants spanning the largest part of the wave function, the dimension of which scales linearly with the size of the polyene. Provided that the effect of the other excitations within the π valence space is taken into account, at least in a perturbative manner through an intermediate effective Hamiltonian formalism (47) one eventually obtains at a very low computational cost a value of the ground state energy very close to that of the full π CASSCF treatment. Moreover, the response of the ground state energy to the variation of the bond alternation computed at this level, which is very different from that of the SCF approximation, is extremely close to that of the full π CASSCF.

4.2 COMPUTATIONAL DETAILS

The lowest members of the all-trans polyene series, from butadiene to decapentaene, have been considered. To verify the predictive ability of our modeling, full π CASSCF calculations have been performed on the next members of the series, involving 6 and 7 double bonds. Ideal planar geometries have been considered, all angles between close C-C and C-C-H atoms being kept equal to 120° , the CH bond length being 1.08 \AA . The mean CC bond length (the average between a single and a double bond length) is 1.40 \AA , and the bond length alternation (δ_{BLA}) between double ($1.40 - \delta_{\text{BLA}} \text{ \AA}$) and single ($1.40 + \delta_{\text{BLA}} \text{ \AA}$) bonds is considered as a degree of freedom. For simplicity δ_{BLA} is kept fixed along the chain, thus ignoring end effects, that is the fact that the bond alternation is actually larger on the external bonds than on the center of the molecule. In the next section the CC bond lengths are 1.35 \AA and 1.45 \AA for the double bonds and for the simple bonds, respectively. These parameters are reported in Table 4.1.

Table 4.1: Standard geometrical parameters.

Parameter	Value
CC double bond	1.35 Å
CC single bond	1.45 Å
CH bond	1.08 Å
Angle	120°

The SCF and CASSCF calculations have been performed using the MOLCAS package in its 7.8 version (48). The ANO-L basis set is used, with contraction (14s9p4d)/[4s3p1d] for the carbon atoms and (8s4p)/[2s1p] for the hydrogen atoms. The study is focused on the physics taking place within the π valence space, *i.e.* the effects treated at the full π CASSCF level. For decapentaene this active space involves more than 63,000 determinants.

The molecule lies in the xy plane, thus the π manifold is spanned mainly by the p_z atomic orbitals of the atoms.

4.3 STRONGLY LOCALIZED MOLECULAR ORBITALS

Our target is to define strongly localized bond MOs. Working in a minimal basis set, with only one p_z atomic orbital per carbon, it is evident how to define a non-polar bond MO between adjacent atoms involved in a double bond. In the linear polyenes with even numbers of atoms the end effects impose the pairing of atoms. For each double bond i , defined between atoms A_i and B_i , the bonding SLMO is

$$\varphi_i = \frac{(a_i + b_i)}{\sqrt{2(1 + \langle a_i | b_i \rangle)}} \quad (4.1)$$

and the antibonding orbital

$$\varphi_i^* = \frac{(a_i - b_i)}{\sqrt{2(1 - \langle a_i | b_i \rangle)}} \quad (4.2)$$

where a_i and b_i are the p_z orbitals on atom A_i and B_i , respectively.

The non orthogonal bonding MOs can be orthogonalized through a least-moving (symmetric) $S^{-1/2}$ transformation, the virtual MOs can be orthogonalized to the bonding MOs by a Gram-Schmidt orthogonalization and orthogonalized among themselves by a $S^{-1/2}$ transformation. The resulting MOs take orthogonalization tails but they keep a strongly localized character.

When working with non-minimal basis sets it is possible to define an optimal valence space starting from a CASSCF procedure, where $2n$ active electrons occupy $2n$ active MOs (n being the number of double bonds in the polyene). The n most occupied MOs are very close

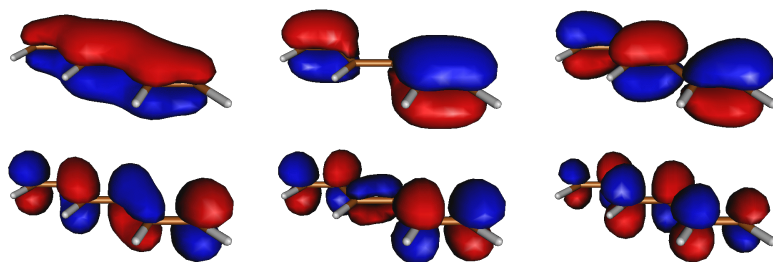


Figure 4.1: Delocalized molecular orbitals for hexatriene.

to the SCF occupied MOs while the n least occupied MOs keep a valence character and present the same nodal properties as the virtual MOs of a SCF calculation in a minimal basis set. This set of MOs actually defines a set of $2n$ orthogonal atom-centered equivalent MOs, obtained by one of the typical localization procedures. It may be for instance Boys' criterion (49) (maximization of the distances between the centroids of the localized orbitals), or the Ruedenberg's one (50) (minimization of the electronic repulsion between the localized orbitals), but here a more direct procedure has been adopted: since the basis set is of Atomic Natural Orbitals (ANO) type, one can look for a unitary transformation of the delocalized active MOs that makes the final orbitals as similar as possible to the $2p_z$ ANO basis functions of the C atoms, thus obtaining orthogonal atomic orbitals (OAOs). Once the OAOs have been obtained, the strongly localized bonding and antibonding MOs (SLMOs) are defined accordingly

$$\varphi_i = \frac{a_i + b_i}{\sqrt{2}} \quad (4.3)$$

$$\varphi_i^* = \frac{a_i - b_i}{\sqrt{2}} \quad (4.4)$$

where a_i and b_i represent the OAOs on the A_i and B_i atoms of the i double bond, respectively.

The delocalized molecular orbitals for the hexatriene molecule and the two types of localized orbitals described above (the strongly localized molecular orbitals and the orthogonal atomic orbitals) are shown in Figures 4.1, 4.2 and 4.3, respectively. In addition, a representation of the determinants written in each of these orbitals bases is reported in Figure 4.4

It is interesting to see in a qualitative way how the Hamiltonian matrix changes using different sets of orbitals. Therefore, a pictorial representation of the Hamiltonian matrices for the hexatriene molecule is reported in Figure 4.5, where the color of each element of the matrices depends on the magnitude of the individual Hamiltonian matrix elements (the diagonal elements have been set to zero to avoid large values on the scale and to highlight the effect of the interactions). As

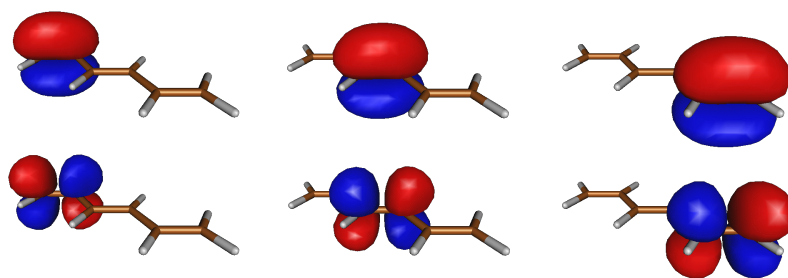


Figure 4.2: Strongly localized molecular orbitals for hexatriene.

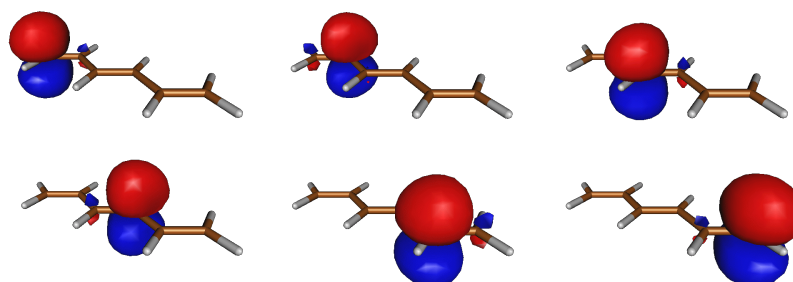


Figure 4.3: Orthogonal atomic orbitals for hexatriene.

one can see, using delocalized molecular orbitals, the Hamiltonian matrix shows many interactions having a small significance, while using localized molecular orbitals there are less interactions with larger magnitude. This effect is even more palpable for orthogonal atomic orbitals, having very few interactions with really large values.

The strategy here adopted can recall the standard VB approach. They differ by two important aspects. Firstly, the “atomic” functions used as building blocks are pure atomic orbitals in VB and OAOs in our approach. This difference, which should look secondary at a first sight, has indeed a dramatic impact on the description of the chemical bond, as it has been shown in details for the simple H_2 case (23, 51, 52) in Chapter 3. Secondly, the bond is described in VB by the singlet coupling of the electrons in the appropriate atomic orbitals (those involved in the bond), while in our case “molecular” orbitals are considered for each bond, thus keeping the local nature of the basis functions, but allowing a minimal delocalization within the bond. Given the clear analogy with VB, we indicate the approach here described with the acronym OVB (orthogonal valence bond). The interpretive power of OVB, together with its computational efficiency (due to the orthogonality of the one electron basis functions) have allowed recently to unravel the intricate nature of the wave function of a few complex systems (20, 53–57).

It is worth noticing that the SLMOs introduced in Eqs. 4.3-4.4 are of CASSCF quality, that is, they are optimized in the molecular reality (therefore, with respect to the pure atomic orbitals, they are polarized and distorted to adapt themselves to the specific molecular situ-

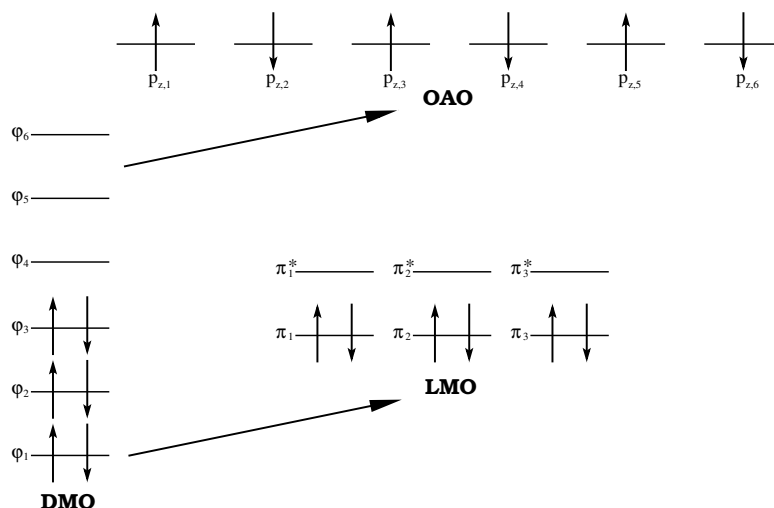


Figure 4.4: Determinants written in different orbitals bases.

ation), sand that a FCI expansion within these orbitals gives exactly the CASSCF wave function and energy. The “Lewis determinant” will be the anti-symmetrized product

$$\Phi_L = \|\prod_{i=1,n} \varphi_i \bar{\varphi}_i\| \quad (4.5)$$

This determinant defines a Fock operator

$$F_L = h + \sum_i^{\text{occ}} (2J_i - K_i) \quad (4.6)$$

here h is the (kinetic+nuclear attraction) mono-electronic operator and the J s and K s are the Coulomb and exchange operators relative to the occupied MOs.

Of course it may seem paradoxical to define the LMOs from a preliminary full π CASSCF calculation. The target of this procedure is purely analytic: it is devoted to an understanding of the relative parts of the delocalization and correlation effects and of their local versus collective character. Alternative procedures may be followed, which start from the single determinant SCF solution. One may consider the corresponding density matrix expressed in the AO basis, truncate it to the basis set of each atom, diagonalize this block of the density matrix and the most occupied vector defines an optimized AO. Then, one may orthogonalize them and return to the preceding procedure, to obtain strongly localized MOs obtained from an SCF step only. The LMO build with this procedure are hereafter labelled (SCF)-SLMOs. The tails of these MOs are not optimal, they do not incorporate any variational inter-bond delocalization. This procedure offers an alternative definition of the π valence space and of the Lewis determinant in this space.

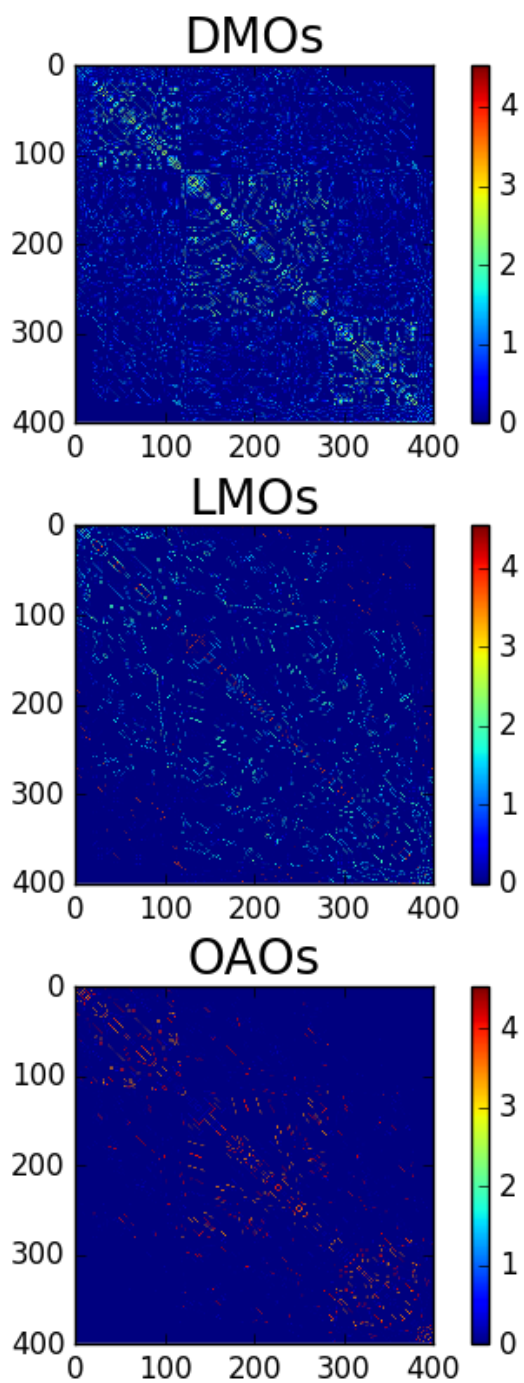


Figure 4.5: Representation of the Hamiltonian matrices with different types of localization (eV), hexatriene

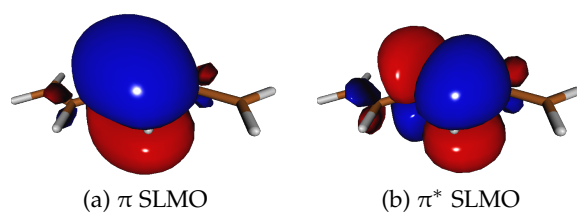


Figure 4.6: Strongly localized molecular orbitals

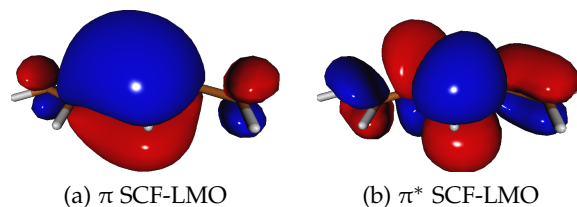


Figure 4.7: SCF localized molecular orbitals

On the other hand, most of the post-HF calculations in terms of localized MOs start by a unitary localizing transformation of the occupied SCF MOs, leaving the SCF determinant invariant. The corresponding SCF LMOs have optimized delocalization tails. The further improvement of the energy by increasing the quality of the wave function is defined as the correlation energy. In practice, the localized approaches for the calculation of the correlation energy also require to localize the virtual MOs. This is not easy in general when using extended basis sets if one wants to use Boys' or Ruedenberg's criteria. A convenient procedure has been proposed by Maynau et al (58). Starting from the eigenvectors of the truncated SCF density matrix one may project the previously defined SLMOs onto the subset of the occupied SCF MOs and orthogonalize these projections. This defines SCF localized MOs (SCF-LMOs). The antibonding counterparts may be orthogonalized to the SCF occupied MOs and orthogonalized between themselves, resulting in a set of localized antibonding valence MOs.

The analysis reported in the present chapter is performed with three sets of localized valence MOs, the SLMOs obtained from the CASSCF MOs, the (SCF)-SLMO and the SCF-LMO, the last two are obtained both from an SCF calculation, the former one being strongly localized, the second one incorporating delocalization effects. The qualitative differences between the SLMOs and the SCF-LMOs appear clearly in Figures 4.6 and 4.7 for the π and π^* orbitals of the central bond of the hexatriene molecule. Focusing on the occupied π orbitals, the orthogonalization (small) tails of the SLMOs on the adjacent-bond atoms present a phase opposite to that of the AOs on the bond, while the SCF-LMOs have an in-phase (large) tail on the adjacent atoms and a negative phase (equally large) tail on the second-neighbor atoms, as shown in the qualitative representation reported in Figure 4.8.

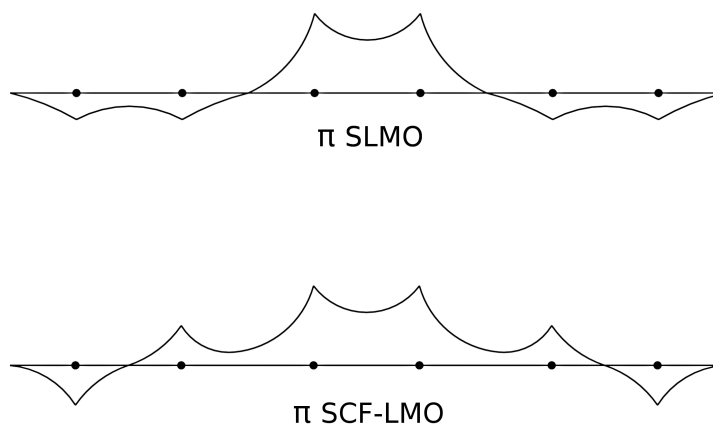


Figure 4.8: Qualitative representation of the orbital tails for SLMOs and SCF-LMOs for the hexatriene molecule.

This difference can be easily understood. Indeed, starting from the Lewis determinant, the orbital optimization may be seen to proceed through the interaction with the singly excited determinants, among which one has the charge transfer (CT) determinants

$$\Phi_{i \rightarrow j^*}^{\text{CT}} = a_j^\dagger a_i \Phi_L \quad i \neq j \quad (4.7)$$

The configuration mixing between Φ_L and $\Phi_{i \rightarrow j^*}^{\text{CT}}$, considered at first order in a perturbation scheme, may be expressed as an orbital mixing

$$\varphi'_i = \varphi_i + \frac{\langle \varphi_{j^*} | F_L | \varphi_i \rangle}{-\Delta E_{i \rightarrow j^*}} \varphi_{j^*} \quad (4.8)$$

The denominator is negative (minus an excitation energy) and the numerator is negative if the i and j bonds are connected by the b_i and a_j OAOs. Indeed, the φ_{j^*} MO has in this case a positive coefficient on a_j , therefore

$$\langle \varphi_{j^*} | F_L | \varphi_i \rangle \approx \frac{\langle b_i | F_L | a_j \rangle}{2} < 0 \quad (4.9)$$

and the coefficient of φ_{j^*} in Equation 4.8 is positive. For this reason in the φ'_i orbital the coefficients of the b_i and a_j OAOs have the same sign. When the i and j bonds are connected by the a_i and b_j OAOs, the numerator is positive given that b_j has a negative sign in φ_{j^*} and therefore

$$\langle \varphi_{j^*} | F_L | \varphi_i \rangle \approx -\frac{\langle a_i | F_L | b_j \rangle}{2} > 0 \quad (4.10)$$

In this case, the coefficient of φ_{j^*} in Equation 4.8 is negative and again in the φ'_i orbital the coefficients of the a_i and b_j OAOs have the same sign.

In conclusion, the SCF MO centered on the bond i takes in-phase tails on the atoms of the neighbor bonds and negative tails on the second neighbor atoms. This feature appears clearly in Figures 4.6 and 4.7, where one may see the difference between the SLMOs and the SCF LMOs, the second ones incorporating inter-bond delocalization effects, while in the first set the tails are required only for the orthogonality constraint.

4.4 SHORT-RANGE CHARACTER OF DELOCALIZATION AND CORRELATION ENERGIES

Let us start from a given zero-order function Φ_0 , which may be either the strongly localized function Φ_L of energy E_{SL} , or the Hartree-Fock single determinant Φ_{SCF} of energy E_{SCF} . Knowing the exact wave function in a given basis, it is always possible, by using the intermediate normalization, to write the energy improvement with respect to this zero-order energy as a sum of contributions from the single and double excitations. In particular for the CASSCF wave function one has:

$$\begin{aligned} E_{CASSCF} - E_{SL} &= E_{singles} + E_{doubles} \\ &= \sum_{ij^*} \left\langle \Phi_L | H | a_{j^*}^\dagger a_i \Phi_L \right\rangle \frac{c_{ij^*}}{c_L} + \sum_{ikj^*l^*} \left\langle \Phi_L | H | a_{l^*}^\dagger a_{j^*}^\dagger a_i a_k \Phi_L \right\rangle \frac{c_{ikj^*l^*}}{c_L} \end{aligned} \quad (4.11)$$

where the coefficients are those of the corresponding determinants in the CASSCF function. The first sum can be seen as the delocalization energy, the second one as the correlation energy, although the term "correlation energy" usually refers to the energy beyond the single determinant approximation.

A similar expression can be written also for the HF wave function, but Φ_L and Φ_{SCF} are built on different MO sets and this complicates the comparison between these two wave functions. In order to simplify the analysis, we consider here an approximation to Φ_{SCF} obtained by a constrained SCF procedure in which only the rotations within the CASSCF active MOs are allowed, obtaining a wave function Φ'_{SCF} and an energy E'_{SCF} which closely approximates the exact SCF wave function and energy ($E'_{SCF} - E_{SCF} = 0.08$ eV for the hexatriene molecule). The simplification brought by this approach is that the constrained SCF step produces a set of MOs for which a CI in the CAS space exactly gives the CASSCF energy E_{CASSCF} .

When starting from the SCF single determinant Φ'_{SCF} , the first sum vanishes, due to the Brillouin's theorem, (2, 34)

$$\begin{aligned} E_{\text{CASSCF}} - E'_{\text{SCF}} &= E'_{\text{doubles}} \\ &= \sum_{ikj^*l^*} \left\langle \Phi_L | H | a_{l^*}^\dagger a_{j^*}^\dagger a_i a_k \Phi_L \right\rangle \frac{c'_{ikj^*l^*}}{c'_{\text{SCF}}} \end{aligned} \quad (4.12)$$

As a first consideration, it is interesting to compare the effect of the single excitations starting from the Lewis determinant to the energy difference between E'_{SCF} and E_{SL} . The values for these two quantities are reported in Table 4.2 for the polyenes here considered (first and second entries) and the comparison confirms that they are very close to each other, indicating the validity of the interpretative model here proposed. Indeed, for all systems one has that E_{singles} is around 90% of $E'_{\text{SCF}} - E_{\text{SL}}$ (third entry in Table 4.2), therefore, as a first approximation, one can write:

$$E'_{\text{SCF}} - E_{\text{SL}} \approx E_{\text{singles}} = \sum_{ij^*} \left\langle \Phi_L | H | a_{j^*}^\dagger a_i \Phi_L \right\rangle \frac{c_{ij^*}}{c_L} \quad (4.13)$$

It is worth of interest to evaluate the spatial extent of the delocalization. To this aim, one can compute the part of the delocalization energy (right term of Equation 4.13) coming from the CT excitations between adjacent bonds

$$E_{\text{deloc}}^{\text{short-range}} \approx E_{\text{CT}} = \sum_{\langle ij^* \rangle} \left\langle \Phi_L | H | a_{j^*}^\dagger a_i \Phi_L \right\rangle \frac{c_{ij^*}}{c_L} \quad (4.14)$$

where the sum runs on adjacent bonds only. Table 4.2 reports the percentage of E_{singles} described by E_{CT} (fourth entry). From these results one clearly see that the delocalization effect in the GS is brought almost entirely by the CT between adjacent bonds, thus debunking the myth that the GS of these systems (and of all conjugated systems) is intrinsically delocalized.

Obviously, equality 4.13 is no longer strictly valid for the exact SCF energy E_{SCF} , but the difference with E'_{SCF} is small and this analysis describes the main effects involved in the passage from Φ_L to Φ_{SCF} .

Similarly, one may study the local character of the correlation energy. It is clear that the largest contributions come from the intra-bond double excitations $a_{i^*}^\dagger a_{i^*}^\dagger a_i a_i$. The percentage of the total correlation energy due to all double excitations (E_{doubles} , fifth entry in Table 4.2) brought by the intra-bond double excitations (E_{IC} , where IC stands for "Internal Correlation") is also reported in Table 4.2, for both Φ_L and Φ_{SCF} (sixth and seventh entries, indicated with % $[E_{\text{IC}}/E_{\text{doubles}}]$ and % $[E_{\text{IC}}^{\text{SCF}}/E_{\text{doubles}}^{\text{SCF}}]$, respectively). Also in this case, one promptly notes that when Φ_L is used as expanding function (sixth entry in Table 4.2), the intra-bond double excitations collect almost all the correlation energy, confirming that the correlation effects are strongly local

Table 4.2: Analysis of the different contributions to the energy of the butadiene (But), hexatriene (Hex), octatetraene (Oct), and decapentaene (Dec) polyenes. See text for the meaning of the different contributions.

	But	Hex	Oct	Dec
$E'_{SCF} - E_{SL}$ (eV)	-1.03	-2.05	-3.07	-4.09
$E_{singles}$ (eV)	-0.91	-1.84	-2.76	-3.69
% [$E_{singles} / (E'_{SCF} - E_{SL})$]	88.62	89.72	90.08	90.25
% [$E_{CT} / E_{singles}$]	99.17	98.64	98.53	98.50
$E_{doubles}$ (eV)	-1.60	-2.41	-3.23	-4.04
% [$E_{IC} / E_{doubles}$]	99.74	99.55	99.43	99.35
% [$E_{IC}^{SCF} / E_{doubles}^{SCF}$]	94.62	92.11	90.65	89.71
% [$E_{IC+ijexc}^{SCF} / E_{doubles}^{SCF}$]	99.41	98.21	97.38	96.82

in this MO basis. With the SCF-LMOs (seventh entry in Table 4.2) this analysis is less clear: indeed the fact that they account for the delocalization effects makes the SCF-LMOs less localized on a given bond. For this reason the intra-bond double excitations do not account for all the correlation energy and the error becomes larger if the number of double bonds increases. It is important to stress that the form of the SCF-LMOs is not affected by the number of double bonds (they keep a local nature, given that they just account for the delocalization between close bonds): what is observed here just indicates that the intra-bond double excitations are not able to account for all the correlation energy (which is due to all double excitations), that, therefore, other double excitations are relevant (*vide infra*), and that this effect increases with the dimension of the system.

The other categories of double excitation with a relevant role are two-bond excitations of the type $a_{j*}^\dagger a_{i*}^\dagger a_i a_{\bar{i}}$ or $a_{i*}^\dagger a_{i*}^\dagger a_j a_{\bar{i}}$ where i and j are adjacent bonds and which describe the coupling of a single excitation within a bond (i) and a CT between i and j , and the double excitations of dispersive character $a_{j*}^\dagger a_{i*}^\dagger a_i a_{\bar{j}}$, again between adjacent bonds in which two single excitations, each one within a given bond, are performed at the same time.

The role of this kind of excitations is more important for the SCF-LMOs; indeed, as one can see from the eighth entry in Table 4.2, indicated with % [$E_{IC+ijexc}^{SCF} / E_{doubles}^{SCF}$], almost all the correlation energy is recovered when they are considered together with the intra-bond double excitations (IC). For the SLMOs, instead, their effect is almost negligible, since more than 99 % of the effect of the double excitations is concentrated in the intra-bond IC contribution.

All these results show that both the delocalization and correlation effects are of short range character, despite the fact that the π electron system of a conjugated molecule is usually considered as a typical delocalized system. From now onward, when considering the SCF solution, the exact SCF LMOs are used.

4.5 REDUCED CI MODEL SPACES

This extreme concentration of the contributions contrasts dramatically with the dispersion of the contributions to the correlation energy when working with canonical MOs. This effect is evident from Figure 4.9, which reports, for both the delocalized and localized orbitals, how the energy converges towards the CASSCF energy (chosen in figure as the zero of the energy) by considering in Equation 4.11 more and more determinants (starting from those with the largest contributions and then including the others in a descending order). The value reported in the ordinate axis can be seen as the absolute value of the correlation energy within the CAS space. The absolute value of the total correlation energy, calculated with respect to the reference determinant (Φ_L or Φ_{SCF}), is smaller when one uses the DMOs set (E_{SCF} is lower than E_{SL}), but the CASSCF energy is approached faster when using SLMOs, due to the large contribution of few, but meaningful, excitations.

It has been demonstrated (59) that with these MOs n^4 double excitations contribute by corrections proportional to n^{-4} (their interaction with the HF determinant scales as n^{-2}), thus to a constant value, while n^3 double excitations contribute by corrections scaling as n^{-2} (their interaction with the HF determinant scales as n^{-1}), thus to a n -scaling correlation energy, as expected. For this reason, reasonable strategies for the calculation of the ground state correlation energy always rely on the use of localized MOs, both for the occupied and for the virtual MOs. The concentration of the contributions observed with the localized MOs suggests that one might use a very limited model space, considering for the systems here studied, besides the Lewis structure, only CT singly excited configurations between adjacent MOs and intra-bond double excitations. The size of this model scales as n only.

The interactions between Φ_L and the intrabond doubly excited determinant (IC) and between Φ_L and the adjacent charge transfer singly excited determinants (CT) are reported in Table 4.3, as well as the excitation energies from Φ_L to these determinants. The interactions show a weak dependence on the position of the bonds, external or internal. Moreover, they are extremely transferable from one polyene to another, since the differences are lower than 0.01 eV. This marked transferability shows that our strongly localized MOs are extremely local.

Table 4.3: Energies of the CT and IC determinants (with respect to the energy of Φ_L) and their interactions with Φ_L . The data are obtained from the CASSCF Hamiltonian matrix built using SLMOs. The data in round brackets are obtained using the second order Intermediate Hamiltonian, those in square brackets are obtained using its diagonal version (which does not affect the interactions). The labels “e”, “qe” and “i” indicate the position of the double bond in the conjugated chain: external, quasi-external and internal, respectively. See text for details.

	Interaction (eV)	Energy (eV)
Butadiene		
L		0.00 (-0.04) [-0.03]
IC	3.73 (3.69)	16.45 (15.38) [14.96]
CT	1.63 (1.64)	10.89 (9.42) [9.25]
Hexatriene		
L		0.00 (-0.07) [-0.07]
IC (e)	3.72 (3.68)	16.43 (14.55) [13.14]
IC (i)	3.80 (3.75)	16.82 (14.75) [13.74]
CT (e→i)	1.58 (1.56)	11.21 (8.46) [7.40]
CT (i→e)	1.64 (1.71)	10.79 (8.31) [7.00]
Octatetraene		
L		0.00 (-0.09) [-0.11]
IC (e)	3.72 (3.68)	16.42 (13.73) [11.34]
IC (i)	3.80 (3.75)	16.82 (13.93) [11.91]
CT (e→i)	1.58 (1.55)	11.20 (7.49) [5.69]
CT (i→i)	1.60 (1.63)	11.12 (7.35) [5.19]
CT (i→e)	1.64 (1.72)	10.78 (7.26) [5.10]
Decapentaene		
L		0.00 (-0.12) [-0.14]
IC (e)	3.72 (3.68)	16.42 (12.91) [9.54]
IC (qe)	3.80 (3.75)	16.80 (13.12) [10.10]
IC (i)	3.80 (3.75)	16.79 (13.11) [10.08]
CT (e→qe)	1.58 (1.55)	11.20 (6.51) [3.91]
CT (qe→i)	1.60 (1.63)	11.11 (6.39) [3.49]
CT (i→qe)	1.60 (1.64)	11.11 (6.32) [3.30]
CT (qe→e)	1.64 (1.72)	10.78 (6.24) [3.28]

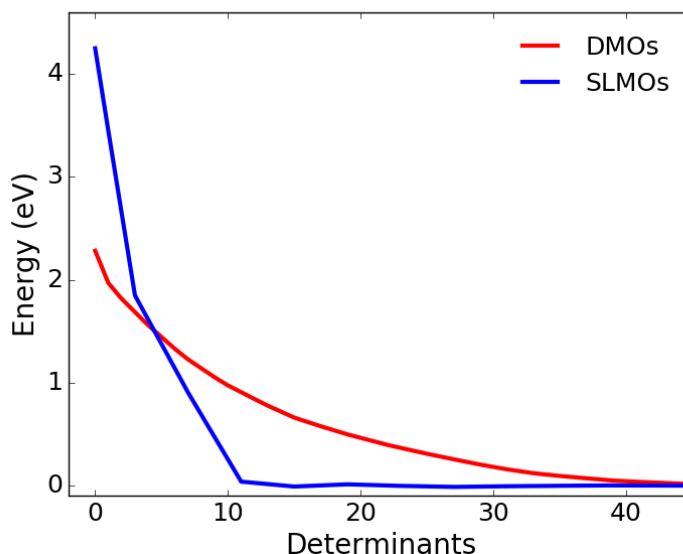


Figure 4.9: Cumulative sum of the contributions to the absolute value of the correlation energy brought by the determinants. The determinants are in a descending order with respect to the value of their contribution. Comparison between delocalized molecular orbitals (DMOs) and strongly localized molecular orbitals (SLMOs). The CASSCF energy is set to zero while the starting point for the two curves is the energy of the lowest determinant (2.28 eV for DMOs and 4.25 eV for SLMOs).

The diagonalization of the CI matrix in this extremely reduced model space does not produce correct energies, as it is apparent from Table 4.4, where the SCF energy is reported together with the energy of the Lewis structure (OVB L, second entry) and the CI energies from the model space containing the Lewis structure plus the CT and IC determinants (OVB L+IC+CT, third entry). By comparing the OVB L+IC+CT energies with the CASSCF energies (also reported in Table 4.4), one notes that the difference increases with the dimension of the system, with the error reaching 0.08 a.u for decapentaene. Two main sources of error affect this result: first of all, different single and double excitations are excluded from our model space, such as, for instance, long range CT and dispersion excitations (two single $\pi \rightarrow \pi^*$ excitations on two different bonds). In principle they give a small contribution, but their number increases with the dimension of the system. The second error is due to the size inconsistency of the approach, that is, the lack of the determinants obtained by the repetition of the excitations considered in the model space on a given determinant of the model space (60). To solve this problem one can be tempted to consider the other singly and doubly excited determinants, but the main contributions are brought essentially by the multiple excitations, since, for instance, an intrabond double excitation

Table 4.4: Energies (in a.u.) for the four polyenes computed at different levels (see text for details) and energy differences (eV) between the OVB-Hint2 L+IC+CT and CASSCF approaches.

	Butadiene	Hexatriene	Octatetraene	Decapentaene
a)SCF	-154.969448	-231.879932	-308.790519	-385.701136
b)OVB L	-154.931624	-231.804746	-308.677826	-385.550904
c)OVB L+IC+CT	-155.015264	-231.933662	-308.847124	-385.757037
d)OVB-Hint2 L	-155.031036	-231.970545	-308.909752	-385.848903
f)OVB-Hint2 L+IC+CT	-155.023773	-231.960727	-308.897818	-385.835122
g)CASSCF	-155.024078	-231.960954	-308.897909	-385.834889
Δ_{f-g} (eV)	-0.0083	-0.0062	-0.0025	-0.0063

on bond k may be applied to a the intrabond double excitation on bond i . A Coupled Cluster formalism might be applied to treat such a repetition of excitations or one can consider methods to eliminate the unlinked contributions of a truncated configuration interaction, such as for instance the (SC)² method (61) but here we simply use a perturbative intermediate effective Hamiltonian formalism (47) (discussed in Section 2.8.1) namely the so-called Shifted Bk technique (62–64). Labelling the model space determinants with $|I\rangle, |J\rangle$, one builds a dressed CI matrix in the model space, the matrix elements of which incorporate the 2nd order effect of the outer-space determinants $|\alpha\rangle$ (those not belonging to the model space),

$$\langle I | H_{\text{int}}^{(2)} | J \rangle = \langle I | H | J \rangle + \sum_{\alpha} \frac{\langle I | H | \alpha \rangle \langle \alpha | H | J \rangle}{E_{\text{SL}} - \langle \alpha | H | \alpha \rangle} \quad (4.15)$$

In our application of this approach, the determinants $|\alpha\rangle$ belong to the CAS-CI space. This method is not strictly size-consistent but, as one can observe in Table 4.4, the diagonalization of this dressed CI matrix provides energies (indicated with OVB-Hint2 L+IC+CT) which deviate from the CASSCF energy by less than 0.01 a.u.. These energies are obtained at a very low cost. The main impact of the dressing can be examined by looking at the results in round brackets in Table 4.3. The amplitude of the modification of the diagonal matrix elements necessarily increases with the size of the molecule since one may repeat more and more processes on top of a local single or double excitation. Asymptotically, the diagonal dressed values may become lower than the energy of the reference determinant, but this is a well-known feature of the dressed CI matrices (see for instance the (SC)² CI technique (65) and all more approximate CEPA methods). The dressing of the diagonal terms may be guessed from linear

extrapolation. Indeed, the number of IC and CT excitations which remain possible on each one of the determinants of the truncated model space increases linearly with the size of the system. Each one of the possible excitations brings a specific energy contribution, a finite increment lowering the diagonal energy of the considered IC or CT determinant. On the contrary, the dressed off-diagonal matrix elements are only marginally modified at second order and they remain extremely transferable.

With the aim to build a model Hamiltonian through extrapolation, that is, looking for an analytic expression of the dressed Hamiltonian matrix elements as a function of the number n of double bonds in the system, however, it is convenient to use a variant of the intermediate Hamiltonian technique, in which the dressing affects only the diagonal elements of the Hamiltonian matrix, leaving the off-diagonal ones as in the bare matrix (66). This “diagonal” dressing is simply:

$$\Delta'_{II} = \Delta_{II} + \sum_{J \neq I} \Delta_{IJ} \frac{c_J}{c_I} \quad (4.16)$$

where Δ_{IJ} represents the second order correction to the generic matrix element $\langle I | H | J \rangle$ (the second term in the right-hand side of Equation 4.15). As one may see from the Equation 4.16, the diagonal shift depends on the coefficients of the state under consideration, making this kind of dressing more state-specific than the general one. Indeed, the dressing reported in Equation 4.15 is also state specific because one has to identify a reference function, here Φ_L , which represent a good qualitative description of the GS and whose energy plays a key role in the dressing. The results obtained from the approach of Equation 4.16 are reported in square brackets in Table 4.3.

The linear extrapolation of these data (considering only the octatetraene and decapentaene in order to reduce the end effects) as a function of n , combined with the linearity of the energy of the Lewis determinant, makes it possible to build a model Hamiltonian (the dimension of which scales linearly) able to predict the energy and the wave function of a polyene with an arbitrary number n of double bonds. The energies obtained following this strategy for the polyenes with six and seven double bonds (twelve and fourteen carbon atoms, respectively) are reported in Table 4.5, together with their CASSCF energy. As one may see from the small values of the errors, the model Hamiltonian is able to well represent the actual systems.

This model Hamiltonian has been used to analyze how the wave function changes when one increases the length of the conjugated chain. Figure 4.10 reports the dependence on the number of double bonds of the weights of the Lewis, CT and IC structures in the wave function computed from the diagonalization of the extrapolated model Hamiltonian. One may notice that the weight of the Lewis determinant is very large for short chains but it rapidly decreases and

Table 4.5: Total energy (a.u.) for the two polyenes with twelve and fourteen carbon atoms computed at the CASSCF level and using the model Hamiltonian whose elements are obtained by extrapolation of the values computed for shorter polyenes. The energy difference (eV) is also reported for the sake of clarity.

Molecule	CASSCF (a.u.)	H model (a.u.)	Error (eV)
12 C	-462.771872	-462.774975	0.08
14 C	-539.708852	-539.712629	0.10

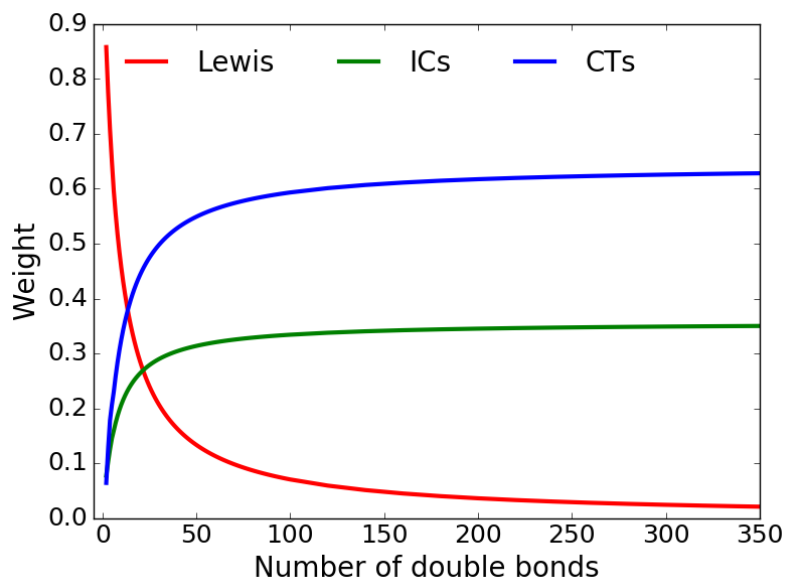


Figure 4.10: Total weights of the Lewis, CT and IC structures in the wave function of the polyenes as a function of the number n of the double bonds. Values computed from the wave function obtained from the diagonalization of the extrapolated model Hamiltonian matrix (see text for details).

goes to zero for long chains. For $n < 12$ it represents the largest component of the wave function, while for larger values of n this role is played by the CT structures.

The fact that the weight of the Lewis determinant tends to zero when the size of the system increases is not symptom of a long range-delocalization. It is simply the effect of the normalization of the wave function, the number of IC and CT increasing linearly with the size of the chain. A similar phenomenon takes place in a model problem of N non-interacting H_2 molecules, the weight of the HF single determinant decreases (in absence of any inter-molecular delocalization).

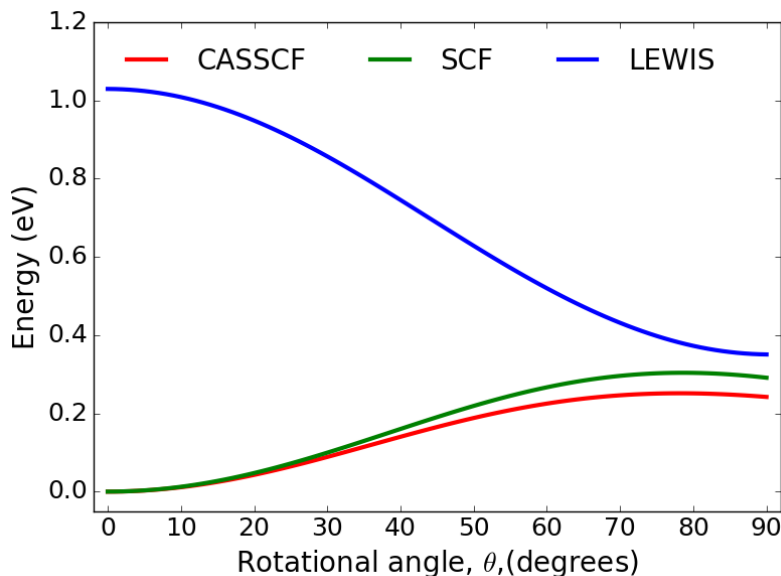


Figure 4.11: Energy of the CASSCF (red), SCF (green) and Lewis (blue) wave function for the butadiene molecule as a function of the rotation angle (rigid rotation of the two ethylene units) around the single C-C bond. The CASSCF energy are reported using the value at the planar geometry (vanishing rotational angle) as zero, the energies of the SCF and Lewis wave functions are reported using the SCF energy at the planar geometry as zero.

4.6 ROTATION AROUND A SINGLE BOND: THE BUTADIENE CASE

The planar geometry of the linear polyenes is often related to the intrinsically delocalized nature of their ground state, a nature which would be strongly modified if planarity is removed, for instance by a rotation around a double bond.

One can wonder how this interpretation can match the consideration reported in the previous section concerning the rather local character of the ground state when it is analyzed in terms of the SLMOs.

In order to clarify this point, the rotation around the single C-C bond in butadiene has been considered (the two ethylene units are rotated rigidly), computing the energy of the CASSCF, SCF and Lewis (Φ_L with SLMOs) wave functions as a function of the rotation angle. These energies are reported in Figure 4.11

One promptly notes that the CASSCF and SCF curves are almost parallel. This indicates that the main effects controlling the dependence of the energy on the rotational angle θ are already present at the SCF level. On the contrary, the E_{SL} curve shows a qualitatively different behavior, with a decreasing of the energy when θ increases, revealing that for the Lewis structure the optimal geometry is for $\theta \simeq 90$ degrees.

The origin of this difference has to be found in the role of the CT structures. Indeed, as reported in the previous section, the energy difference between E_{SL} and E_{SCF} ($\simeq 1$ eV) is due to the CT structures, which evidently have a larger impact at $\theta = 0$ than at $\theta = 90$ degrees.

The energy of the CT structures (all equivalent in this molecule), together with their interactions with the Lewis structure as a function of θ is reported in Table 4.6. From this table it is apparent that the energy of the CT structures is lowered when θ increases (the value in Table 4.6 are reported with respect to E_{SL}) and the interaction, large for $\theta = 0$, rapidly goes to zero when θ approaches 90 degrees. For this reason E_{SL} and E_{SCF} are almost degenerate at $\theta = 90$ and the SLMOs are almost identical to the SCF LMOs (both the delocalization tails and the orthogonalization tails become negligible).

Table 4.6: Energy of the CT structures and their interactions with the Lewis structure as a function of θ . The energy is computed considering as zero the energy of the Lewis structure, E_{SL} , at the same value of θ . Angles in degrees, energies and interactions in eV.

θ	0	10	20	30	40
Energy	10.8878	10.8741	10.8336	10.7700	10.6910
Interaction	1.6272	1.5979	1.5112	1.3713	1.1855
θ	50	60	70	80	90
Energy	10.6075	10.5313	10.4703	10.4281	10.4043
Interaction	0.9635	0.7160	0.4529	0.1822	0.0893

As a conclusion, one can state that a system of independent ethylene units would have a non planar geometry and that the presence of the delocalization brought by the CT structures, even if limited to the neighbour double bonds, is the responsible for the planar structure of the polyenes.

It is worth noticing that this analysis cannot be performed with the SCF LMOs. Indeed, they leave unchanged the SCF wave function, and therefore the energy of the Lewis-like structures built with these LMOs has the same behavior as the CASSCF energy. This good behavior is due to a marked modification of the nature of the SCF LMOs, which include delocalization tails at $\theta = 0$ while they are strongly localized on the double bonds for $\theta = 90$.

4.7 BOND ALTERNATION DEPENDENCE OF THE GROUND STATE ENERGY

It seems important to see whether our approximate treatments are able to reproduce the dependence of the ground state energy on the bond alternation. The dependence of the equilibrium ground state

energy of conjugated systems on the level of considered theoretical model has been the subject of many studies (67–74) and has a relevance also for the correct estimation of the excitation energy in molecules of biological interest (75). This problem is here considered in details for the decapentaene molecule. For modelization purposes, end-effects have not been taken into account and all double bonds are considered to change equally. The dependence on the BLA coordinate δ_{BLA} of the CASSCF energy is reported in Figure 4.12, from which one can see that the energy minimum is obtained for $\delta_{BLA} = 0.05 \text{ \AA}$ (that is, for a double bond length of 1.35 \AA). Figure 4.12 reports also the dependence on δ_{BLA} of the energy computed at other levels. In particular, one can observe that the bond alternation is grossly overestimated at the SCF level where the minimum is at $\delta_{BLA} = 0.07$ (1.33 \AA and 1.47 \AA for the double and single bond lengths, respectively).

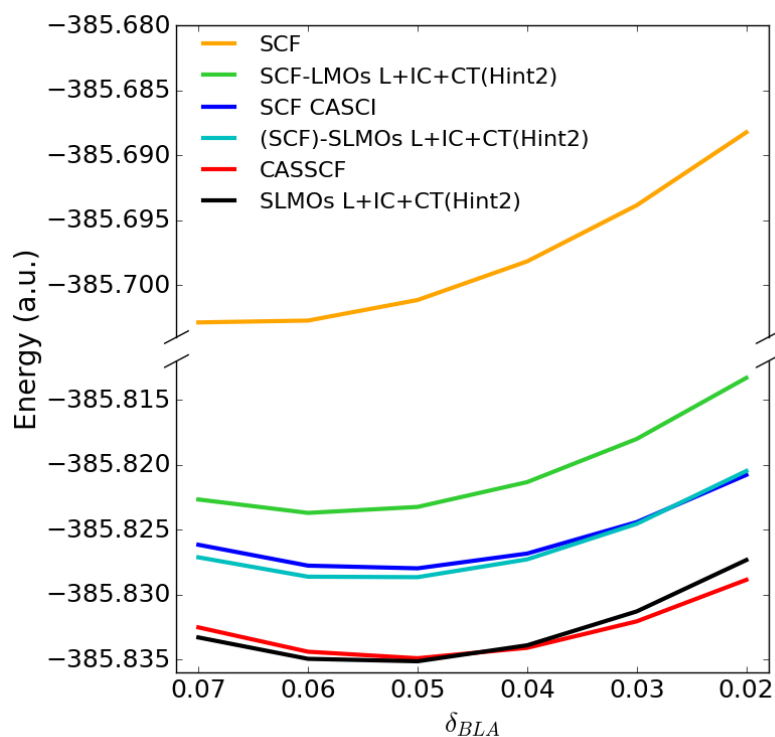


Figure 4.12: Decapentaene: dependence of the energy computed at different levels on the BLA coordinate (δ_{BLA} , see text for details).

As expected, using the SLMOs Hint(2) in the reduced model space gives a PES extremely close to the CASSCF one. It is interesting to notice that with the (SCF)-SLMOs, the energy is higher than the CASSCF value by $\simeq 0.006$ (a.u.) but the dependence on the bond alternation is correctly described. Also in this case, as expected, using these MOs the diagonalization of the dressed intermediate Hamiltonian gives an energy very close to the CASCI value. Starting from SCF localized MOs the dressed intermediate model Hamiltonian gives significantly

poorer results and the incorrect dependence of the SCF energy on δ_{BLA} is only partially improved.

Table 4.7: Bare and dressed energies (E, eV), interactions with the Lewis structure (Int, eV) and coefficients (C) of a Charge Transfer determinant in decapentaene (excitation from the internal bond to the quasi-external one): dependence on δ_{BLA} . The model space considered is the L+IC+CT, both bare or dressed with the Hint(2) procedure values are reported.

δ_{BLA}	0.07	0.06	0.05	0.04	0.03	0.02
E bare	11.4885	11.2951	11.1052	10.9185	10.7351	10.5549
E dressed	7.0762	6.6997	6.3178	5.9299	5.5353	5.1333
$\Delta E_{\text{dress-bare}}$	-4.4123	-4.5954	-4.7874	-4.9886	-5.1998	-5.4216
Int bare	1.5426	1.5691	1.5959	1.6230	1.6504	1.6783
Int dressed	1.5840	1.6124	1.6412	1.6703	1.6999	1.7301
$\Delta \text{Int}_{\text{dress-bare}}$	0.0414	0.0433	0.0453	0.0473	0.0495	0.0518
C bare	0.0798	0.0813	0.0827	0.0841	0.0855	0.0869
C dressed	0.1077	0.1106	0.1136	0.1166	0.1197	0.1228
$\Delta C_{\text{dress-bare}}$	0.0279	0.0293	0.0309	0.0325	0.0342	0.0359

The analysis in terms of local MOs here reported offers an interpretation of the change of the optimal geometry when going from the SCF to the CASSCF treatment. The effective excitation energy of the CT determinants (with respect to the energy of the reference Lewis determinant) is reduced by more than 4 eV (Table 4.7). As a consequence the coefficients of the CT components of the wave function are significantly increased by the dressing. Moreover, the effective energy of the CT structures decreases when one reduces the bond alternation. The augmented role of the CT structures in the wave function due to the determinants outside the model space pushes the system toward a geometry where the CTs have a lower energy, that is, toward a decrease of the bond alternation. This effect is responsible for the reduction of the bond alternation by the correlation in the π valence shell. A qualitative Valence Bond interpretation of this effect can be formulated as follows: in a CT component, the electrostatic field is no longer the mean field of the CASSCF electronic distribution, a dipole is created, to which the electrons of the surrounding bonds should react, polarizing toward the instantaneous positively charged bond and away from the negatively charged bond.

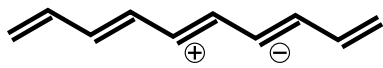
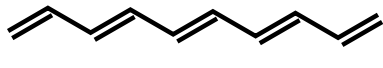
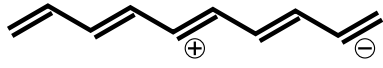
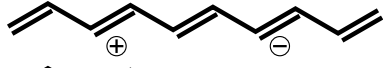
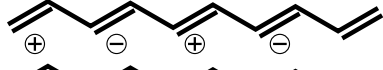
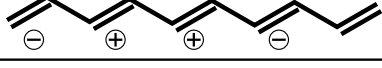
This polarization can be easily explained analyzing how the dressing affects the charge distribution of a charge transfer determinant. In the intermediate effective Hamiltonian formalism the dressed CT may be written, in accordance with Equation 4.15, as:

$$|\text{CT}'\rangle = |\text{CT}\rangle + \sum_{\alpha} c_{\alpha} |\alpha\rangle \quad (4.17)$$

where α indicates the determinants outside of the model space interacting with $|CT\rangle$ and the coefficients c_α are obtained as:

$$c_\alpha = \frac{\langle \alpha | H | CT \rangle}{E_{SL} - \langle \alpha | H | \alpha \rangle} \quad (4.18)$$

Table 4.8: Different charge distributions, and their weights, contributing to a $i \rightarrow qe$ dressed CT wave function ($|CT\rangle'$) in decapentaene with SLMOs.

Charges	Weight	Cumulative Weight
	0.8243	0.8243
	0.1074	0.9317
	0.0268	0.9585
	0.0186	0.9771
	0.0093	0.9865
	0.0071	0.9936

A simple analysis of the $|CT\rangle'$ wave function (once normalized) can be performed by taking advantage of the local nature of the MOs. Indeed, each determinant represents a well defined charge distribution and the square of its coefficient can be considered as the weight of this charge distribution in $|CT\rangle'$. Therefore, the charge on each bond can be estimated as the sum over all determinants in $|CT\rangle'$ of the charge on the bond for the determinant times its weight. The results, for an $i \rightarrow qe$ CT in decapentaene with SLMOs, are reported in Table 4.8. As one can see, after the dressing the weight of the charge distribution corresponding to the “naked” CT ($|CT\rangle$) is reduced to 82%, while other charge distributions have gained importance, such as the one in which all bonds are neutral (11%) and the two corresponding to the hole and particle propagation (2% and 3%, respectively). The resulting effects is that the charges on the two bonds involved in the CT are weakened and the charges are delocalized along the chain.

These effects are highlighted in Figure 4.13, where the net charges on each bond, calculated from the previous weights, are reported. After the dressing, the net charges on the bonds involved in the charge transfer are no longer unitary and a charge delocalization on the neighbouring bonds appears. Moreover, the total charge is vanishing, as expected, but when one sums only the positive (or the negative) charges, the results is not one. This is due to the influence of the neutral charge distribution which reduces the charge separation. It is worth stressing that the neutral charge distribution reported in Table

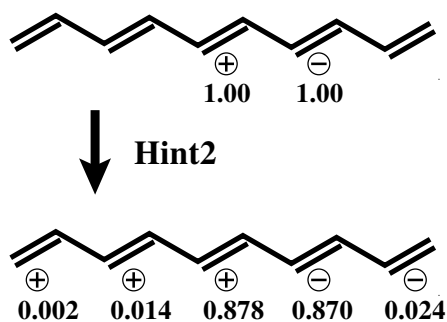


Figure 4.13: Net charges on each bond for a $i \rightarrow qe$ CT in decapentaene with SLMOs, before and after the Hint(2) dressing.

4.8 is not related to the Lewis structure (included in the model space and therefore not considered in the dressing procedure) but rather to other structures presenting two electrons for each double bond.

4.8 CONCLUSIONS

The nature of the ground state of the first terms of the linear all-trans polyene series has been analyzed making use of strongly localized bonding and antibonding π orbitals within the OVB approach. Such an analysis allows to separate the delocalization effect from the correlation effect. Both have been found to be local effects, the delocalization involving a π bonding orbital and the two neighbour π^* antibonding orbitals, while the electronic correlation mainly is due to the intra bond correlation. The rather local character of the delocalization in the ground state of conjugated π systems is in contrast with the accepted view, for which these systems have a strongly delocalized nature.

The reduced number of relevant electronic structures has allowed to define a model space within the space of the CAS determinants, the dimension of which scales linearly with the number of double bonds n , and to build an effective intermediate Hamiltonian spanning this model space. The effective intermediate Hamiltonian has been computed at second order in perturbation theory, following two different strategies: one in which all elements of the matrix are in principle dressed and the other where only the diagonal elements are modified at second order. The last choice has been found to be particularly efficient for the definition of a model Hamiltonian, the element of which can be easily expressed as a linear function of n , thus allowing the estimation of the CASSCF energy for large values of n .

The study reported in this chapter is an example of the effectiveness of the OVB approach and opens the way to the analysis of the wave functions of the excited and ionized states of the conjugated systems, a complex problem with many interesting possible applications, which will be analyzed in the next chapter.

LINEAR CONJUGATED POLYENES: CATIONS AND EXCITED STATES

In the previous chapter, the neutral ground state of the series of linear conjugate polyenes has been analyzed in details, by means of the orthogonal valence bond and intermediate Hamiltonian theories, allowing to get new insights on their electronic structure. Beyond the ground state, the ionized and excited states of these systems are even more interesting, at least from a technological point of view. The cations, for instance, play a central role as model for the rationalization of relevant properties such as superconductivity and organic conductivity; while the excited states are crucial for the study of optical and photochemical properties.

In the following sections, a preliminary study of the cations and excited states of polyenes is reported, following the procedures analyzed before for the ground state.

5.1 CATIONS

For the study of the cations, the first three elements of the linear conjugated polyenes series are taken into account: butadiene, hexatriene and octatetraene. For comparison purposes, the basis sets and geometrical parameters are the same used for the ground state, which are reported in Section 4.2. For the same reason, the orbitals employed for the analysis are the strongly localized molecular orbitals (SLMOs) optimized for the neutral ground state. Therefore, the wave function is obtained through a CASCI procedure which optimizes the CI coefficients in the CAS space without changing the orbitals.

The orthogonal valence bond structures for the cations are obtained with the same procedure used for the ground state. The main difference to be taken into account is the spin multiplicity. Indeed, the ground state for the neutral systems is a singlet while the for the cations it is a doublet.

The most important determinant of the ground state of the neutral molecules, in terms of weight, is the so-called Lewis determinant, whose weight represents a large fraction of the wave function of the first term of the polyenes series, as reported in Table 5.1. For the cations, instead, one cannot identify a unique determinant such as the Lewis one, because the ionization process may be virtually localized on any of the bonding π orbitals. Therefore, for n double bonds one has n almost degenerate determinants representing the situation in which one electron has been “extracted” from that specific bond. In

Table 5.1: Weights of the dominant structures in the ground state and in the lowest state of cations.

	weight Lewis (neutral)	weight LI (cation)	n. LI
Butadiene	0.91026	0.83778	2
Hexatriene	0.86705	0.69989	3
Octatetraene	0.82578	0.58391	4
Decapentaene	0.78645	0.48841	5

the following, these structures are referred to as local ions (LI). As one may see from Table 5.1, the total weight of these structures is dominant in the wave function, even if their importance is lower than the Lewis for the ground state.

The local ions may interact with each other in different ways, generating n states whose energy is quite similar. As stated below, these states can be well represented together within the intermediate Hamiltonian scheme. One may think about them as “particular” states sharing a similar nature. It is therefore interesting to consider all these states in the following analysis.

The most important determinants to be considered in addition to the local ions are the charge transfer (CT) and the internal correlation (IC) ones, in accordance to the ground state case (see Figures 5.1 and 5.2 for a representation of these excitations for the neutral ground state). It must be taken into account, however, that in the cations these excitations depends on the position of the positive charge and therefore one obtains several kinds of CTs and ICs.

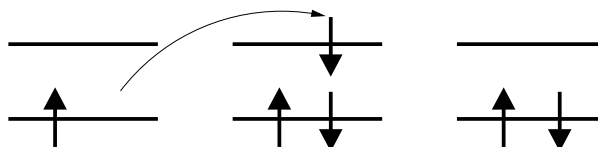


Figure 5.1: Charge transfer (CT) excitation in hexatriene neutral ground state.

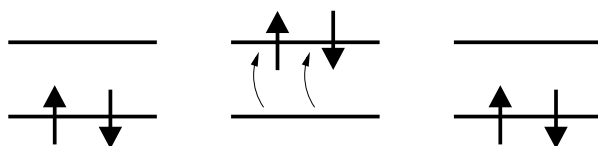


Figure 5.2: Internal correlation (IC) excitation in hexatriene neutral ground state.

Let us consider the hexatriene molecule. One has three double bonds and three bonding π SLMOs, therefore the positive charge may

be localized in three different positions, two of them being equivalent (the terminal ones). The determinant with the charge on the internal bond is more stabilized than the others and it has a lower energy and a larger weight in the ground state's wave function.

When the ionized charge is on a terminal bond, there are four different possible charge transfer processes. The first one is reported in Figure 5.3 and it is referred to as charge transfer triple charge (CTTC). The alternation of the charges makes this determinant very stable, for instance, when compared to the one reported in Figure 5.4. The latter is always a CTTC, but it presents two positive charges on adjacent bonds which destabilize the structure. Therefore, only the first CTTC plays an important role in the wave function and has to be included in the model space for the application of the intermediate Hamiltonian technique.

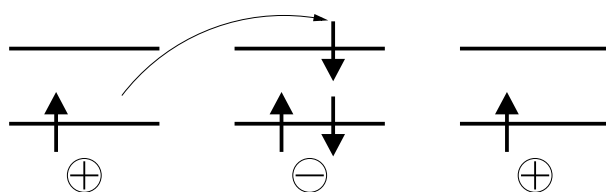


Figure 5.3: Charge transfer triple charge (CTTC) excitation in hexatriene.

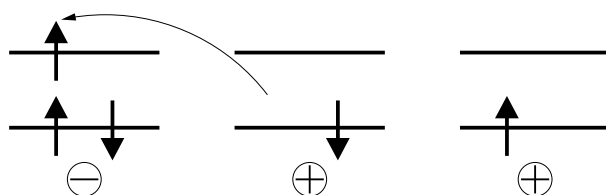


Figure 5.4: Non-alternated charge transfer triple charge (CTTC) excitation in hexatriene.

Another determinant to be included in the model space is reported in Figure 5.5. This kind of charge transfer results in a stabilizing shift of the charge towards the center of the molecule. Conversely, the charge transfer in the opposite direction results in the very unstable structure shown in Figure 5.6.

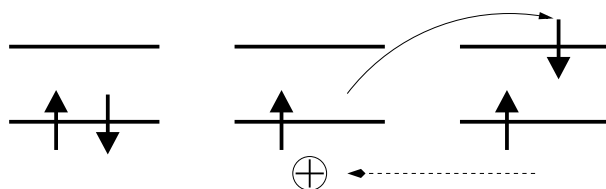


Figure 5.5: Charge transfer single charge (CTSC) excitation in hexatriene.

Starting from the local ions with the positive charge localized on the central bond, instead, there are only two possible charge transfer processes, among which only one plays an important role in the wave

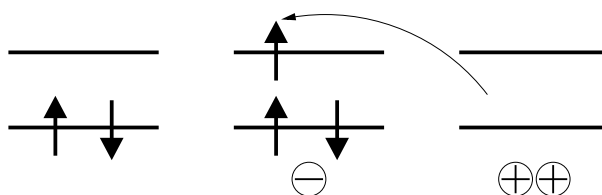


Figure 5.6: Unstable charge transfer excitation in hexatriene.

function and has to be included in the model space. This is reported in Figure 5.7 and consists in a charge transfer single charge analogue to the one shown in Figure 5.5. The other one is represented in Figure 5.8 and it is clearly unstable due to the value and position of its charges.

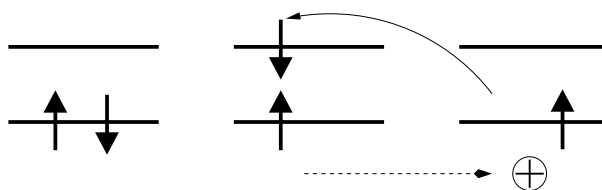


Figure 5.7: Charge transfer single charge (CTSC) excitation in hexatriene.

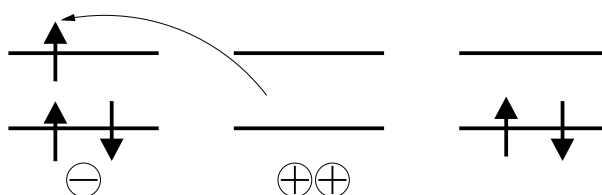


Figure 5.8: Unstable charge transfer excitation in hexatriene.

As one may see from the first entries of Tables 5.2, 5.3 and 5.4 (OVB LI and OVB LI+CT), considering the relevant charge transfer determinants discussed above (here indicated as CT for simplicity) in addition to the local ions greatly improves the description of all the n states considered. This results may be further improved considering also the internal correlation (IC) determinants (OVB LI+CT+IC). However, the error with respect to the CASCI energy increases with the length of the chain, as already seen for the neutral ground state (Table 4.4). The proposed solution to this behavior is the application of the second order intermediate Hamiltonian theory. As reported in the tables, the dressing allows to obtain energies value in very good agreement with the CASCI energy for all the states considered. Therefore, the procedures defined for the neutral ground state works well also for the cations with only minor revisions.

It is interesting to see that the results obtained using the model space spanned only by the LI and CT determinants are very good, even without the presence of the internal correlation determinants. Therefore, the cations differ from the neural systems, where the IC are

of fundamental importance for their description. This is not surprising, considering the lower number of possible IC excitations doable on the local ions and the intrinsic delocalized nature of a ionized molecule.

Table 5.2: CI energies of butadiene cation, before and after the Hint2 dressing.

Butadiene	I	II
OVB LI	-154.612847	-154.507513
OVB LI+CT	-154.655818	-154.561514
OVB LI+CT+IC	-154.676176	-154.581325
OVB-Hint2 LI	-154.709296	-154.576473
OVB-Hint2 LI+CT	-154.689733	-154.592542
OVB-Hint2 LI+CT+IC	-154.687981	-154.588368
CAS-CI	-154.685491	-154.588230

Table 5.3: CI energies of hexatriene cation, before and after the Hint2 dressing.

Hexatriene	I	II	III
OVB LI	-231.509934	-231.431948	-231.360056
OVB LI+CT	-231.583723	-231.491791	-231.442849
OVB LI+CT+IC	-231.622080	-231.532799	-231.478511
OVB-Hint2 LI	-231.693624	-231.575371	-231.502643
OVB-Hint2 LI+CT	-231.663000	-231.577346	-231.519799
OVB-Hint2 LI+CT+IC	-231.659795	-231.573550	-231.516893
CAS-CI	-231.655009	-231.573713	-231.519722

5.2 EXCITED STATES

The analysis of the spectroscopic properties of conjugate polyenes is not straightforward, especially for what concerns the shortest terms of the series. Indeed, one has to take into account what follows:

- the first excited states are very close in energy;
- their energetic order is not univocally defined;
- they may present a neutral or covalent nature.

Table 5.4: CI energies of decapentaene cation, before and after the Hintz dressing.

Octatetraene	I	II	III	IV
OVB LI	-308.395098	-308.338269	-308.272920	-308.223291
OVB LI+CT	-308.487170	-308.406015	-308.344441	-308.323076
OVB LI+CT+IC	-308.542945	-308.466674	-308.402937	-308.374882
OVB-Hintz LI	-308.659865	-308.561446	-308.479490	-308.439086
OVB-Hintz LI+CT	-308.622191	-308.546391	-308.483892	-308.452306
OVB-Hintz LI+CT+IC	-308.618157	-308.541894	-308.479609	-308.450610
CAS-CI	-308.611796	-308.543088	-308.490717	-308.457117

The ground state geometry of these molecules belongs to the C_{2h} point group, with four irreducible representations: A_g , A_u , B_g and B_u . The first two excited states are indicated with $2^1A_g^-$ and $1^1B_u^+$, where the labels "+" and "-" refer to the particle-hole pseudo-symmetry. Indeed, numbering the occupied orbitals starting from the HOMO (and descending in energy) and the unoccupied orbitals starting from the LUMO (and increasing in energy), one may see that in an independent particle model the orbital energies are symmetrically disposed ($\epsilon_{i'} = -\epsilon_i$) and the energy of the configuration obtained with the excitation $i \rightarrow j'$ (the HOMO \rightarrow LUMO + 1, for instance) is the same of the one obtained with $j \rightarrow i'$ (the HOMO - 1 \rightarrow LUMO, for instance). These two degenerate configurations may be combined in-phase or out-of-phase, generating the plus (covalent) and minus (neutral) states, respectively. More details concerning the effect of this symmetry on the nature of the excited states and the selection rules can be found in Ref. (76).

The relative energetic order of the first two excited state is not clear, at least for the first terms of the polyenes series. Starting from octatetraene, indeed, the $2^1A_g^-$ is known to be the first excited state, while for shorter polyenes it remains a matter of discussion. In hexatriene, for instance, these two states are virtually degenerate (76).

The $1^1A_g^- \rightarrow 2^1A_g^-$ transition is forbidden both for spatial symmetry and for the particle-hole pseudo-symmetry ($2^1A_g^-$ is the *dark* state), while the transition to $1^1B_u^+$ (the *bright* state) is allowed and it can be observed experimentally with a strong absorption. Given the quasi-degeneracy of the two states, this absorption completely hides the very weak transition to the $2^1A_g^-$ state.

The ionic $1^1B_u^+$ state is of simple theoretical interpretation within the molecular orbitals scheme, being represented mainly by the HOMO \rightarrow LUMO excitation. The covalent $2^1A_g^-$, conversely, is a complex mixing of HOMO - 1 \rightarrow LUMO, HOMO \rightarrow LUMO + 1 and $[HOMO \rightarrow LUMO]^2$ and its nature cannot be easily understood within the MO scheme. Using a local approach, instead, this state can be seen as a sin-

glet obtained from the product of two triplet excitation localized on the two halves of the molecule. This interpretation has been deduced using semi-empirical methods (77, 78) and it will receive an *ab-initio* confirmation, based on orthogonal valence bond, in the following of this chapter.

5.2.1 Computational details

The computational details are the very same used for the study of the neutral ground state (Section 4.2). The orthogonal valence bond analysis is made using the strongly localized molecular orbitals (SLMOs, or simply LMOs), optimized for the neutral ground state.

5.2.2 Orthogonal valence bond structures

As seen in the previous chapter, the ground state is described to a good approximation using just a three types of determinants: the Lewis, the charge transfer (CT) and the internal correlation (IC) structures. However, as shown in Table 5.5 for hexatriene and Table 5.6 for octatetraene, the weight of these determinants is very small in the $2^1A_g^-$ excited state. The wave function for this state has a strong multireference nature and the individuation of a meaningful model space (useful for the interpretation of the electronic structure) is not straightforward.

Table 5.5: Weight of Lewis, CT and IC determinants in the ground state and in the $2^1A_g^-$ state, hexatriene

	weight in GS	weight in $2^1A_g^-$
Lewis	0.730	0.065
IC (e)	0.034	0.001
IC (i)	0.033	0.001
CT (e→i)	0.027	0.014
CT (i→e)	0.030	0.009

Analyzing the wave function of both hexatriene and octatetraene, it results that the most important determinants have four unpaired electrons, two α and two β , occupying four different orbitals: two bonding π orbitals (hereafter indicated with a and b) and the two corresponding π^* (hereafter a^* and b^*). There are several ways to arrange the spin of the four electrons in four orbitals, therefore the number of these determinants is large and their weights are small. Taking into account such a large number of determinants would result in a difficult interpretation of the wave function and of its nature.

Table 5.6: Weight of Lewis, CT and IC determinants in the ground state and in the $2^1A_g^-$ state, octatetraene

	weight in GS	weight in $2^1A_g^-$
Lewis	0.633	0.065
IC (e)	0.029	0.002
IC (i)	0.029	0.001
CT (e→i)	0.024	0.001
CT (i→i)	0.025	0.006
CT (i→e)	0.027	0.000

To overcome this problem, a convenient procedure is to perform a contraction of these determinants into new structures, which allows to concentrate the information contained in a large numbers of determinants in a few but meaningful structures. Basically, this consists in taking into consideration only a small number of structures obtained as linear combination of a larger number of determinants.

The contraction coefficients used in the linear combinations are obtained looking at the spin eigenfunctions of a system composed of four unpaired electron. In order to do this, one has to build the branching diagram shown in Figure 5.9. It indicates that in the case of four unpaired electrons one may obtain a quintet ($S = 2$), three triplets ($S = 1$) and two singlets ($S = 0$). Given that the $2^1A_g^-$ state is a singlet, the contraction coefficients are those coming from the singlet eigenfunctions.

In order to do this, one has to subsequently apply the lowering operator, $S_- = S_-(1) + S_-(2) + S_-(3) + S_-(4)$, to the highest multiplicity state, that is, the $S_z = 2$ component of the quintet, allowing one to obtain its $S_z = 1$ and $S_z = 0$ components.

$$\Phi_{S_z=2}^q = \|aa^*bb^*\| \quad (5.1)$$

$$\begin{aligned} \Phi_{S_z=1}^q &= S_- \Phi_{S_z=2}^q = \\ &= \frac{1}{2} (\| \bar{a}a^*bb^* \| + \| a\bar{a}^*bb^* \| + \| aa^*\bar{b}b^* \| + \| aa^*b\bar{b}^* \|) \end{aligned} \quad (5.2)$$

$$\begin{aligned} \Phi_{S_z=0}^q &= S_- \Phi_{S_z=1}^q = \\ &= \frac{1}{\sqrt{6}} (\| \bar{a}\bar{a}^*bb^* \| + \| \bar{a}a^*\bar{b}b^* \| + \| \bar{a}a^*b\bar{b}^* \| + \\ &\quad + \| a\bar{a}^*\bar{b}b^* \| + \| a\bar{a}^*b\bar{b}^* \| + \| aa^*\bar{b}\bar{b}^* \|) \end{aligned} \quad (5.3)$$

The various components of the quintet describe the coupling of two local triplets on the A and B double bonds.

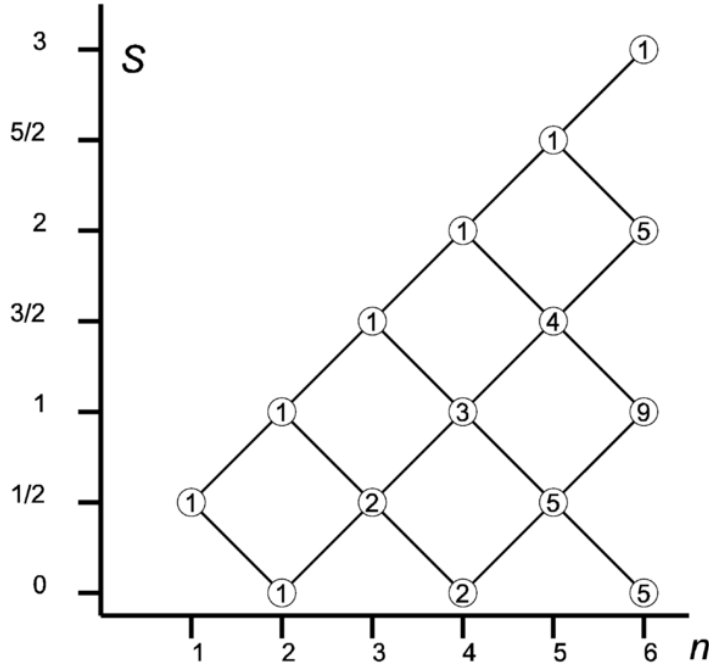


Figure 5.9: Spin branching diagram. n is the number of electrons and S indicates the total spin of the obtained spin eigenfunction.

The $S_z = 1$ components of the triplets are chosen to be orthogonal to the $S_z = 1$ component of the quintet:

$$\Phi_{S_z=1}^{t_1} = \frac{1}{2}(\|\bar{a}a^*bb^*\| + \|a\bar{a}^*bb^*\| - \|aa^*\bar{b}b^*\| - \|aa^*b\bar{b}^*\|) \quad (5.4)$$

$$\Phi_{S_z=1}^{t_2} = \frac{1}{2}(\|\bar{a}a^*bb^*\| - \|a\bar{a}^*bb^*\| + \|aa^*\bar{b}b^*\| - \|aa^*b\bar{b}^*\|) \quad (5.5)$$

$$\Phi_{S_z=1}^{t_3} = \frac{1}{2}(\|\bar{a}a^*bb^*\| - \|a\bar{a}^*bb^*\| - \|aa^*\bar{b}b^*\| + \|aa^*b\bar{b}^*\|) \quad (5.6)$$

One can see that they describe the coupling of a triplet on one of the double bonds with a triplet or singlet on the other bond.

Then, to obtain the $S_z = 0$ of the triplets one applies the lowering operator to the above functions, which leads to:

$$\Phi_{S_z=0}^{t_1} = \frac{1}{\sqrt{2}}(\|\bar{a}a^*bb^*\| - \|aa^*\bar{b}b^*\|) \quad (5.7)$$

$$\Phi_{S_z=0}^{t_2} = \frac{1}{\sqrt{2}}(\|\bar{a}a^*\bar{b}b^*\| - \|a\bar{a}^*b\bar{b}^*\|) \quad (5.8)$$

$$\Phi_{S_z=0}^{t_3} = \frac{1}{\sqrt{2}}(\|\bar{a}a^*b\bar{b}^*\| - \|a\bar{a}^*\bar{b}b^*\|) \quad (5.9)$$

Finally, the two singlets are calculated as functions orthogonal to the $S_z = 0$ components of the quintet and the triplets:

$$\Phi^{s_1} = \frac{1}{2\sqrt{3}}(2\|\bar{a}\bar{a}^*b b^*\| - \|\bar{a}a^*\bar{b}b^*\| - \|\bar{a}a^*b\bar{b}^*\| - \|\bar{a}\bar{a}^*\bar{b}b^*\| - \|\bar{a}\bar{a}^*b\bar{b}^*\| + 2\|a a^*\bar{b}\bar{b}^*\|) \quad (5.10)$$

$$\Phi^{s_2} = \frac{1}{2}(\|\bar{a}\bar{a}^*\bar{b}b^*\| - \|\bar{a}a^*b\bar{b}^*\| + \|\bar{a}\bar{a}^*b\bar{b}^*\| - \|a a^*\bar{b}\bar{b}^*\|) \quad (5.11)$$

Among these two singlets, the first describes a singlet coupling of two local triplets on the two double bonds, while the second singlet comes from the coupling of two singlets on the two double bonds.

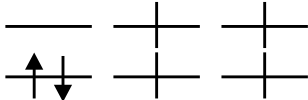
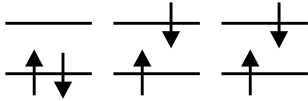
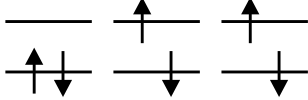
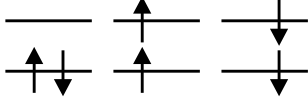
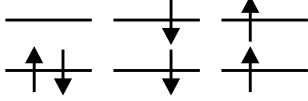
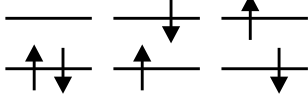
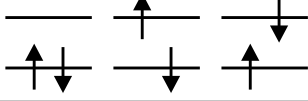
Therefore, the new structures may be obtained contracting the determinants using the coefficients shown in the above equations. By comparison with the full wave function, one may see that for the $2^1A_g^-$ excited state, only the first singlet spin eigenfunction is relevant (Equation 5.10). This is evident from Tables 5.7 and 5.8, which show that the coefficients of the determinants in the wave function (overlooking the phase, which depends on how the determinants are written inside the program package) are almost proportional to the coefficients in Equation 5.10.

The structures here considered, labelled T_2T_3 , describe the excitation $\pi_2 \rightarrow \pi_2^*$ coupled with the excitation $\pi_3 \rightarrow \pi_3^*$. They can be seen as local triplets, localized on each bond, interacting together.

Obviously, there are other similar structures to be considered for the description of the wave function. In Table 5.9, the main contracted structures, in terms of weight, of the hexatriene CASSCF wave function are reported. In addition to the T_2T_3 structure already described (and its symmetry partner T_1T_2), one may see the T_1T_3 structure, which differs from the previous only for the distance between the two excitations (responsible for the slightly smaller weight) and the $T_1T_2T_3$ structure, that is, the coupling between three triplet excitations, one per bond (this structure is the results of the contraction of 20 determinants). Together with the Lewis determinant, these contracted structures cover the 56% of the wave function, a very good result considering the highly multireference nature of the $2^1A_g^-$ excited state.

The case of octatetraene is very similar to hexatriene. Of course, one has to consider more excited structures, included the ones with three and four unpaired electrons. The relative weights of these structures are almost equal to hexatriene, while their total weight sums up to 45%. This has to be compared to the 56% of hexatriene.

Table 5.7: Example of new structure (T_2T_3) obtained from the contraction of several determinants in hexatriene. Both the CASSCF wave function coefficients and the contraction coefficients are reported.

			T_2T_3 structure	Weight = 0.150
Determinant	Wave function c.	Contraction c.		
	0.1093	$1/2\sqrt{3}$		
	0.1093	$1/2\sqrt{3}$		
	-0.2235	$-1/\sqrt{3}$		
	-0.2235	$-1/\sqrt{3}$		
	-0.1138	$-1/2\sqrt{3}$		
	-0.1138	$-1/2\sqrt{3}$		

5.2.3 Truncated CI matrices

As stated in the previous section, a possible solution to the highly multireference nature of the wave function of the $2^1A_g^-$ excited state can be achieved using a contraction scheme. This allows to identify a subset of relevant structures which play an important role in a given electronic state.

For hexatriene and octatetraene, the most important structures are the ones identified as the coupling between local triplets, labelled as T_xT_y , where x and y are indices referring to the bond in which the triplet excitation occurs. Specifically, the leading structure, both for hexatriene and octatetraene, is the T_2T_3 (that, in hexatriene, is equivalent to T_1T_2 for symmetry reasons). It is interesting to analyze how these structures interact with the other structures belonging to the CAS space. Table 5.10 and 5.11 report the most relevant interactions, together with the weight of the interacting structures in the CASSCF wave function.

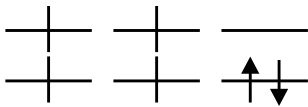
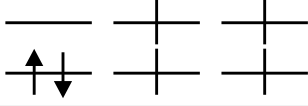
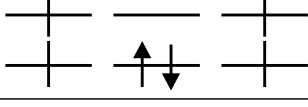
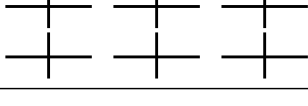
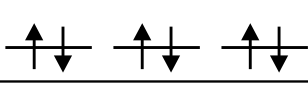
Table 5.8: Example of new structure (T_2T_3) obtained from the contraction of several determinants in octatetraene. Both CASSCF the wave function coefficients and the contraction coefficients are reported.

				T_2T_3 structure	Weight = 0.097
Determinant	Wave function c.			Contraction c.	
	0.0884	$1/2\sqrt{3}$			
	0.0884	$1/2\sqrt{3}$			
	-0.1816	$-1/\sqrt{3}$			
	-0.1816	$-1/\sqrt{3}$			
	-0.0932	$-1/2\sqrt{3}$			
	-0.0932	$-1/2\sqrt{3}$			

In addition to the internal correlation and charge transfer excitations made on top of the T_2T_3 structures, similar to those already seen in the analysis of the ground state, there are other relevant excitations to be taken into account. The $p_{21}T_2T_3$ structures, for instance, represents the propagation of a particle (an electron) from the antibonding orbital π_2^* to the adjacent antibonding π_1^* , while the $h_{21}T_2T_3$ represent the hole propagation from the bonding orbital π_2 to the adjacent π_1 . As reported in the tables, their weight in the wave function is not negligible both for hexatriene and octatetraene and they have a strong interaction with the T_2T_3 structure.

It must be noted that the interactions reported in tables are transferable from hexatriene to octatetraene, and they are similar to the interactions taking place in the ground state (see Table 4.3). Therefore, it would be possible to derive a model Hamiltonian similar to the one developed for the ground state, allowing the study of the larger terms of the linear conjugate polyenes series. However, to achieve this task a much deeper analysis of the $2^1A_g^-$ state is compulsory, including the definition of a comprehensive model space and the application of

Table 5.9: Contracted structures with their weight in the hexatriene wave function.

Representation	Structure	Weight
	T_1T_2	0.150
	T_2T_3	0.150
	T_1T_3	0.131
	$T_1T_2T_3$	0.066
	Lewis	0.065

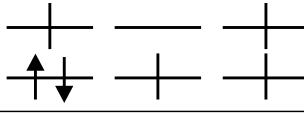
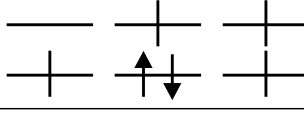
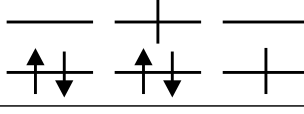
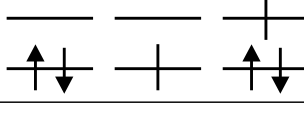
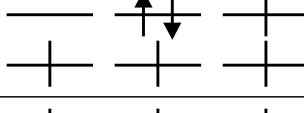
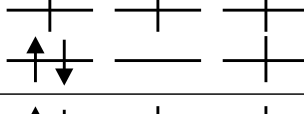
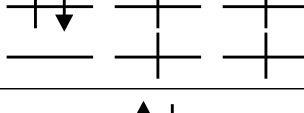
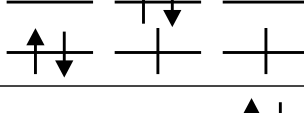
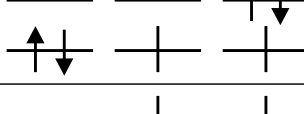
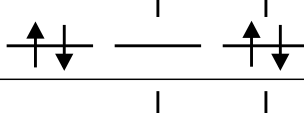
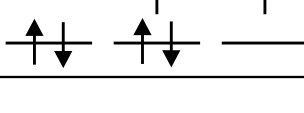
an intermediate Hamiltonian scheme that would present more difficulties compared to the case of the ground state. For this reason, it will be addressed in future works.

For now, the model space here defined contains the relevant structures reported in the above tables and the energies of the truncated CI obtained in this space are reported in Table 5.12. For hexatriene, both the ground state and the $2^1A_g^-$ are well represented using only 41 contracted structures (involving 176 determinants out of 400 defining the CAS space). The error in the excitation energy (the energy difference between the two states) is less than 0.5 eV and it is acceptable in a truncated scheme. For octatetraene, however, the same error increases to more than 2 eV, indicating that a more refined model space is needed to achieve adequate results. It must be stressed, anyway, that in the case of octatetraene these results are obtained using 60 structures involving only 491 determinants out of the 4900 determinants of the CAS space.

5.2.4 Conclusions

Preliminary results on the analysis of the $2^1A_g^-$ state of hexatriene and octatetraene have been reported, highlighting the difference in the electronic structures when compared to the ground state. The highly multireference nature of the wave function does not allow a clear definition of a model space involving few determinants but the use of contracted structures helps to solve this problem. Given the sat-

Table 5.10: Interactions with the T_2T_3 structure and weights in the CASSCF wave function of some relevant structures in hexatriene.

Representation	Structure	Weight	Int. with T_2T_3 (eV)
	$p_{21}T_2T_3$	0.042	1.89
	$h_{21}T_2T_3$	0.041	1.43
	CT_{32}	0.014	2.18
	CT_{23}	0.009	2.11
	$CT_{12}T_2T_3$	0.008	1.55
	$CT_{21}T_2T_3$	0.008	1.60
	$IC_1T_2T_3$	0.009	3.72
	$p_{32}T_2T_3$	0.006	2.31
	$p_{23}T_2T_3$	0.006	2.33
	$h_{32}T_2T_3$	0.004	1.75
	$h_{23}T_2T_3$	0.003	1.77

isfactory description of the wave function using only few structures, it has been demonstrated, using *ab-initio* methods, that the $2^1A_g^-$ state is indeed a singlet obtained from the linear combination of products of two triplet excitations localized on two double bonds of the molecule. Further improvements are needed, especially for what concerns the definition of a comprehensive model space suitable for the applica-

Table 5.11: Interactions with the T_2T_3 structure and weights in the CASSCF wave function of some relevant structures in octatetraene. Given the symmetry of the molecule, only half of the structures is reported.

Representation	Structure	Weight	Int. (eV)
	$p_{21}T_2T_3$	0.021	1.89
	$h_{21}T_2T_3$	0.020	1.43
	CT_{23}	0.006	2.15
	$IC_1T_2T_3$	0.005	3.72
	$p_{23}T_2T_3$	0.003	2.29
	$CT_{21}T_2T_3$	0.004	1.60
	$CT_{12}T_2T_3$	0.004	1.55

Table 5.12: Energies of the truncated CI for hexatriene and octatetraene. The structures here considered are those reported in Tables 5.10 and 5.11, together with other relevant ones.

	GS		$2^1A_g^-$	
	Hexa	Octa	Hexa	Octa
N. determinants	400	4900	400	4900
E_{CASSCF}	-231.960954	-308.897909	-231.724769	-308.689296
N. structures	41	60	41	60
$E_{contracted}$	-231.945874	-308.854582	-231.693452	-308.567601
ΔE (eV)	-0.41	-1.18	-0.85	-3.31

tion of the intermediate Hamiltonian method leading to the possibility of defining a model Hamiltonian able to reproduce the behavior of the excited states of larger polyenes.

Since the discovery of benzene in the nineteenth century, aromatic compounds have been a matter of interest due to their particular properties. Both the theoretical and experimental literature is filled with contributions concerning these compounds. From a quantum chemistry point of view, a complete understanding of the peculiar electronic structure and reactivity of benzene and its derivatives is of paramount importance.

In this chapter, an orthogonal valence bond (OVB) reading of the CASSCF wave function of benzene is reported, using the same tools developed in the above parts of this work. For what concerns the benzene molecule, a similar approach has been followed by Hirao in 1996 (79), who performed an analysis of the CASSCF wave function based on orthogonal valence bond structures, using the so-called CASVB method. Although being very interesting, in this study the attention has been focused on the weights of the structure in the CASSCF wave function, while the energy of the structures and their mutual interactions have been ignored. It is more interesting, indeed, to understand why some structures are more important than others, and this can be achieved knowing their energies and how they interact among themselves.

In the following, several approaches have been exploited, each one based on a different contraction scheme of the Slater determinants composing the wave function. As evident from what reported below, each one of these schemes offers a different point of view allowing one to understand different aspects of the electronic structure of this system.

6.1 COMPUTATIONAL DETAILS

The ground state of benzene is computed at the hexagonal experimental geometry (bond lengths of 1.397 Å for C-C and of 1.084 Å for C-H) using the cc-pVDZ correlation consistent double zeta basis set (80), which has contraction (9s,4p,1d)/[3s,2p,1d] for the C atoms and (4s,1p)/[2s,1p] for the H atoms. The molecule lies in the xy plane with the π orbitals obtained as combinations of the p_z atomic orbitals. The geometry and the basis set have been chosen to allow a clear comparison with the results reported in Ref. (79). Complete Active Space Self Consistent Field (CASSCF) calculations have been performed using the Molcas 7.8 package (48). The active space contains the six π electrons in the six π active orbitals.

The localization of the molecular orbitals and the OVB reading of the CASSCF wave function have been done using a set of codes developed in the Theoretical Chemistry group of the University of Ferrara.

6.2 ORBITALS

The six symmetry-adapted (delocalized) CASSCF π active orbitals are depicted in Figure 6.1: they belong to one of the irrep of the molecular symmetry point group (D_{6h}) and they closely resemble the MOs computed in the simple Hückel method, with the only difference that they are optimized in the molecular reality.

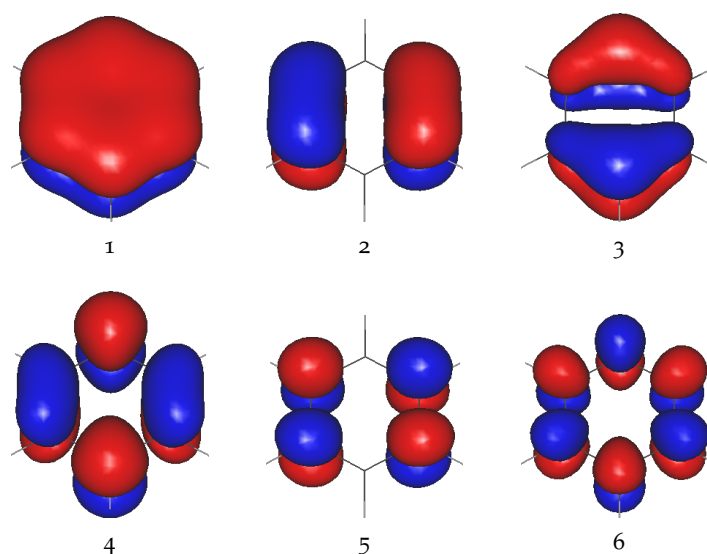


Figure 6.1: Symmetry adapted delocalized molecular orbitals of benzene.

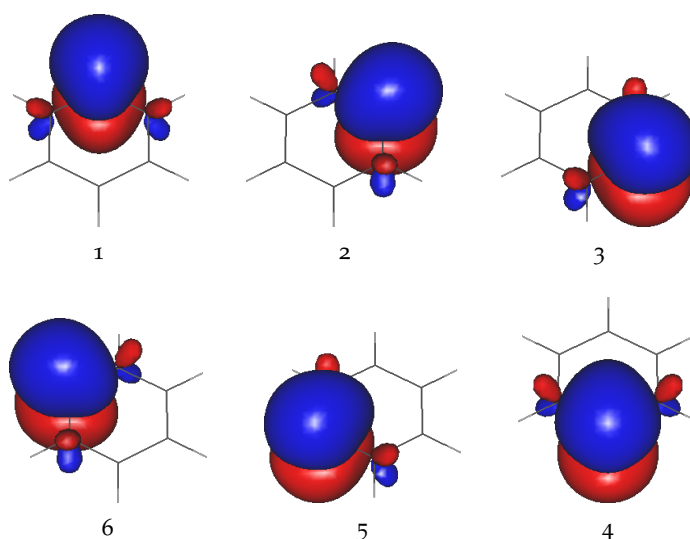


Figure 6.2: Atomic-like localized molecular orbitals of benzene.

By exploiting the invariance property of the CAS wave function with respect to any unitary transformation among the active orbitals, the symmetry adapted MOs can be localised on the carbon atoms, maintaining the orthogonality constraint (51, 79). Many methods to obtain such localized molecular orbitals (LMOs) have been developed and they can be based on some internal criterion (49, 50), or on external criteria (see Section 4.3). In the localization procedure here used, the unitary transformation maximises the overlap of the transformed orbitals with a set of (possibly non orthogonal) strongly localized reference orbitals, which in the present case are one of the p_z functions of the basis set (the same function on the various C atoms). In the simple case of benzene, this is equivalent to the localization transformation which one can deduce from simple symmetry considerations.

The localized MOs (OAOs) are shown in Figure 6.2. For each OAO, two out-of-phase orthogonalization tails on the adjacent C atoms can be observed. The consequences of such tails have been widely investigated by both VB and OVB points of view (23, 81, 82), as well as in Chapter 4. In a recent paper (23), the role of these orthogonalization tails in the H_2 has been reconsidered and it has been shown that, rather than describing a delocalization, they actually account for a reduction of the density of a given OAO on the neighbor atoms.

By performing a full CI within the OAOs active space one recovers the CASSCF wave function as a linear combination of the determinants written in terms of OAOs, which in turns can be interpreted as OVB structures (OVB-S), that is, possible distributions of the electrons in the OAOs. These determinants can then be combined to build Rumer structures (RS), which are normalized linear combinations of structures showing a singlet coupling of the electrons involved in a bond. The Rumer structures are arbitrarily built with reasonable criteria, and they represent just one of the possible choices to couple the electrons in the molecule. Finally, the Rumer structures can be combined in order to satisfy the molecular symmetry (symmetry adapted RS, SA-RS).

As a result, the CAS wave function can be expanded on different objects, all based in OAOs: OVB-S, RS or SA-RS, grouped for order of ionicity (defined as the number of + and - carbon atoms couples in the molecule) as shown in table 6.1, where the number of structures for each case is reported. Such objects are not necessarily orthogonal, even working with an orthogonal one-electron basis. In particular, only the RS and SA-RS characterized by the same distribution of charge may be non orthogonal, while two RS or SA-RS with different charge distribution are orthogonal objects.

In the following sections, a closer insight to the structure of the Hamiltonian matrix for each expansion basis is given. Also, the reasons of the non-orthogonality of RS and SA-RS is further examined.

Table 6.1: Number of OVB, Rumer and symmetry-adapted Rumer structures (OVB-S, RS, and SA-RS, respectively) spanning active space of benzene, sorted for the order of ionicity.

	Neutral	Single Ionic	Double Ionic	Triple Ionic
OVB-S	20	180	180	20
RS	5	60	90	20
SA-RS	2	6	11	3

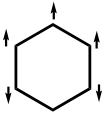
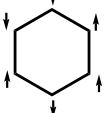
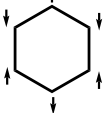
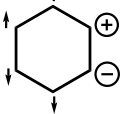
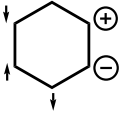
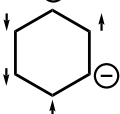
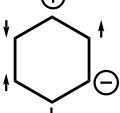
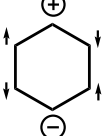
6.3 OVB STRUCTURES

The reading of the wave function granted by OVB-S allows the individuation of effective parameters. Under this view, the determinants are orthogonal, in contrast with the classic VB structures. The OVB-S with a large weight in the CASSCF wave function and their energies are shown in Table 6.2.

From this table, it is evident that determinants carrying the same charge distribution are almost degenerate. This is an expected result since the differences in energy are due to exchange terms, usually small quantities. The OVB-S with the lowest energy, D₁, presents four couples of neighbor parallel spins, and their energy expression contains, besides other terms common to all neutral structures, four stabilizing exchange integrals between neighbor electrons (hereafter indicated with K_{ab}). The D₂ structures have only two couples of neighbor parallel spins and their energy expression contains the same terms as the D₁ case but only two exchange integrals. Hence, the energy of D₂ is higher than that of D₁ by $2 K_{ab}$ and the energy of D₂ is lower than the one of D₃ (where all neighbor spins are antiparallel) by the same quantity. One can note that since the exchange integral between local orbitals decreases almost exponentially, the interaction between electrons on atoms not directly linked is almost vanishing.

By diagonalization of the neutral subspace only, the lowest singlet eigenvalue is higher in energy than some of the quintets by a quantity of 0.076 eV and than the septuplet by a quantity of 0.241 eV. Since the septuplet describes the complete uncoupling of the electrons in the molecule, its energy is based only on the great number of exchange interactions. Once more, it is worth noticing that the neutral OVB-S does not describe a bonding situation: all the eigenvalues (either septuplet, quintets or singlets) are almost degenerate. In the neutral structures the electrons are strongly constrained on their site and the only stabilization inside the neutral subspace comes from the exchange integrals. Since the neutral singlet structures count less exchange integrals (K_{ab}) than the septuplet and than some of the quintets, they are expected to be higher in energy. In order to achieve a correct description of the chemical bond in OVB, the interaction between neutral

Table 6.2: Energy (E) and coefficient in the CASSCF wave function (C) of the most important OVB-S. A symbol is associated to each OVB-S for the discussion (see text) and the number of similar (degenerate) structures is also reported. The energy of the D₁-like structures (-230.154175 hartree) is taken as reference.

Symbol	Deg.	OVB-S	Coeff.	E (eV)
D ₁	6		0.029	0.000
D ₂	12		0.102	0.279
D ₃	2		0.232	0.525
D ₄	24		0.064	7.563
D ₅	24		0.100	7.690
D ₆	48		0.025	10.511
D ₇	48		0.049	10.645
D ₈	24		0.041	11.325

and ionic OVB-S must be considered: the effect introduced by such interaction represents the possibility to delocalize the electrons on neighboring sites. It must be highlighted that this is the same effect seen in the OVB analysis of the hydrogen dimer in Chapter 3.

Starting from the energy of D₁ (or a neutral OVB-S whatsoever) it is possible to esteem the energy of the single ionic structures. This can be achieved by considering the sum of the Ionization Potential (IP) and Electron Affinity (EA) absolute values, as well as the stabilization integrals due to the charge separation of one bond, two bonds or

three bonds: such values are addressed hereafter with $J_{1\ 2}$, $J_{1\ 3}$ and $J_{1\ 4}$ respectively. The energies of the ionic forms computed in this way are reported in Table 6.3, where the values of IP and EA (following the Koopmans' approach) and of $J_{1\ 2}$, $J_{1\ 3}$ and $J_{1\ 4}$ are also reported.

Table 6.3: IP, EA and estimated energy values (referred to the energy of D1 in Table 6.2). The estimated energies are obtained from the difference between IP+EA and the J terms.

	IP=9.509 eV	
	EA=7.045 eV	
IP+EA=16.554 eV		
orthoionic	$J_{1\ 2}=8.798$ eV	estimated energy= 7.756 eV
metaionic	$J_{1\ 3}=5.579$ eV	estimated energy=10.975 eV
paraionic	$J_{1\ 4}=4.879$ eV	estimated energy=11.675 eV

Even though the IP and EA values are calculated without taking into account the orbital relaxation for the cation and the anion, the estimated energies of the single ionic structures are in good agreement with the ones obtained at CAS level for all simply ionic structures.

Examining further the ionic structures, it is evident that the charge transfer which generates an ionic structure has a major impact on the energies of the OVB-S, *e.g.* the neutral D1 and single ionic D4 configurations differ by 7 eV. For the single ionic OVB-S, the energies increase with the charge separation, as happens from D4 to D6.

The coefficients of the OVB-S in the CASSCF wave function do not follow what is expected from their energies. As one can notice, a higher energy do not imply a lower coefficient. For the neutral OVB-Ss, D1 D2 and D3, which are close in energy, differences up to one order of magnitude on the coefficients are observed, with the highest energy OVB-S (D3) showing the largest coefficients. A similar effect is found also for the ionic OVB-Ss: although D6 is 0.8 eV lower in energy than D8, its coefficient is almost half of that of D8's one.

In order to understand the origin of this behavior, an analysis of the interactions between the OVB-Ss is required.

The study of the interactions considers only the main interaction elements (which are mono-electronic or coulombic in nature), neglect-

ing the exchange terms: the exchange interactions (0.15 eV) are at least one order of magnitude lower than the coulombic ones (3.8 eV). This approximation aims to highlight the main effects on the coefficients coming from the interactions, although one has to keep in mind that the results are approximated. The main interaction elements are found between OVB-S differing by the transfer of one electron between neighbor atoms. This interaction is usually called hopping integral and indicated with t_{ab} . In the present study, the hopping integral was found to be 3.8 eV.

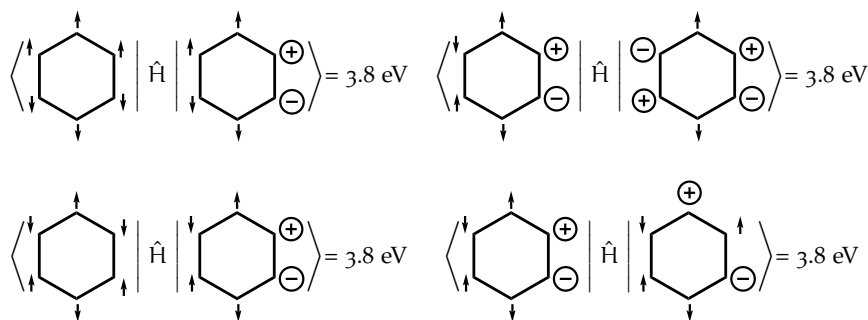


Figure 6.3: Interactions between OVB-S differing by the transfer of one electron between neighbor atoms.

As one can notice from Figure 6.3, these interactions appear either within the same ionic subspace (bottom right part) or between OVB-S of different ionicity. The spin distribution in a given OVB-S has a negligible influence on the t_{ab} values, but the possibility to transfer an electron (with its spin) to a neighboring atom strongly depends on the spins in the sites involved in the CT: the transferred electron must satisfy Pauli's exclusion principle. For this reason, only 4 charge transfer to neighboring atoms can be performed on the D₁ OVB-S (Figure 6.4, left), hence it interacts by t_{ab} with 4 single ionic OVB-S. On the other hand, all CTs (12) are allowed on the D₃ OVB-S (Figure 6.4, right), so it interacts by t_{ab} with 12 single ionic OVB-Ss. Such a high number of strong interactions explains why the coefficients in the CASSCF wave function of the D₃ OVB-S are much larger than those of the D₁ OVB-Ss, despite the fact that they are higher in energy.

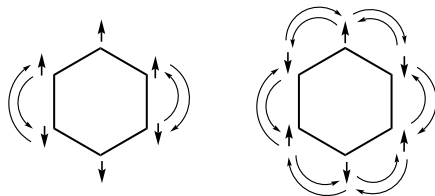


Figure 6.4: Possible charge transfers for D₁ and D₃.

6.4 RUMER STRUCTURES

The Rumer structures are the most chemist-friendly representation of the electronic structure of a molecule. They have such a central role that they are normally called *de facto* "VB structures". From the graphical point of view, they are represented reporting the "bonding scheme" between the atoms, such as, for instance the two Kekulé structures reported in Figure 6.5.

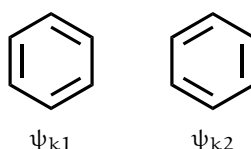


Figure 6.5: The two Kekulé structures.

If also the ionic forms are considered, 175 Rumer structures can be drawn, corresponding to the 175 possible singlet spin coupling for this system.

In order to connect the RSs to the OVB-Ss, one can write a given RS as a wave function in which the two electrons forming a bond are coupled as a singlet. Here we follow the same strategy, but using OAOs instead of pure atomic orbitals. An example is given in the following: the Kekulé structures reported in Figure 6.5 can be obtained as

$$\begin{aligned}\psi_{k1} &= \left\| \left(\frac{1\bar{2} - \bar{1}2}{\sqrt{2}} \right) \left(\frac{3\bar{4} - \bar{3}4}{\sqrt{2}} \right) \left(\frac{5\bar{6} - \bar{5}6}{\sqrt{2}} \right) \right\| \\ \psi_{k2} &= \left\| \left(\frac{6\bar{1} - \bar{6}1}{\sqrt{2}} \right) \left(\frac{2\bar{3} - \bar{2}3}{\sqrt{2}} \right) \left(\frac{4\bar{5} - \bar{4}5}{\sqrt{2}} \right) \right\|\end{aligned}\quad (6.1)$$

and, by developing ψ_{k1} one has:

$$\begin{aligned}\psi_{k1} &= \frac{1}{2\sqrt{2}} \left(\|1\bar{2}3\bar{4}5\bar{6}\| - \|1\bar{2}3\bar{4}5\bar{6}\| + \|1\bar{2}\bar{3}4\bar{5}6\| - \|1\bar{2}\bar{3}4\bar{5}6\| + \right. \\ &\quad \left. \|1\bar{2}\bar{3}4\bar{5}6\| - \|1\bar{2}3\bar{4}5\bar{6}\| + \|1\bar{2}3\bar{4}5\bar{6}\| - \|1\bar{2}\bar{3}4\bar{5}6\| \right)\end{aligned}\quad (6.2)$$

In Figure 6.6 the composition of the first Kekulé structure in terms of the eight neutral OVB-Ss is shown. The coefficient of the OVB-Ss in the linear combination are fixed by the bonding scheme defined in the RS.

A similar development can be done for ψ_{k2} . It is worth noticing that among the OVB-Ss spanning ψ_{k1} , only two are in common with ψ_{k2} : the two all-alternated spin determinants (also known as Neel structures) $\|1\bar{2}3\bar{4}5\bar{6}\|$ and $\|\bar{1}2\bar{3}4\bar{5}6\|$ are included in both Kekulé structures. Such determinants are responsible for the overlap between

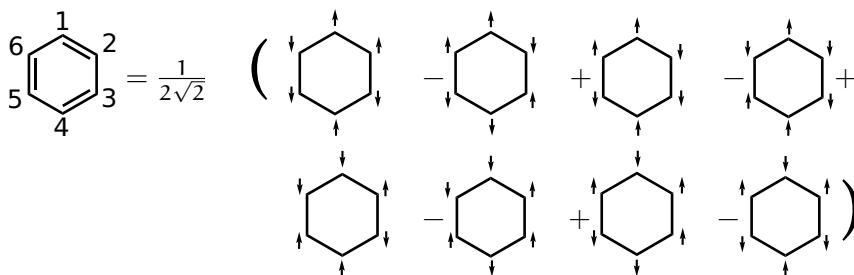


Figure 6.6: Eight neutral OVB-Ss generating the first Kekulé structure, as described in Equation 6.2.

ψ_{k1} and ψ_{k2} . Following this scheme it is easy to compute the overlap between two general RSs and, for the two Kekulé RSs, one has:

$$\langle \psi_{k1} | \psi_{k2} \rangle = S_{k_1, k_2} = \frac{1}{4} \quad (6.3)$$

The 175 RSs can be organized in 22 groups of degenerate structures (connected by symmetry operations), shown in Figure 6.7. They are hereafter indicated by the corresponding acronym (see caption of Figure 6.7).

The energies of the RSs are reported in Table 6.4, together with their coefficient in the CASSCF wave function. A few general trends can be identified. The energy of the RSs is mainly controlled by the order of ionicity and by the distance and disposition of the charges following three intuitive rules: i) the larger the ionicity order, the higher the energy; ii) the farther the opposite charges (for instance in the singly ionic structures) the higher the energy; iii) the energy is lower if positive and negative charges are alternate.

Concerning the bonding scheme, the energy is lower if the bonds connect farther atoms: the energy of the Dewar RSs is lower than the energy of the Kekulé RSs (and similarly for the other cases). This result can look counter-intuitive, but actually it is not within the OVB scheme: the singlet coupling of two electrons on two different atoms increases the energy with respect to the triplet coupling by a quantity $2 K_{ab}$. This quantity decreases almost exponentially with the distance. In the Kekulé RSs there are three singlet couplings between close atoms, while in the Dewar RSs one of this coupling is between distant atoms, leading to a lower energy for such RSs.

Similarly to the OVB-S case, the magnitude of the coefficient does not reflect the energy ordering. Indeed, according to Table 6.4, the RS with the lowest energy (the D RS, Figure 6.7) does not have the largest coefficient. Again, this result can be understood considering the interactions between the RSs.

The largest interactions are found, once more, between RSs differing by a charge transfer between neighbor atoms. This quantity is a

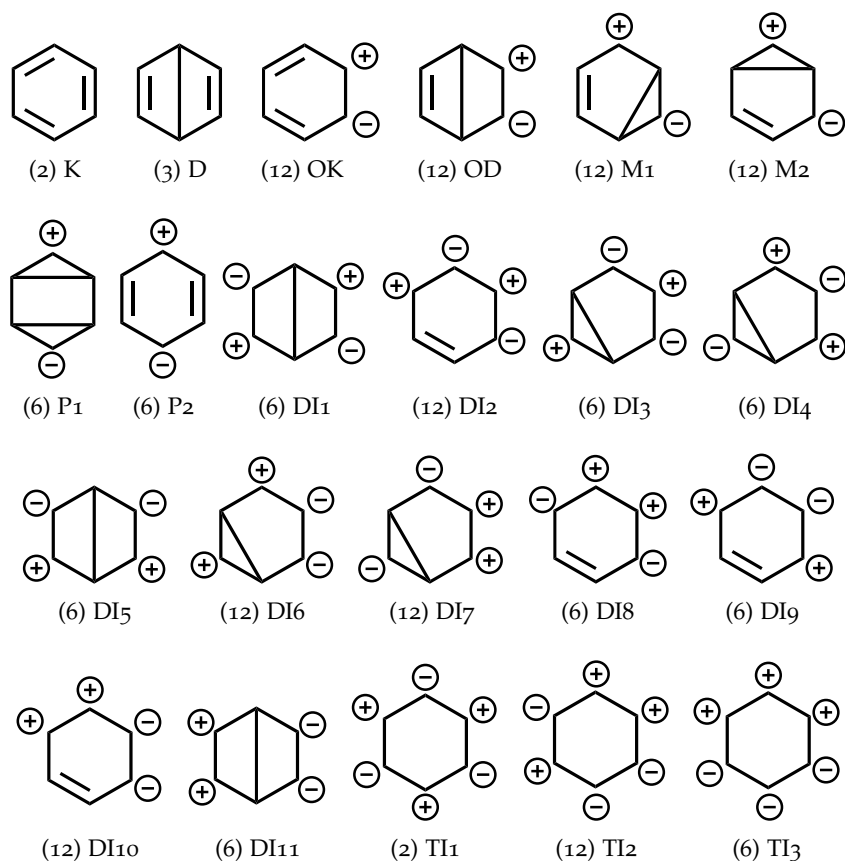


Figure 6.7: Rumer structures. Multiplicity for each group of degenerate structures is reported in round brackets. For each group an acronym is reported to identify the group (K=Kekulé, D=Dewar, OK= Ortho ionic Kekulé, OD= Ortho ionic Dewar, M=Meta ionic, P= Para ionic, DI=Double Ionic, TI= Triple Ionic).

hopping integral and is indicated here with T_{ab} to distinguish it from the t_{ab} related to the same quantity in the case of the OVB-Ss.

In the example shown in Figure 6.8 (the first Kekulé structure, ψ_{k1} , and a structure obtained by a charge transfer on it, ψ_{ok1}) the interaction is 5.4 eV. By expanding ψ_{k1} and ψ_{ok1} on the OVB-S basis, one verifies that each one of the eight OVB-S of ψ_{k1} presents an interaction with only one of the four OVB-S of ψ_{ok1} , in particular, the one with the same spin distribution for the four unpaired electrons. Moreover, the contribution of this couple of OVB-Ss to T_{ab} is t_{ab} . The signs of the coefficients of the two OVB-Ss in ψ_{k1} and ψ_{ok1} and that of the interaction are equal so that the product has a positive sign. Finally, it is worth noticing that ψ_{k1} contains all the OVB-S interacting with the OVB-S of ψ_{ok1} , the other twelve neutral OVB-S showing a vanishing interaction with them. These considerations have important consequences also for other type of interactions. In conclusion,

Table 6.4: Energies and coefficients in the CASSCF wave function of the Rumer Structures (RSs).

Bond group	C _{OVB}	E _{OVB} (eV)	Bond group	C _{OVB}	E _{OVB} (eV)
K	0.209	0.218	DI4	0.061	14.576
D	0.079	0.000	DI5	0.048	16.666
OK	0.128	7.852	DI6	0.055	17.933
OD	0.072	7.634	DI7	0.055	17.933
M1	0.047	10.787	DI8	0.019	22.266
M2	0.047	10.787	DI9	0.019	22.266
P1	0.024	11.275	DI10	0.013	25.624
P2	0.059	11.697	DI11	0.005	29.250
DI1	0.097	13.040	DI12	0.087	15.779
DI2	0.071	13.870	TI1	0.025	25.567
DI3	0.061	14.576	TI3	0.002	40.948

there are eight additive interactions of magnitude $t_{ab}=3.8$ eV. Hence, the interaction between ψ_{k1} and ψ_{ok1} is:

$$\langle \psi_{k1} | \hat{H} | \psi_{ok1} \rangle = \frac{n_{t_{ab}} t_{ab}}{4 \sqrt{2}} = \frac{8 \cdot 3.8 \text{ eV}}{4 \sqrt{2}} = \sqrt{2} \cdot 3.8 \text{ eV} = 5.4 \text{ eV} \quad (6.4)$$

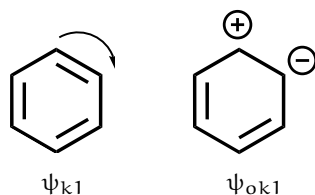


Figure 6.8: The first Kekulé structure and the OrthoKekulé generated by a charge transfer on it.

A simple scheme of interaction is shown in Figure 6.9. As one can notice, the T_{ab} magnitude is either of 3.8 eV or 5.4 eV. The magnitude of T_{ab} depends on the number of OVB-Ss spanning each RS, a quantity which is a function of the ionicity order of the RSs (it is $2^{\#b}$ where $\#b$ is the number of bonds in the π -manifold) and which is reported in Table 6.5. The interactions between RSs are the interaction between OVB-S multiplied by a scaling factor k_{sc} , which is the number of t_{ab} integrals between the OVB-S spanning each RS, divided by the product of the normalization constants.

By generalizing this result, the interaction between RSs which differ for a charge transfer and belong to different orders of ionicity is 5.4 eV,

Table 6.5: Number of determinants spanning each structure, sorted by each order of ionicity.

Neutral	Single Ionic	Double Ionic	Triple Ionic
$n_{\text{det}}^{\text{N}}=8$	$n_{\text{det}}^{\text{I}}=4$	$n_{\text{det}}^{\text{D}}=2$	$n_{\text{det}}^{\text{T}}=1$

while the interaction between RSs differing for a CT and belonging to the same order of ionicity is 3.8 eV, since the scaling factor k_{sc} in such case is one.

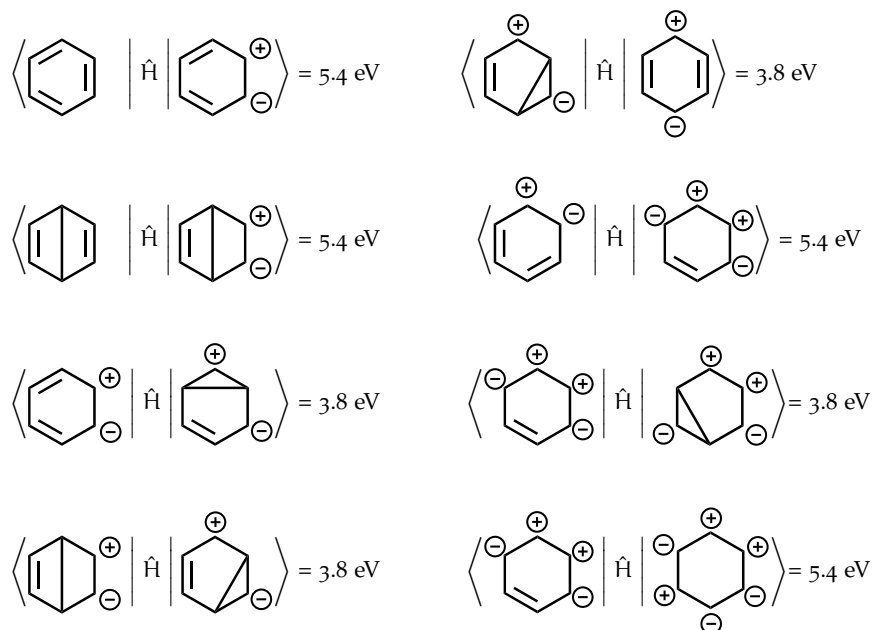


Figure 6.9: Interaction pattern between Rumer structures.

Besides these interactions many other non-negligible off diagonal terms appear in the Hamiltonian matrix expressed on the RS structure basis. As in the previous case, they connect RS differing by a CT between neighbor C atoms but in this case the bond pattern of the remaining electrons is different in the two RSs. To clarify the origin and magnitude of these interactions, let us consider explicitly an example, where three structures are considered: ψ_{k1} , ψ_{k2} , and ψ_{ok1} , one of the singly ionic structure obtained by a short range charge transfer on ψ_{k1} . The interaction $\langle \psi_{k1} | \hat{H} | \psi_{ok1} \rangle$ is $T_{ab} = 5.4$ eV as shown in the previous example. One can note that the overlap $S_{k2,k1} = \langle \psi_{k2} | \psi_{k1} \rangle$ is a measure of the fraction of OVB-S in ψ_{k1} also present in ψ_{k2} with the same sign, minus those with an opposite sign, and recalling that:

- the OVB-S in ψ_{k1} are all those (and only those) interacting with the OVB-S of ψ_{ok1} ;
- each OVB-S in ψ_{k1} interacts with only one OVB-S of ψ_{ok1} ;

- the interaction different from zero are always t_{ab} (the sign being positive if the sign of the two OVB-S is considered);

one can show that the interaction between ψ_{k2} and ψ_{ok1} can be computed simply as:

$$\langle \psi_{k2} | \hat{H} | \psi_{ok1} \rangle = \langle \psi_{k2} | \psi_{k1} \rangle \langle \psi_{k1} | \hat{H} | \psi_{ok1} \rangle = S_{k2,k1} T_{ab} = \frac{1}{4} T_{ab} \quad (6.5)$$

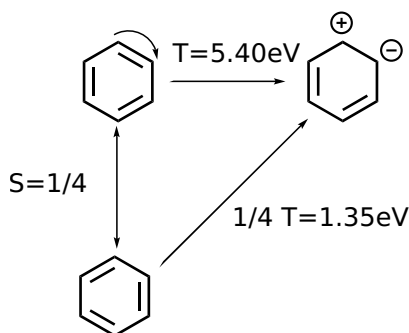


Figure 6.10: Graphic representation of Equation 6.5.

These considerations can be generalized for the whole Hamiltonian matrix: the relations developed for the neutral and singly ionic subspaces are valid also for the interactions between other RS connected by single excitation between two close atoms.

As found for the OVB-S, the number and magnitude of the interactions observed for each RS deeply influences its coefficient in the CASSCF wave function. To identify these interactions, let us note that for a given RS one must consider only the CT between close atoms. The two atoms involved in the CT can present a bond or not in the RS. In the first case, one has two $T_{ab} = \sqrt{2}t_{ab}$ interactions with the RSs presenting a CT on this bond (see Equation 6.4). In the second case, the atoms not involved in the CT can in principle present different bonding scheme and the interaction can be computed using Equation 6.5.

An example can help at this point. Let us compute the number and magnitude of the interactions shown by one of the Kekulé structure (say ψ_{k1}). One can verify that there are:

- six interactions with the ionic structures which can be obtained from ψ_{k1} by a CT on a bond: the value of each interaction is $T_{ab} = \sqrt{2} t_{ab}$;
- six interactions with ionic structures which can be obtained from ψ_{k2} by a CT on a bond: the value of each interaction is $T_{ab} = 1/(2\sqrt{2}) t_{ab}$ (recall that $\langle \psi_{k2} | \psi_{k1} \rangle = 1/4$);
- twelve interactions with ionic structures which can be obtained from the Dewar RSs by a CT on a bond (four CTs for each Dewar RS): the value of each interaction is $T_{ab} = -1/\sqrt{2} t_{ab}$ (recall that $\langle \psi_{k1} | \psi_{Dewar} \rangle = -1/2$).

On the other hand, considering one of the Dewar structure, one has

- four interactions with the ionic structures which can be obtained from it by a CT on a bond: the value of each interaction is $T_{ab} = \sqrt{2} t_{ab}$;
- eight interactions with ionic structures which can be obtained from another Dewar structure by a CT on a bond: the value of each interaction is $T_{ab} = 1/(2\sqrt{2})t_{ab}$ (recall that overlap between two Dewar structure is $1/4$);
- twelve interactions with ionic structures which can be obtained from the Kekulé structures by a CT on a bond (6 CTs for each Kekulé): the value of each interaction is $T_{ab} = -1/\sqrt{2} t_{ab}$.

Obviously, the diagonalization of the Hamiltonian matrix is a complex problem, in particular here, given that the metric of the basis is not the unit matrix (the RSs are not orthogonal), but one can understand, from these simple considerations, while in the CASSCF wave function the Kekulé structures have a coefficient larger than the Dewar structures (structures 1 and 2 respectively in Table 6.4), even if their energy is higher.

From a general point of view, by comparing two structures with the same same ionicity order and similar energies, it is simple to understand that a higher number of short range bonds ensures a larger coefficient in the CASSCF wave function.

It is worth noticing that the coefficient of the single ionic structures in Ψ_{str} is comparable in magnitude with the coefficient of the neutral structures (structures 1 and 3 in Table 6.4). The high number of short range charge transfer on the single ionic RSs play a key role in explaining such a high coefficient, despite the fact that they are 7 eV higher than the neutral RSs. As shown in Figure 6.11, the singly ionic structures are linked to each other, to the neutral RSs and to the double ionic RSs by a short range charge transfer.

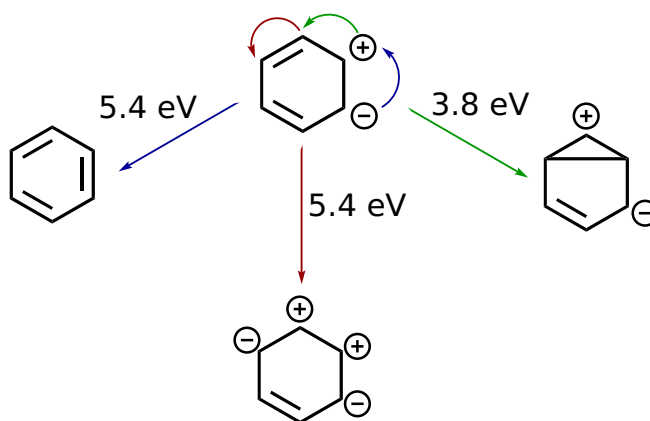


Figure 6.11: Possible short range charge transfers on a singly ionic structure.

6.5 LINEAR COMBINATIONS OF STRUCTURES

An even more compact reading of the CAS wave function is achieved by considering symmetry adapted linear combinations of RSs (SA-RSs). A simple example of the total symmetric (A_1 irrep) SA-RS obtained from one of the OrthoDewar structure is shown in Figure 6.12 and is hereafter indicated with $\psi_{\text{OD}}^{A_1}$, where the subscript OD follows the notation used in Figure 6.7.

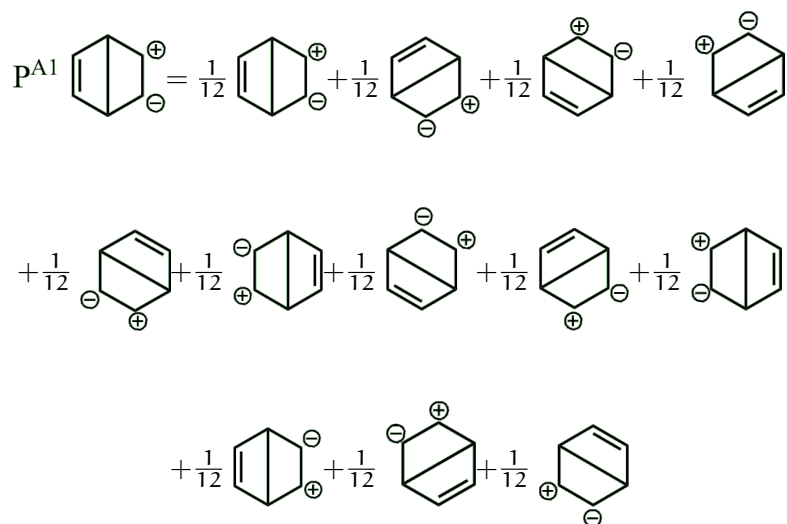


Figure 6.12: The A_1 symmetry adapted linear combination of OrthoDewar structures.

Such grouping allows to compact the Hamiltonian matrix to a 22 SA-RSs basis. The energies and interactions associated to the most important of these functions are reported in Table 6.6.

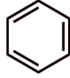
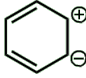

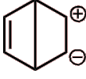
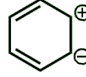

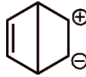

By considering the number of RS included in each SA-RS, it is simple to rationalize the interaction pattern. Let us consider, for instance, a Kekulé structures and its CT (line 1, in Table 6.6). The interaction between the respective RSs is 5.4 eV, as already seen in the previous section. The normalization constant for the sum of the two Kekulé structures ($\psi_K^{A_1}$) is $\frac{1}{\sqrt{2.50}}$ (the overlap between them is 0.25). The twelve OrthoKekulé structures, instead, are orthogonal, hence the normalization constant for their SA-LCS ($\psi_{\text{OK}}^{A_1}$) is $\frac{1}{\sqrt{12}}$. Each Kekulé has an interaction of 5.4 eV ($T_{k1,ok1}$) with 6 OrthoKekulé RSs, and of 1.3 eV with the other six OrthoKekulé ($S_{k1,k2} T_{k1,ok1}$), giving

$$\langle \psi_K^{A_1} | \hat{H} | \psi_{\text{OK}}^{A_1} \rangle = \frac{12 T_{k1,ok1} + 12 S_{k1,k2} T_{k1,ok1}}{\sqrt{2.50} \cdot 12} = 14.79 \text{ eV} \quad (6.6)$$

in good agreement with the result reported in Table 6.6. The same procedure can be applied when considering other SA-RSs.

For instance, the interaction between the Dewar and OrthoDewar SA-RSs is computed to be 12.48 eV, in good agreement with the 12.68

Table 6.6: Energies and interactions of symmetry adapted linear combination of RS. Only one RS for each SA-RS is represented. The reference value is the energy of the linear combination of Dewar structures ψ_D^{A1} (-230.106682 hartree).

E_{SA-RS} (eV)		E_{SA-RS} (eV)	Int (eV)
0.058	 → 	7.435	14.58
0.000	 → 	7.197	12.68
7.435	 → 	10.403	4.84
7.197	 → 	10.403	5.67

eV exact value. The interactions shown in lines 3 and 4 of Table 6.6 should be approximatively around the T_{ab} value, since all of the SA-LCS involved have the same normalization constants. The 0.83 eV difference (in opposite direction) in the interaction reported for line 3 and 4 is the outcome of minor interactions (around 0.3-0.4 eV) of the orthoionic RSs with other metaionic RSs differing for a long range CT.

6.6 ORDER OF IONICITY

The effect of compacting the ground state wave function can also be studied by considering an extreme contraction of the RSs. Indeed, one can consider linear combinations of all OVB-Ss belonging to one specific order of ionicity using their coefficient in the CASSCF wave function as contraction coefficient (and then normalizing the so obtained wave function). One has in this approach only four functions on which the CASSCF wave function is expanded: the neutral (ψ^N), singly ionic (ψ^{I1}), doubly ionic (ψ^{I2}), and triply ionic (ψ^{I3}) wave functions. The Hamiltonian matrix expressed on such a basis is reported in Table 6.7.

As one can notice, the energy of $|\psi^{I1}\rangle$ is only 1 eV higher than $|\psi^N\rangle$. Recalling that each singly ionic OVB-S is 7 to 11 eV higher in energy than the neutral OVB-Ss (as shown in Table 6.2), the great stabilization of $|\psi^{I1}\rangle$ can simply be explained by considering the large num-

Table 6.7: The Hamiltonian matrix expressed in the ψ^N , ψ^{I_1} , ψ^{I_2} , and ψ^{I_3} basis (see text). The energies are reported in eV and the reference energy is the energy of the contracted neutral wave function ($\langle\psi^N|\hat{H}|\psi^N\rangle$).

\hat{H}	$ \psi^N\rangle$	$ \psi^{I_1}\rangle$	$ \psi^{I_2}\rangle$	$ \psi^{I_3}\rangle$
$\langle\psi^N $	0.00	-13.64	0.06	0.00
$\langle\psi^{I_1} $	-13.64	1.08	-15.68	0.06
$\langle\psi^{I_2} $	0.06	-15.68	6.08	-11.75
$\langle\psi^{I_3} $	0.00	0.06	-11.75	19.16

ber of t_{ab} interactions among the OVB-Ss composing it: the orthoionic OVB-Ss interact strongly with the metaionic ones, and the metaionic determinants interact strongly with the paraionic ones. Such effect is evident in the energy of $|\psi^{I_2}\rangle$ as well, where each OVB-S of this ionicity is at least 13 eV higher than the neutral OVB-Ss, while the energy of $|\psi^{I_2}\rangle$ is just 6 eV higher than $|\psi^N\rangle$. The overall composition of the ground state wave function in this basis is :

$$\Psi_{GS} = 0.27 |\psi^N\rangle + 0.38 |\psi^{I_1}\rangle + 0.27 |\psi^{I_2}\rangle + 0.08 |\psi^{I_3}\rangle \quad (6.7)$$

Since $|\psi^N\rangle$ and $|\psi^{I_1}\rangle$ have similar energies, the interactions play a key role in determining their coefficient in the GS wave function. Indeed, the great number of t_{ab} interactions between the singly ionic OVB-Ss and both the neutral and the doubly ionic ones leads $|\psi^{I_1}\rangle$ to gain weight in the GS. The strong interactions of $|\psi^{I_2}\rangle$ with $|\psi^{I_1}\rangle$ and $|\psi^{I_3}\rangle$ make the coefficient of the contracted double ionic wave function equal to the coefficient of the neutral one, despite the fact that $|\psi^{I_2}\rangle$ is 6 eV higher in energy than $|\psi^N\rangle$.

6.7 CONCLUSIONS

Starting from the energy of the OVB structures, the energy of the Rumer structures has been evaluated. Such investigation has revealed that the energy of the Rumer structures is dominated by the Coulomb field, while the fluctuation of the exchange field has a small effect. The t_{ab} parameter has been identified as critical in order to draw a scheme of interaction between either the OVB structures, or the Rumer structures or the symmetry-adapted linear combination of the structures. The main interactions between the Rumer structures can be seen as a scaling factor multiplying the hopping integral between the OVB structures, while smaller interactions are related to the overlap between structures. All these results can be easily obtained analytically by simple considerations regarding the normalization factors, the number of interactions between determinants and the number of determinants in common among the Rumer structures. Similarly, the

interactions between symmetry adapted linear combinations of structures can be rather well rationalized following the method developed for the Rumer structures. Such a simple model may be employed in the study of more complex conjugated systems. The important role of the short range charge transfer allows indeed to greatly reduce the number of effects to take into account when working with aromatic compounds.

MAGNETIC SYSTEMS: STUDY OF BINUCLEAR COPPER COMPLEXES

The rationalization of the physical mechanisms controlling the interaction between unpaired electrons in magnetic systems has been a matter of study in molecular magnetism for decades. Driven by this aim, different models have been proposed to interpret the magnetic coupling, as that of Anderson (83) in the solid state physics domain, and the models introduced by Kahn and Briat (84) and by Hay, Thibeault, and Hoffmann (85) conceived for magnetic transition metal complexes. Mainly devoted to the study of binuclear complexes with $S=1/2$ centers, these models only took into account the unpaired electrons occupying the magnetic orbitals, a and b , and their success resides in providing simple expressions for the magnetic coupling constant J on the basis of a reduced number of parameters, K_{ab} , t_{ab} and U . K_{ab} is the direct exchange between the active orbitals, t_{ab} is the hopping integral between magnetic centres and U is the energy difference between the ionic forms, with two electrons in the same magnetic center, and the neutral ones, containing one unpaired electron per magnetic site.

These models have been successful in qualitatively describing the nature of the interaction, but as very soon de Loth *et al.* (86) have shown and many posterior applications have corroborated (87–92), these *active-electron-only* approximations are not able to provide J values in agreement with the experiment, J being in general at least one order of magnitude too small or even of incorrect sign. Indeed, the seminal work by de Loth *et al.* put in evidence that the other electrons play a key role on the magnetic coupling, by means of different processes such as the hole and particle polarization, spin polarization, ligand to metal and metal to ligand charge transfer (LMCT and MLCT), and combined (higher order) effects. They have proposed an expression of J based on second-order perturbation theory (PT), which only takes into account the differential effect playing a role on the energy difference between the states involved in the coupling. The procedure has been useful for rationalizing the magnetostructural behaviour of several Cu(II) binuclear compounds (88, 93, 94), and it has been quickly surpassed by the variational version, the difference dedicated configuration interaction (DDCI) approach by Malrieu and coworkers (95, 96), which ensure the introduction of higher-order effects and avoids the intrinsic convergence problems of the perturbation expansion. The first DDCI calculation was carried out by Broer and Maaskant (97) with the aim to analyze the magnetostructural

correlations in the $[\text{Cu}_2\text{Cl}_6]^{-2}$ complex. From then on, the DDCI approach has been particularly successful in the quantitative evaluation of the magnetic coupling constants in many solid and molecular magnetic systems (98) and at present it is considered as the reference method in this field.

The possibility to access quantitative estimations of J using the DDCI method has renewed the interest in the rationalization of the magnetic interaction and stimulated a series of works dedicated to the analysis of the physical effects governing the coupling at DDCI level (99–101). The DDCI space contains different classes of determinants, characterized by the number of inactive doubly occupied (*holes*, h) and virtual (*particles*, p) orbitals involved in the excitation. Among all excitations in the DDCI space, those carrying the largest effect on the coupling constant are the $1h1p$ determinants (responsible for the stabilization of the ionic forms and the introduction of the spin polarization mechanisms) and the $2h1p$ and $1h2p$ excitations, which contribute to a large fraction (30%–50%) of the coupling. The $2h1p$ determinants only bring a small antiferromagnetic contribution when acting directly on the CAS space, far away from the large effect found at DDCI level. This suggests that their impact is not related to a direct coupling with the ionic and neutral forms (second- and third-order effects), but it must be mediated by the indirect coupling through other electronic configurations (a higher-order effect). This proposal has been supported by a series of class-partitioned CI calculations where the variational space is step-by-step increased by different classes of excitations (101). The meticulous analysis of the so-obtained J values support a complex mechanism where the $2h1p$ excitations acquire their key role only in presence of the LMCT and $1h1p$ determinants. The origin of this cooperative effect could be related to a stabilization of the ionic and LMCT configurations due to the $2h1p$ and $1h1p$ excitations, resulting in a remarkable amplification of the AF character of J .

It is worth noticing that this analysis has been performed on wave functions based on the triplet CASSCF molecular orbitals (MOs) expanded in a minimal CAS. It takes into account the relative energy of the intermediates generated on this basis, and the amplitude of the interaction terms following arguments such as Brillouin's theorem. The use of the singlet CASSCF MOs only marginally modifies the scheme reported. However, if DDCI natural orbitals are employed, which magnetic orbitals are more delocalized on the ligands than the CASSCF ones (102), both the excitation energies and the interaction terms are affected. Hence, the relative importance on the magnetic coupling of each interaction pathway is also revised, some pathways negligible on the basis of canonical MOs become dominant, other appear to contribute at lower order of perturbation.

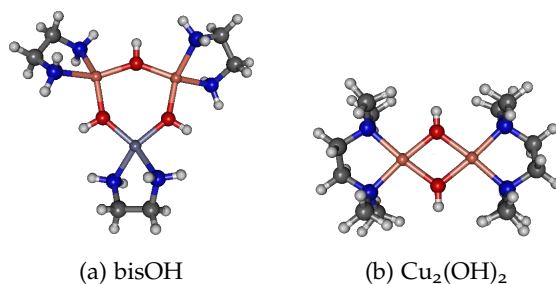


Figure 7.1: Geometries of the systems here considered.

In this work we provide *direct* and *numerical* evidences of the cooperative effect introduced by the $2h1p$ excitations and the whole set of mechanisms controlling the magnetic coupling. Based on the Orthogonal Valence Bond (OVB) reading of the wave function and the use of the Intermediate Hamiltonian theory, a rational strategy is proposed to analyze and finally quantify the physical effects in terms of the modification of some interaction terms and the lowering of the effective energy of those configurations strongly affecting the coupling.

This strategy provides the clues to classify the determinants able to provide a quantitative estimate of J on two groups, those that need to be treated variationally and those whose effect can be introduced by perturbation. The former group contains a reduced number of excitations (less than 0.05% of the whole space), those with a large interaction with the model space or a large impact on the effective energies of the determinants in the model space. The resulting CI matrix is dressed by the effect of the excitations belonging to the second group at second-order in perturbation theory (PT). This perturbative + variational strategy could be a powerful tool to deal with large and complex polynuclear magnetic systems, with the best skills of the variational methods and the low-cost requirements and high performance of the perturbation approach. To illustrate this strategy, two antiferromagnetic systems have been here considered, a binuclear model related to one of the native intermediates of the multicopper oxidases cycle (*vide infra*) and a binuclear Cu(II) complex, with similar ligands in the metal coordination spheres.

7.1 DESCRIPTION OF THE SYSTEMS AND COMPUTATIONAL DETAILS

Two antiferromagnetic binuclear Cu(II) systems have been considered. Geometries have been taken from X-Ray crystal data (103, 104) and are shown in Figure 7.1.

The system referred as bisOH in Figure 7.1 is obtained from the tris(μ -hydroxy)tricopper(II) complex, $[\text{Cu}_3(\text{dbed})_3(\mu\text{-OH})_3](\text{ClO}_4)_3$ (referred to as trisOH), by the substitution of a Cu atom by a Zn atom. The trinuclear complex trisOH is a bio-mimetic compound that mod-

els one of the native intermediates of the multicopper oxidases catalytic cycle. (104–107) In this complex, with a rigorous D_3 symmetry, the Cu centers are arranged in a triangle, connected to each other by an hydroxo group. The Cu-OH-Cu angle is 140.5° and the Cu-OH distance is 1.96 Å. The bidentate N,N' -di-*tert*-butylethyldiamine (dbed) ligand completes the coordination sphere of each metal atom. The magnetic interaction between the Cu(II) centers in the trimeric complex is antiferromagnetic, resulting in a spin-frustrated two-fold (four-fold considering the spin degeneracy) degenerate doublet ground state. In the frame of the isotropic exchange Heisenberg-Dirac-Van Vleck (HDVV) Hamiltonian, (108–110)

$$\hat{H}_{\text{Heis}} = - \sum_{i < j} J_{ij} \hat{S}_i \cdot \hat{S}_j \quad (7.1)$$

these degenerate 2E doublet states are separated by an energy of $3J/2$ from the quartet state 4A_2 . The fitting of the magnetic susceptibility data (104) yields a J value of $\approx -210 \text{ cm}^{-1}$ and then a doublet-quartet splitting energy of $3J/2 \approx -315 \text{ cm}^{-1}$. The EPR and variable-temperature variable-field magnetic circular dichroism (VTVH MCD) spectra demonstrate the existence of competing effects of an antisymmetric exchange and symmetry lowering, additional to the dominant isotropic exchange coupling. These terms are important to explain the observed magnetic and spectroscopic data at low temperature (105).

The electronic structure and EPR g tensors of the trisOH system together with many other inorganic models of the trinuclear Cu(II) site of the multicopper oxidases have been previously studied by multireference ab initio calculations (111), including CASPT2, MS-CASPT2, DDCI and MRCI calculations. As the authors claimed, these multireference methods only yield qualitatively correct results, the main issue being the correct description of the relative energies of the ground doublet and the excited quartet states. Table 7.1 collects the doublet-quartet gap (Δ) and J values obtained by Vancoille et al. (111) for trisOH. In general, the calculated CASPT2 values of the magnetic coupling constant are lower than the experimental ones, while DDCI largely overestimates the doublet-quartet gap. The inclusion of the spin-orbit coupling effect only modifies in some wavenumbers the J values. As the authors noticed, the underestimation of the CASPT2 values is somewhere expected, but the large overestimation of the DDCI values is *highly unusual* for this method.

In the present study we focus on the evaluation of the isotropic exchange coupling constant J . For this purpose, the simplified binuclear bisOH model is employed, where one of the Cu(II) atoms is replaced by a diamagnetic Zn(II) ion. To reduce the computational cost, the external *tert*-butyl groups are replaced by H, with a fixed N-H distance of 1.02 Å.

The second system explored, named $\text{Cu}_2(\text{OH})_2$ in Figure 7.1, consists in two Cu(II) centers bridged by two hydroxo groups, [Cu(tmen)

Table 7.1: Variational and perturbation estimates from Ref. 111 of the doublet-quartet gap, Δ , and magnetic coupling constant, J , (in cm^{-1}) for the trisOH system.

	Δ	$J = 2\Delta/3$
Exp	-315	-210
CASSCF(27,15)/CASPT2	-105	-70
CASSCF(27,15)/CASPT2/MS-CASPT2	-112	-75
DDC2(3,3)	-875	-583
DDCI(3,3)	-718	-479

OH]₂Br₂. The Cu atoms present a square-planar coordination, where the Cu-O-Cu angle is 104.1° and the Cu-OH distance is 1.90 Å. The coordination sphere is completed with tmen=N,N,N',N'-tetramethylethylenediamine (103). The two Cu(II) centers present a strong antiferromagnetic coupling with $J = -509 \text{ cm}^{-1}$, relative to the HDVV Hamiltonian. (103)

Both systems contain only two active $S=1/2$ antiferromagnetically coupled centers and J can be evaluated from the singlet-triplet energy difference, $J = E(S) - E(T)$. For the sake of comparison, for both systems we have used the basis sets employed in Ref. 111: the ANO-S basis sets with contraction [6s4p3d2f] for Cu and Zn atoms, [3s2p1d] for O, N and C atoms, and [2s] for H atoms. All CASSCF calculations have been performed using the MOLCAS 7.8 program package (48). The OVB analyses (23, 52, 112) are made with *ad-hoc* codes developed by the Ferrara group. The CASDI (113, 114) code has been used for DDCI calculations.

Several sets of MOs have been employed, both delocalized and localized. As will be discussed later, the DDCI calculations show a strong dependence on the MOs, differently to what is usually expected. The common strategy based on the use of the CASSCF orbitals optimized for the triplet state is not able to well describe the physics of the systems here considered. A set of natural orbitals (obtained from the diagonalization of the average singlet and triplet DDCI one-particle density matrices) allows one to overcome this problem.

7.2 THE LEWIS LOCALIZATION METHOD

Several methods can be found in literature for the generation of localized orbitals optimized at the mean field level (both single reference or multireference). In most of them, the MOs are firstly optimized in a standard procedure and the final canonical (delocalized) MOs are then localized. To this aim, most of the localization methods (49, 50,

115) use an intrinsic criterion of localization, in general by maximizing some localization function, while other localization procedures are based on an extrinsic criterion, as, for instance, the projection of localized MOs on the canonical SCF ones. The method employed in this article belongs to the latter group, in which a set of strongly localized (not optimized) MOs built using the Lewis method (*vide infra*) is projected on a set of optimized MOs.

In the Lewis approach, the first step is to build a set of (non optimized) localized orbitals. The procedure starts with a representation of the molecule following the idea of the Lewis' structures, where different kinds of orbitals appear. One may identify bonding and antibonding orbitals between neighbour atoms, atom centered doubly occupied orbitals (as, for instance, core orbitals) and unoccupied diffuse orbitals. The lone pairs can also be considered as atom centered orbitals. Moreover, orbitals involving more than two atoms may be considered, such as partially delocalized π (occupied or not) orbitals distributed on a small part of the molecule. The user must build all core and valence orbitals, while the virtuals are automatically generated by the program as atom centered orbitals. In summary, this step corresponds to a thorough analysis of the system under study, and this is, obviously, far from looking like a black box. Indeed, a large degree of freedom is given to the user who, at the end, is required to have a good understanding of the chemical nature of the molecule.

The guess local (non orthogonal) orbitals are orthogonalised through a hierarchical orthogonalisation method, which consists of a series of $S^{-1/2}$ and projection (Gram-Schmidt) steps. The first priority is given to the core orbitals, as they are responsible for the largest part of the energy of the system. They are orthogonalised among themselves through a $S^{-1/2}$ procedure. The second class corresponds to the active orbitals. They are projected on the space complementary to the space spanned by the core orbitals (Gram-Schmidt projection) and orthogonalised among themselves through a $S^{-1/2}$ transformation. The next class is the valence and, finally, the virtual orbital, for which a similar strategy is applied.

Once the guess local orthogonal orbitals are generated, they can be used as starting point for a CASSCF calculation (116) or projected on an optimized set of MOs, the CASSCF MOs or the natural DDCI MOs, as it is the case in this work. Each orbital space (doubly occupied, active, and virtual) is projected separately. Compared to a localization method based on an intrinsic criterion, for which a simple keyword is enough to get a set of localized orbitals, the Lewis approach is more demanding for the user, even if it is computationally very efficient. One must however emphasize that all orbitals can be localized without difficulty, in particular the virtual ones. Indeed, the localization criteria appearing in the most common methods require in general the presence of electrons in the orbitals, so that localizing the vir-

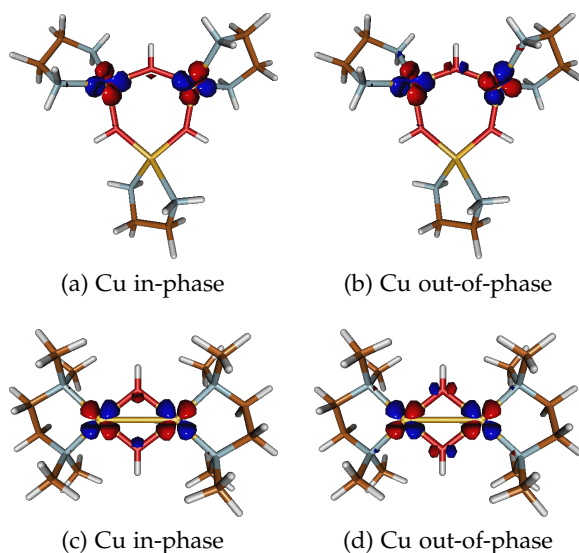


Figure 7.2: Triplet CASSCF(2,2) active orbitals for bisOH(a,b) and Cu₂(OH)₂(c,d).

tual MOs can be difficult. Finally, the application of methods based on intrinsic criteria can give orbitals that, even if they have a small spatial extension and they are therefore local, do not correspond to bonds, lone pairs, or any of the orbitals typical of the Lewis' description. The advantage of working with orbitals that exactly correspond to the Lewis description of the molecular architecture is helpful in particular in a VB logic, as it will be evident in the following.

7.3 RESULTS AND DISCUSSION

7.3.1 *Difference Dedicated CI results*

The common approach for the evaluation of J in systems with two unpaired electrons is based on the use of the triplet CASSCF MOs, where the active space contains the singly occupied $3d$ orbitals of the metallic centers (or in-phase and out-of-phase combinations of them). These orbitals are not purely atomic given that they show tails on the surrounding ligands. Afterwards, the application of the DDCI method on this minimal active space usually gives J values in good agreement with the experimental data (see for instance, Ref. 98 and references therein).

Figure 7.2 shows the triplet CASSCF(2,2) active orbitals for bisOH and Cu₂(OH)₂. In both cases, they have a dominant Cu $3d_{x^2-y^2}$ character. For the Cu₂(OH)₂ system, each Cu center presents a square-planar coordination, and the $3d_{x^2-y^2}$ orbitals are in the same plane of the OH bridges. In contrast, in the bisOH system, the Cu coordination polyhedra are distorted with respect to the square-planar one,

with the two N atoms slightly rotated out of the plane containing the Cu atoms and the OH ligands (tetrahedral distortion). As a result, the active $3d_{x^2-y^2}$ orbitals are not in the same plane. Actually, the active orbitals are not strictly speaking $3d_{x^2-y^2}$ orbitals, but hereafter we maintain this notation for simplicity.

When the triplet MOs are employed in the DDCI calculations, the resulting J values are largely underestimated with respect to the experimental ones, as shown in Table 7.2. This result is particularly surprising for $\text{Cu}_2(\text{OH})_2$, because previous studies with the same methodology have provided a nice agreement with the experimental J value. (101, 117, 118) The only difference between these studies and this work is the Cu basis set. The incorporation of the f basis functions has been related to a slight underestimation of J on previous studies (119). The marked effect found here will be discussed in a forthcoming paper, here we will focus on the impact on J of the nature of the MOs and of the size and composition of the active spaces.

Table 7.2: Magnetic coupling constants J (in cm^{-1}) at DDCI(2/2) level with different sets of MOs.

	bisOH	$\text{Cu}_2(\text{OH})_2$
Triplet MOs	-109	-350
Natural CAS+S MOs	-125	-394
Natural DDCI MOs	-150	-493
J_{exp}	-210	-509

Regarding the nature of the MOs, the question whether the CASSCF MOs are well suited for the variational or perturbation treatments of the electron correlation in magnetic systems has been previously raised by different authors (120–122). In perturbation treatments, the use of a minimal active space CASCI zeroth-order wave function with the triplet (or the singlet) orbitals usually gives underestimated values of J . A general accepted strategy to get better results is to extend the CAS with a set of virtual d -orbitals (introducing the radial correlation of the $3d$ electrons), and a few selected occupied ligand orbitals, which partially introduce at zeroth-order the effects brought by the LMCT (7, 98, 123, 124). Alternatively, it is possible to rest on the minimal active space if optimized (not in terms of the lowest energy) MOs are employed to build the reference wave functions, as those resulting from an average CASSCF calculation involving the two lowest CASSCF singlet states, mainly neutral and ionic in nature (120). This procedure gives magnetic MOs which are more delocalized on the ligands, leading to a stabilization of the ionic forms, thus reducing U , and to an increase of the hopping integral between the magnetic

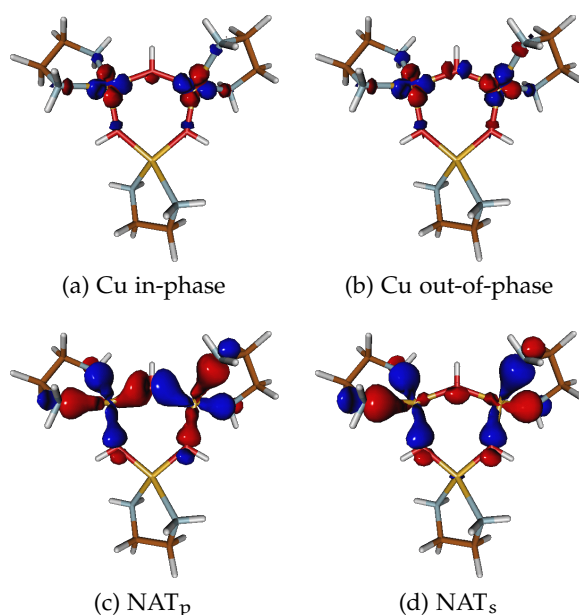


Figure 7.3: Natural orbitals for bisOH from the average density matrices of the DDCI singlet and triplet wave functions: (a) and (b) magnetic orbitals, (c) and (d) ligand centered natural orbital antisymmetric and symmetric with respect to the OH axis.

orbitals. They resemble the natural DDCI orbitals and provide a significant improvement of the CASPT2 and NEVPT2 results. (120, 125)

Among variational treatments, the DDCI J values have been traditionally considered highly independent of the MOs, with the exception of organic conjugated biradicals, where DDCI calculations on the basis of a minimal active space produces very poor results and an optimized set of MOs is required to obtain quantitative results (120, 121).

To this aim, two MO sets have been generated, the natural MOs obtained by the diagonalization of the average density matrix computed from the CAS(2,2)+S and from the DDCI wave functions. Table 7.2 reports on the J values obtained with these two sets of MOs at DDCI(2,2) level. The use of the natural DDCI MOs significantly improves the result for the bisOH system and gives a quantitatively correct estimate of J for the $\text{Cu}_2(\text{OH})_2$ compound. The impact of the MOs set is then noticeable and somewhat unusual for the DDCI approach, in any case larger than what has been reported so far.

Figures 7.3 and 7.4 show the magnetic orbitals of the natural DDCI MOs set for the bisOH and $\text{Cu}_2(\text{OH})_2$ molecules, respectively. One may qualitatively note that, compared to the corresponding triplet CASSCF MOs (Figure 7.2), these orbitals are more delocalized both on the ethylenediamine ligand and on the bridging hydroxy group(s). Indeed, it is well known that natural orbitals partially describe the delocalization of the active electrons on the ligand orbitals. (102, 126,

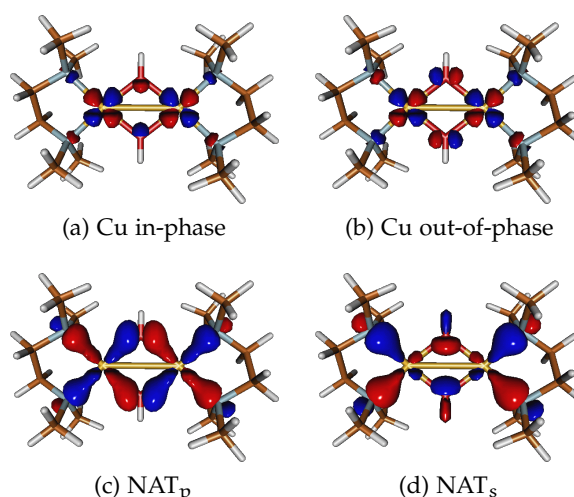


Figure 7.4: Natural orbitals for $\text{Cu}_2(\text{OH})_2$ from the average density matrices of the DDCI singlet and triplet wave functions: (a) and (b) magnetic orbitals, (c) and (d) ligand centered natural orbital antisymmetric and symmetric with respect to the OH axis.

127) Such a difference between the mean field singly occupied orbitals and the natural orbitals of a correlated wave function is present also in complexes with only one metal center and in recent works (56, 57) it has been explained as a different composition of the wave function in OVB terms. In particular the mean field approach (here CASSCF(2,2)) attributes an excessively large weight to the OVB structure with the unpaired electron on the metal center. Moreover, the importance of the metal-ligand delocalization has been also invoked as key ingredients of the non-orthogonal CI (NOCI) approach (128–130), first applied to the prediction of magnetic couplings in La_2CuO_4 by Van Oosten et al. (131, 132).

The results in Table 7.2 indicate that using optimized MOs it is possible to have a good value of J for $\text{Cu}_2(\text{OH})_2$, while for the bisOH system at best only 70% of the experimental value is recovered. Actually, this is not an isolate case, similar behaviour can be found for other binuclear transition metal complexes (98, 120). Looking in detail the characteristics of both systems, besides the number of bridges, the main differences come from: i) the Cu-Cu bond distances (3.0 Å in $\text{Cu}_2(\text{OH})_2$ and 3.69 Å in bisOH); ii) the Cu-OH-Cu bond angle, 105° in $\text{Cu}_2(\text{OH})_2$ and 140° in bisOH, and iii) the coordination polyhedron of the Cu centers, square-planar for $\text{Cu}_2(\text{OH})_2$ and slightly distorted square-planar in the bisOH molecule.

As a consequence of these structural differences, the OH group in bisOH acquires a special relevance. To check whether the OH bridge is conveniently represented in the active space, we decide to extend the active space with two orbitals mainly located on the hydroxy group(s). Two different OH orbitals are relevant in this case, those

able to overlap with the in-phase and out-of-phase combinations of the magnetic 3d orbitals, that is the sp hybrid orbital aligned with the O-H bond, and the O $2p_z$ orbital, aligned with the Cu-Cu axis.

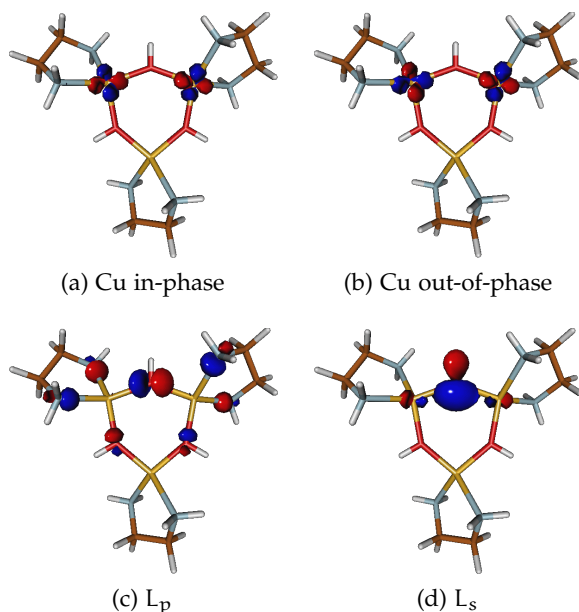


Figure 7.5: Localized most relevant orbitals for bisOH (Lewis procedure on natural DDCI MOs set, see text).

Different approaches can be conceived to identify the MOs needed to extend the CAS. One possibility is to use the occupation numbers of the natural orbitals as a criterion to identify the extra orbitals. The two occupied orbitals with the largest deviation with respect to a doubly occupation (NAT_s and NAT_p) are represented in Figures 7.3c and 7.3d for bisOH and Figures 7.4c and 7.4d for $Cu_2(OH)_2$. NAT_s is symmetric with respect to the OH axis, while NAT_p is antisymmetric.

Two CI spaces have been explored, a CAS(6,4)+S space with all the $1h$, $1p$ and $1h1p$ excitations with respect to the CAS(6,4), and the CAS(6,4)+DDC2 space, including also the double excitations involving two active orbitals (*i.e.* the $2h$ and $2p$ determinants). This strategy has been proposed in the past as an alternative to DDCI for the systems where the DDCI space is too huge and the calculation becomes unfeasible (118, 127, 133). When applied to our systems this strategy has different effect on the two systems considered (Table 7.3). In the case of $Cu_2(OH)_2$, the behavior is the same as that found in previous studies. The results obtained with the extended CAS are around the experimental value, representing 90% to 110% of the accepted value. In the case of bisOH, the situation is different. The extended CAS enhances the AF coupling and improves the agreement with the expected J value, but the agreement with the experimental value remains not fully satisfactory.

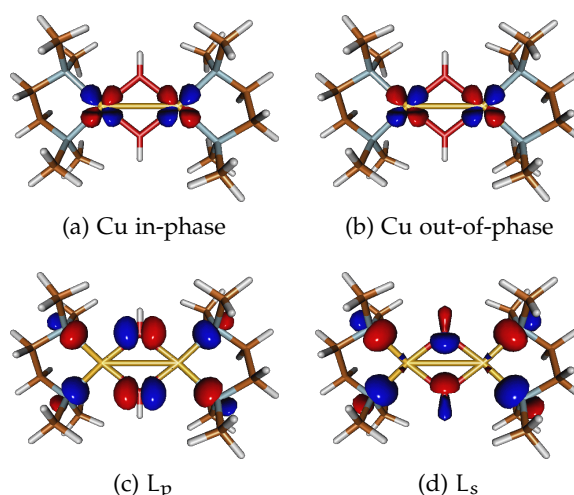


Figure 7.6: Localized most relevant orbitals for $\text{Cu}_2(\text{OH})_2$ (Lewis procedure on natural DDCI MOs set, see text).

Instead of using the occupation number as criteria, it is possible to localize the whole set of DDCI natural orbitals (with the *Lewis* procedure) and select those orbitals with a significant weight on the bridge(s). The resulting localized MOs are depicted in Figures 7.5 and 7.6 for bisOH and $\text{Cu}_2(\text{OH})_2$, respectively. The MOs labelled as L_s and L_p correspond to those with a large weight on the O sp hybrid and the O $2p_z$ orbitals, or in their out-of-phase combinations in the case of $\text{Cu}_2(\text{OH})_2$. L_s and L_p orbitals are symmetric and antisymmetric with respect to the O-H axis, respectively. The localization facilitates as well the identification of the *core* and *virtual* orbitals that can safely be frozen and deleted, respectively, thus reducing the computational cost of these calculations.

The results obtained with this extended CAS, are almost stable for $\text{Cu}_2(\text{OH})_2$ with respect to the DDCI(2,2), as shown in Table 7.3, while they are nicely improved for bisOH. In particular at the CAS(6,4)+DDC2 level, the J values obtained with the localized DDCI natural MOs agree with the experimental values for both systems. The main difference with respect to the delocalized set comes from the bisOH system, where the use of localized bridging orbitals significantly improves the J estimates at both levels. This can be related to the localization procedure, which allows for a larger control on the nature of the MOs included in the active space. In the case of $\text{Cu}_2(\text{OH})_2$, the two extra orbitals after localization maintain essentially the same shapes as the delocalized ones, but the tails on Cu 3d have been eliminated and the weight on OH has slightly increased. In the case of bisOH, the delocalized ligand orbitals have a dominant weight on N, in particular for the NAT_s one (Figure 7.3d), while the weight on OH is negligible. The origin of this difference can be found in the structural characteristics of bisOH, with a tetrahedral distortion in the Cu coordination sphere

that places the N and OH ligands in different molecular planes, and the larger Cu-OH-Cu angle (140° vs 105° in $\text{Cu}_2(\text{OH})_2$) that reduces the overlap between the O sp hybrid and the Cu $3d_{x^2-y^2}$ orbitals. The localization allows us to select a well defined MO on the bridge, for both symmetries, but it is important to keep in mind the differences between the L_s orbitals of the two systems, that will have implications for the dominant magnetic pathways, as discussed in next section.

Table 7.3: Magnetic coupling constants J (in cm^{-1}) using extended CAS and Lewis localized natural DDCI MOs.

		bisOH	$\text{Cu}_2(\text{OH})_2$
Delocalized MOs	CAS(6,4)+S	-205	-462
	CAS(6,4)+DDC2	-175	-568
Localized MOs	CAS(6,4)+S	-212	-447
	CAS(6,4)+DDC2	-232	-522
J_{exp}		-210	-509

In summary, the use of an extended active space on the basis of the localized MOs seems to be a key ingredient to obtain a quantitative agreement with the experimental J value in bisOH system. To explore the origin of this effect, an orthogonal valence-bond analysis of the CAS(6,4)+DDC2 wave functions is performed for both systems. It is worth noticing that during the OVB analysis, for practical purposes, orthogonal atomic 3d orbitals have been used, instead of the in-phase and out-of-phase combinations of them as shown in the previous figures. This does not change in any way the results of the calculations.

7.3.2 Orthogonal Valence-Bond analysis

In the following the Orthogonal Valence-Bond analysis of the CAS(6,4) + DDC2 wave functions is performed for the bisOH and $\text{Cu}_2(\text{OH})_2$ systems using the *Lewis* localized average natural orbitals.

The CAS(6,4) space consists in sixteen different OVB Slater determinants (indicated also with the term "structures" or "forms" in the following) of four different types: *neutral*, *ionic*, *charge transfer* and *double charge transfer*. Calling a and b the 3d active orbitals localized on the Cu atoms and s and p the L_s and L_p orbitals of the bridge (or their combinations in the case of $\text{Cu}_2(\text{OH})_2$), the neutral determinants are $||s\bar{s}p\bar{p}a\bar{b}||$ and $||s\bar{s}p\bar{p}b\bar{a}||$. These two determinants are degenerate and their in-phase and out-of-phase combinations identify a singlet and a triplet state, respectively. The ionic determinants are $||s\bar{s}p\bar{p}a\bar{a}||$ and $||s\bar{s}p\bar{p}b\bar{b}||$ and they show a charge separation between the two magnetic centers. Together with the neutral structures, they form the

one-band model CAS(2,2). The other determinants of the CAS space are charge transfer structures, specifically LMCT, with a transfer of electrons from the bridge ligands to the Cu atoms. A representative of a single CT is $||s\bar{s}p\bar{a}a\bar{b}b||$ and it refers to the excitation of a spin down electron from the p bridge orbital to the a metallic center. There are eight different single LMCT forms, considering the spin and the involved metallic center. The last four determinant are double LMCT forms: $||s\bar{s}a\bar{a}b\bar{b}||$ for a double CT from the p orbital, $||p\bar{p}a\bar{a}b\bar{b}||$ from the s orbital and $||s\bar{p}a\bar{a}b\bar{b}||$ a mixed double CT involving both the s and p orbitals.

A graphical representation of these structures is reported in Table 7.4, together with the corresponding Slater determinant and their energy with respect to the energy of the neutral determinant. The ionic determinants are very high in energy in both systems, U being ~ 24 -25 eV. The charge transfer structures have different energy depending on the system. For $\text{Cu}_2(\text{OH})_2$, the double charge transfer forms have an energy similar to that of the ionic ones, while the energy of the LMCT structures, ΔE_{CT} , is definitely lower. In bisOH, on the contrary, the excitations involving the s orbital (LMCT s in the following, CT s in short) is much higher in energy than those involving the p orbital (LMCT p, CT p in short). Indeed, the LMCT p is 13 eV above the neutral determinant, while this gap increases to 29 eV (even larger than U) in the case of the LMCT s. The double charge transfer involving the L_s orbital (DCT s) is particularly destabilized, by more than 60 eV. In fact, for the bisOH system all excitations involving the s orbital are higher in energy than in $\text{Cu}_2(\text{OH})_2$ (they are at almost twice the energy). This suggests that the s orbital is much lower in energy (more stabilized) in bisOH and that it plays a different role on the mechanism of the magnetic coupling in these systems.

The most important interactions between the 16 OVB structures are shown in Table 7.5. The K_{ab} and t_{ab} parameters are the same of the one-band model while the others are characteristic of an extended two-band model. More in details:

- K_{ab} : the direct exchange between the magnetic orbitals, it is the interaction between the two neutral structures.
- t_{ab} : the hopping integral, it is the interaction between ionic and neutral determinants.
- t_{CT}^{N} : it is the interaction between a neutral determinant and the LMCT. Two different terms can be distinguished depending on the type of ligand orbital (s or p) involved in the CT, labelled as CTs or CTp, respectively. The interaction is strong only when the unpaired electrons on the Cu atom and on the ligand have the same spin in the LMCT and in the neutral determinants, or in other words, when they are connected by a single-excitation.

Table 7.4: OVB structures and their energies. The energy of the neutral determinant is taken as the reference.

Type	Structure	Det.	Deg.	Energy (eV)	
				bisOH	Cu ₂ (OH) ₂
Neutral	$ \begin{array}{c} a \uparrow \downarrow \quad \downarrow b \\ p \uparrow \downarrow \\ s \uparrow \downarrow \end{array} $	$ s\bar{s}p\bar{p}a\bar{b} $	2	0.00	0.00
Ionic	$ \begin{array}{c} a \uparrow \downarrow \quad \text{---} b \\ p \uparrow \downarrow \\ s \uparrow \downarrow \end{array} $	$ s\bar{s}p\bar{p}a\bar{a} $	2	23.96	25.25
CT p	$ \begin{array}{c} a \uparrow \downarrow \quad \downarrow b \\ p \uparrow \text{---} \\ s \uparrow \downarrow \end{array} $	$ s\bar{s}p\bar{a}a\bar{b} $	4	13.11	11.29
CT s	$ \begin{array}{c} a \uparrow \downarrow \quad \downarrow b \\ p \uparrow \downarrow \\ s \uparrow \text{---} \end{array} $	$ s\bar{a}p\bar{p}a\bar{b} $	4	29.04	12.67
Double CT p	$ \begin{array}{c} a \uparrow \downarrow \quad \uparrow \downarrow b \\ p \text{---} \\ s \uparrow \downarrow \end{array} $	$ s\bar{s}a\bar{a}b\bar{b} $	1	24.96	21.36
Double CT s	$ \begin{array}{c} a \uparrow \downarrow \quad \uparrow \downarrow b \\ p \uparrow \downarrow \\ s \text{---} \end{array} $	$ p\bar{p}a\bar{a}b\bar{b} $	1	60.73	24.06
Mixed CT	$ \begin{array}{c} a \uparrow \downarrow \quad \uparrow \downarrow b \\ p \uparrow \downarrow \\ s \uparrow \text{---} \end{array} $	$ s\bar{p}a\bar{a}b\bar{b} $	2	40.07	22.11

- t_{CT}^I : it is the interaction between an ionic determinant and the LMCT. As in the previous case, there is a strong interaction only when they are connected by a single-excitation, that is, when the same Cu atomic orbital is doubly occupied in both determinants.
- t_{CT}^{DCT} : it is the interaction between the double charge transfer and the LMCT forms. In this case, the value is the same for all LMCT forms.

Table 7.5: Absolute values of the main interactions (in eV) in the CASCI(6,4) matrix on the basis of the OVB determinants.

name	matrix element	interaction (eV)	
		bisOH	$Cu_2(OH)_2$
K_{ab}	$\langle s\bar{s}p\bar{p}a\bar{b} H s\bar{s}p\bar{p}b\bar{a}\rangle$	0.02	$1 \cdot 10^{-3}$
t_{ab}	$\langle s\bar{s}p\bar{p}a\bar{b} H s\bar{s}p\bar{p}a\bar{a}\rangle$	0.72	0.03
t_{CTp}^N	$\langle s\bar{s}p\bar{p}a\bar{b} H s\bar{s}p\bar{a}a\bar{b}\rangle$	2.97	3.17
t_{CTs}^N	$\langle s\bar{s}p\bar{p}a\bar{b} H s\bar{a}p\bar{p}a\bar{b}\rangle$	1.55	3.24
t_{CTp}^I	$\langle s\bar{s}p\bar{p}a\bar{a} H s\bar{s}p\bar{b}a\bar{a}\rangle$	1.36	2.03
t_{CTs}^I	$\langle s\bar{s}p\bar{p}a\bar{a} H s\bar{b}p\bar{p}a\bar{a}\rangle$	0.62	1.35
t_{CTp}^{DCTp}	$\langle s\bar{s}p\bar{b}a\bar{a} H s\bar{s}a\bar{a}b\bar{b}\rangle$	2.59	3.24
t_{CTs}^{DCTs}	$\langle s\bar{b}p\bar{p}a\bar{a} H p\bar{p}a\bar{a}b\bar{b}\rangle$	1.09	3.25

From Table 7.5 one can note that K_{ab} and t_{ab} are relatively small compared to the other terms. Indeed, the LMCT show a strong interaction with the ionic and neutral determinants, highlighting their fundamental role in the description of the physics of the system. In bisOH the interactions involving the ligand L_s orbital are smaller than the corresponding parameters concerning the L_p orbital. All interactions, with the only exception of K_{ab} and t_{ab} , are larger in $Cu_2(OH)_2$ than in bisOH, in agreement with the relative values of their magnetic coupling constants.

The knowledge of these parameters allows the identification of the main pathways governing the magnetic interaction. In the one-band model, J can be calculated using the well-known equation

$$J = 2K_{ab} - \frac{4t_{ab}^2}{U} \quad (7.2)$$

where the first term is a ferromagnetic contribution that takes into account the direct exchange between the neutral forms (K_{ab} being always positive) and the second term is antiferromagnetic and considers the kinetic exchange through the ionic determinants, as shown in Figure 7.7a.

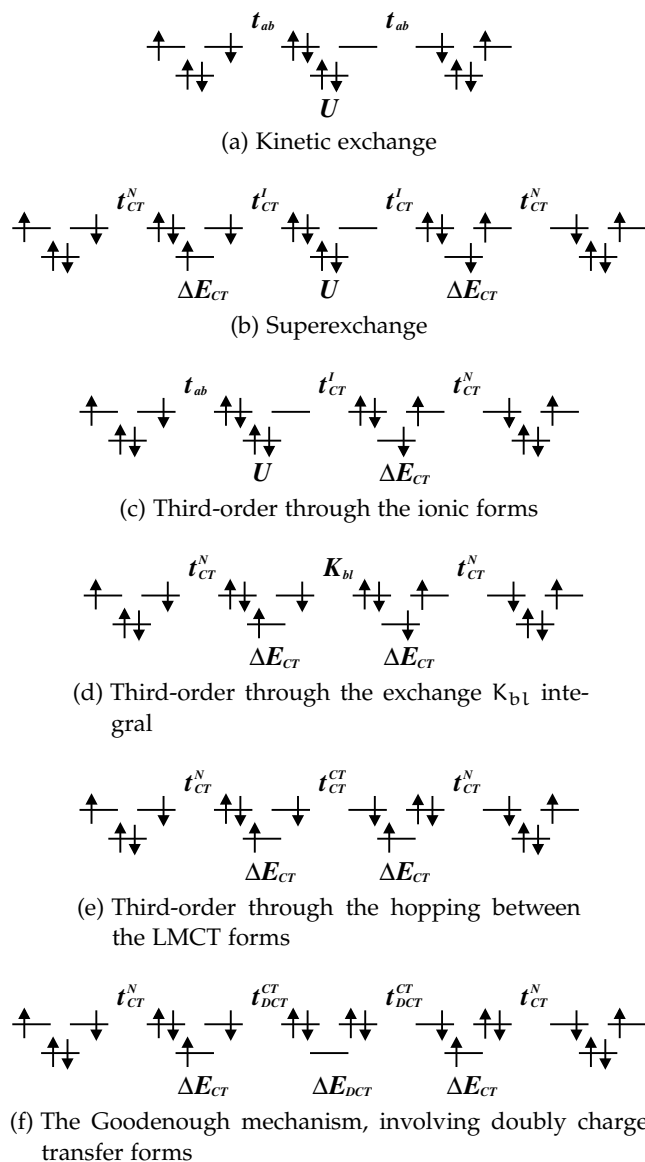


Figure 7.7: Main pathways governing the magnetic interaction

As well known, this one-band model involving only the ionic and neutral determinants significantly underestimates the J value. The deviation is particularly severe in those systems where the active centers are far apart from each other, and both the kinetic and direct exchanges are negligible. The model then needs to explicitly introduce the ligand orbitals, leading to a two-band model. In this model other interaction paths are conceivable and some of them are of key importance. For instance, the superexchange path that involves, besides the ionic structures, also the LMCT forms (see Figure 7.7b) plays a crucial role for a correct description of the energy splitting.

The contribution to the magnetic coupling is antiferromagnetic, and it depends on the hopping integrals, t_{CT}^N and t_{CT}^I , following:

$$J \leftarrow -4 \frac{(t_{CT}^N)^2 \cdot (t_{CT}^I)^2}{\Delta E_{CT}^2 \cdot U} \quad (7.3)$$

Depending on the nature of the ligand orbital, s or p , two different contributions can be distinguished, passing through the LMCT s or LMCT p forms. To return to the one-band model, these contributions can be included in an effective hopping integral, calculated as following:

$$t_{ab}^{eff} = t_{ab} + \frac{4 \cdot t_{CT}^N \cdot t_{CT}^I}{\Delta E_{CT}} \quad (7.4)$$

Since in bisOH t_{ab} has not a negligible value, in this case it is possible to conceive also third-order pathways, as that reported in Figure 7.7c, which contributes to J as:

$$J \leftarrow 8 \frac{t_{ab} \cdot t_{CT}^I \cdot t_{CT}^N}{U \cdot \Delta E_{CT}} \quad (7.5)$$

Two other third-order mechanisms are also possible, reported in Figures 7.7d and 7.7e. Here, K_{bl} is the interaction between two LMCT structures only differing for the spins of the two unpaired electrons on the ligand l and metallic b orbitals. For $l=p$, the integral is $K_{bp} = \langle s\bar{s}p\bar{a}a\bar{b}|H|s\bar{s}b\bar{a}a\bar{p}\rangle$. $t_{CT}^{CT} = \langle s\bar{s}p\bar{a}a\bar{b}|H|s\bar{s}p\bar{a}b\bar{b}\rangle$ is the interaction between two LMCT structures only differing on the doubly occupied Cu orbital. They contribute, respectively, by

$$J \leftarrow 4 \frac{t_{CT}^N \cdot K_{bl} \cdot t_{CT}^N}{\Delta E_{CT}^2} \quad (7.6)$$

and by

$$J \leftarrow 4 \frac{t_{CT}^N \cdot t_{CT}^{CT} \cdot t_{CT}^N}{\Delta E_{CT}^2} \quad (7.7)$$

to the magnetic exchange. These contributions are proportional to the inverse of the energy of the charge transfer forms, therefore, for bisOH they are more important for the LMCT involving the p orbital than for those involving the s orbital.

Using energetic arguments, it is possible to also consider pathways involving the doubly ionic structures, or doubly charge transfer forms, known as the Goodenough mechanism in solid state physics (134, 135), as shown in Figure 7.7f. Their contribution is:

$$J \leftarrow -8 \frac{(t_{CT}^N)^2 \cdot (t_{DCT}^{CT})^2}{\Delta E_{CT}^2 \cdot \Delta E_{DCT}} \quad (7.8)$$

and similar expressions can be written for the pathways with the mixed double charge transfer forms (MCT). The impact of each doubly ionic form on J will depend on their relative energies (Table 7.4). These energies are similar in the case of $\text{Cu}_2(\text{OH})_2$, while only the DCT p structures are expected to play a significant role in the case of bisOH. It is worth noticing that most of these mechanisms involve the interaction between the LMCT and neutral forms, t_{CT}^{N} . If CASSCF triplet MOs are employed, this interaction t_{CT}^{N} in the CASCI matrix is vanishing due to Brillouin's theorem, (100) since the LMCT are single excitations with respect to the neutral forms. However, when using natural MOs, these terms are far of being negligible, as shown in Table 7.5. Hence, the Goodenough mechanism, usually considered as non-relevant due to the high energy of the doubly ionic and the almost vanishing interaction with the LMCT, is responsible for additional antiferromagnetic pathways when working with natural MOs. This role results in a non-negligible weight of the doubly ionic structures in the singlet wave function.

Other paths are possible considering higher orders in perturbation. In an extended model as the one here considered, one should evaluate hundreds of different paths. In the traditional DDCI procedure the diagonalization procedure takes into account all interactions at every possible order in perturbation. In this way one may obtain the correct J value but the physics of the system remains hidden. The use of the Intermediate Hamiltonian (see Section 2.8.1) theory allows one to overcome this problem.

For the systems studied in this work, the main model space (see Sec. 2.8.1) is clearly identified by the two degenerate neutral determinants. The identification of the intermediate model space is not straightforward. At a glance, the most natural choice is the rest of the CAS space: ionic, charge transfer and double charge transfer structures. Hence, the model space (main +intermediate) contains 16 determinants. Therefore, the outer space contains all other determinants of the CAS(6,4)+DDC2 space and using Equation 2.122 one may dress the 16 by 16 bare Hamiltonian matrix with the effect of the other determinants, which are 1,794,393 for bisOH and 792,324 for $\text{Cu}_2(\text{OH})_2$.

The results obtained from the application of this procedure are shown in Table 7.6 (entries with $\tau = \infty$, *vide infra*). As one can see, the J value obtained from the diagonalization of the Hamiltonian in the full model space, J_{bare} , is not even qualitatively correct for bisOH, producing a ferromagnetic splitting. On the other hand, the diagonalization of the bare matrix dressed under the effect of the DDC2 space, provides the correct magnetic behaviour (J_{Hint2} in Table 7.6) but the splitting is strongly overestimated for both systems.

In order to understand the reason why this procedure fails, one can look at the bare and dressed Hamiltonian matrix elements, reported in Table 7.7 ($B_{\text{CAS}(6,4)}$ and $D_{\text{CAS}(6,4)}$ columns, respectively).

Table 7.6: Magnetic Coupling Constants (in cm^{-1}) obtained with different *brute-force* thresholds.

System	τ	n. det	J_{bare}	J_{Hint2}
bisOH	∞	16	44.9	-1090.7
	0.010	208	29.43	-316.17
	0.009	220	11.00	-298.59
	0.008	232	11.00	-298.59
	0.007	250	-11.02	-255.50
	0.006	258	-11.18	-255.72
	0.005	274	-46.52	-217.41
	0.004	308	-46.99	-220.57
	0.003	438	-99.20	-168.73
	0.002	632	-99.48	-164.17
	0.001	1081	-108.98	-204.55
$\text{Cu}_2(\text{OH})_2$	∞	16	-64.5	-1725.5
	0.020	128	-221.62	-357.20
	0.019	164	-39.04	-820.78
	0.018	176	-199.40	-516.74
	0.015	192	-204.02	-505.08
	0.009	212	-200.82	-494.16
	0.007	214	-227.81	-485.50
	0.005	222	-230.76	-484.53
	0.004	230	-233.53	-482.91
	0.003	374	-247.86	-481.17
	0.002	448	-255.73	-484.53
0.001	883	-287.60	-520.41	

Table 7.7: Bare (B) and dressed (D) Hamiltonian matrix elements (in eV) obtained using different model spaces: CAS(6,4) and the more extended CAS(6,4)+selected, where selected stands for $d \rightarrow d^* + 1h N + 1h Cu3d$ (see text).

System	Element	$B_{CAS(6,4)}$	$D_{CAS(6,4)}$	$D_{CAS(6,4)+selected}$
bisOH	E_0	0.0	0.0	0.0
	U	23.96	5.72	15.22
	ΔE_{CTp}	13.11	2.12	7.71
	ΔE_{CTs}	29.04	13.09	16.58
	ΔE_{DCTp}	24.96	8.39	15.94
	ΔE_{DCTs}	60.73	41.61	45.40
	ΔE_{MCT}	40.07	21.63	27.00
$Cu_2(OH)_2$	E_0	0.0	0.0	0.0
	U	25.19	7.78	18.10
	ΔE_{CTp}	11.29	1.57	6.93
	ΔE_{CTs}	12.67	2.84	8.09
	ΔE_{DCTp}	21.36	4.94	13.49
	ΔE_{DCTs}	24.06	8.26	16.41
	ΔE_{MCT}	22.11	6.03	14.54

It clearly appears that the ionic, the CT and the double CT structures withstand a very large stabilization by about 18, 12 and 16 eV, respectively. This large stabilization is the footprint of excitations contained in the outer space that strongly interact with the model space. In such a case, their effect cannot be treated through perturbation theory. To overcome this problem one has to include these excitations into the intermediate space, at the cost of losing its simplicity.

Several ways to identify these determinants have been tested. A *brute-force* method consists in the definition of a threshold τ and in the inclusion in the model space of all the determinants of the outer space whose absolute perturbative contribution to a given matrix element of the model space is larger than τ , following the logic of the CIPSI algorithm. (136) Table 7.6 collects the results obtained with this method, ranked in order of decreasing τ . The first row with $\tau = \infty$ corresponds to a model space containing only the CAS(6,4) determinants. As the most important excitations are included in the model space, the large overestimation of J_{Hint2} is progressively corrected. The J_{bare} values gradually improve with the size of the space and they converge to the DDC2 values. However, the behaviour of J_{Hint2} is rather erratic, in particular for bisOH system. Different τ values are required to obtain J_{Hint2} of similar quality for both systems. The con-

tributions are larger and concentrated in a smaller number of determinants in the case of $\text{Cu}_2(\text{OH})_2$, while they are individually smaller and much more spread out in the case of bisOH.

Hence, the *brute-force* method solves the problem of the over-stabilization of the structures in the model space but its dimension increases very fast and in an uncontrolled way, resulting in a difficult interpretation of the results. Actually, using a different selection procedure it turns out that the number of determinants which have to be included in the model space is quite small and their nature well defined. One may find these structures both manually looking at the most important excitations in the *brute-force* method or using the orbital entanglement maps (see Section 2.9), which allow one to identify the most important orbitals that are needed for the description of the system.

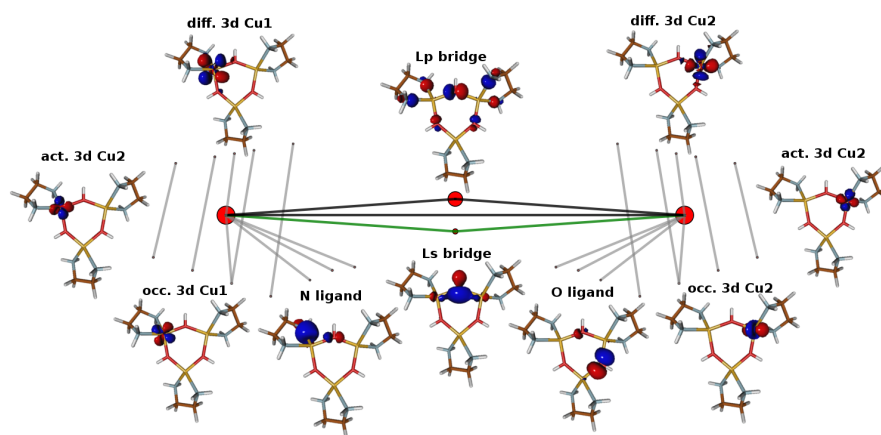


Figure 7.8: Entanglement measures for bisOH. Triplet wavefunction, CAS(6,4)+DDC2.

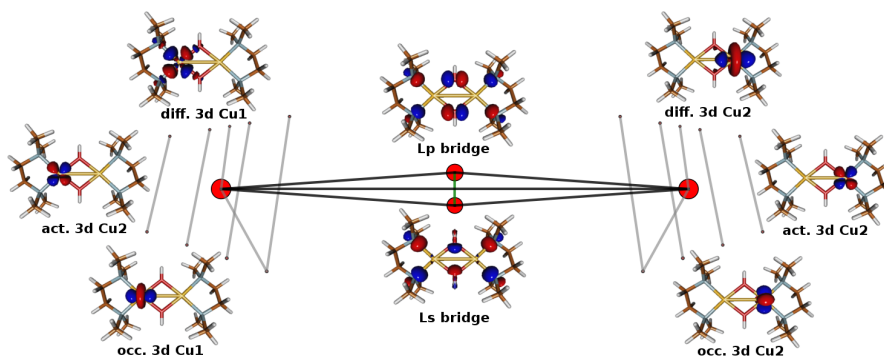


Figure 7.9: Entanglement measures for $\text{Cu}_2(\text{OH})_2$. Triplet wavefunction, CAS(6,4)+DDC2.

The entanglement maps of the triplet CAS(6,4)+DDC2 wavefunction for bisOH and $\text{Cu}_2(\text{OH})_2$ are reported in Figures 7.8 and 7.9, respectively. Similar maps are obtained for the singlet. The data have been obtained using a code recently developed within this thesis

work. In the figures, each point corresponds to a localized orbital and the size of the red-dot is proportional to its one-orbital entropy. The color of the lines connecting two dots represents the magnitude of their entanglement: black if $I_{i,j} > 0.1$, green if $0.01 < I_{i,j} \leq 0.1$ and grey if $0.001 < I_{i,j} \leq 0.01$.

The orbitals reported are only those presenting a significant entanglement value. As one can see, besides the active orbitals there are, both for bisOH and $\text{Cu}_2(\text{OH})_2$, the non-active Cu 3d orbitals with their diffuse counterparts. Moreover, for bisOH the occupied orbitals of both the nitrogen and the hydroxo ligands are also present. A strong entanglement between two orbitals means that they are involved in excitations that play a crucial role in the wave function. Thus, from the entanglement maps one can deduce a qualitative picture of the wave function. For instance, it is clear that for bisOH the L_p orbital plays a more important role than L_s , while in $\text{Cu}_2(\text{OH})_2$ the two orbitals are almost equally important.

The entanglement maps help us identifying (at least in the present case) a small but meaningful model space, showing the key role of a small number of 1h and 1h1p excitations in the description of the coupling:

- (i) the single excitations from the non-active 3d Cu orbitals to their diffuse counterparts, in the following referred to as $d \rightarrow d^*$ excitations. Each metallic center has four non-active 3d functions, resulting in eight different excitations per center.
- (ii) the single excitations from the non-active Cu 3d orbitals to the active Cu 3d, referred to as $1h \text{ Cu}3d$.
- (iii) the single excitations from the lone pair N orbitals to the active Cu 3d orbitals. They correspond to ligand to metal charge transfer forms, labelled as $1h \text{ N}$, and seems to be important only for bisOH. It is worth noticing that these excitations introduce the ligand-to-metal delocalization. In $\text{Cu}_2(\text{OH})_2$ this delocalization is introduced via the L_s and L_p orbitals, both with a non-negligible weight on the lone pair N orbitals. In bisOH, however, only the L_p contains a certain weight on N. This can explain the different role of these excitations in both systems.
- (iv) in minor extension, and only for bisOH, the single excitations from the neighbour OH ligand orbitals to the active Cu 3d.

In principle, these excitations act on each determinant of the CAS(6,4) model space. However, after carefully testing, the most important $d \rightarrow d^*$ excitations are those acting on the CAS determinants with two electrons on the same magnetic Cu 3d orbital on which the excitation is applied. In other words, these structures correspond to local excitations on the ionic, LMCT and double charge transfer forms.

With respect to the DDCI formalism on the basis of a minimal active space, these excitations belong to the $1h1p$ class when acting on the ionic forms, to the $2h1p$ set when acting on the CT forms, and to the $3h1p$ group if they act on the double charge transfer forms. They allow for the orbital relaxation of the “overloaded” Cu center, promoting electrons from the occupied $3d$ shells to the diffuse ones, thus lowering the effective energy of the ionic and CT forms. This effect has been invoked in our previous analysis (101), but here we provided numerical evidences of the impact of these excitations on the magnetic coupling and the evidence that these considerations are also corroborated by the entanglement measures. This selected set of $d \rightarrow d^*$ excitations are the only ones considered for the enlargement of the model space. Different groups of these excitations have been added and the resulting model spaces are used in the intermediate Hamiltonian procedure. The so-obtained J values are shown in Table 7.8. It is evident that the $d \rightarrow d^*$ excitations bring the key effect. When they are included in the model space, the diagonalization of the dressed Hamiltonian matrix produces quantitatively correct results, a coupling of $J=-516 \text{ cm}^{-1}$ for $\text{Cu}_2(\text{OH})_2$, the expected value being -522 cm^{-1} , and $J=-304 \text{ cm}^{-1}$ for bisOH, still overestimated with respect to the CAS(6,4)+DDC2 value (-232 cm^{-1}). Looking at the Hamiltonian matrix elements within this space, it becomes obvious why these determinants must be included in the intermediate model space. Indeed, even if their energies are more than 50 eV higher than the neutral determinants, their interaction with the ionic and the charge transfer structures is surprisingly large, being of the order of 5-6 eV. It is clear that it is not possible to treat an effect of this magnitude through a perturbation approach. The key role of these $d \rightarrow d^*$ excitations can be related to the improvement usually observed in the CASPT2 evaluations of J when the minimal active space is extended with a set of formally virtual d -orbitals (referred as the $3d'$ shell) (7, 98, 123, 124). A similar effect of the $d \rightarrow d^*$ excitations has been recently observed also in simple mononuclear Cu complexes, where the lowering of the LMCT energy and the corresponding increase of their coefficient in the wave function has important consequences on the spin density (56, 57). Actually, the key effect of the $d \rightarrow d^*$ excitations on the magnetic coupling was originally predicted by the pioneer work of de Loth et al. (88), but technical constraints at that time prevented a numerical evaluation through calculations using extended basis sets for Cu atoms.

The effect of the $1h \text{ Cu}3d$ is negligible for both systems, while the incorporation of the $1h N$ excitations has a marked effect for bisOH. Indeed, the J_{bare} value for bisOH becomes antiferromagnetic in nature, and the application of the Intermediate Hamiltonian theory produces a quantitatively correct result for this system, $J=-220.3 \text{ cm}^{-1}$. In the case of system $\text{Cu}_2(\text{OH})_2$ the impact of the $1h N$ excitations is negli-

Table 7.8: Magnetic Coupling Constants (in cm^{-1}) obtained with the Intermediate Hamiltonian theory using different model spaces

Model Space	n. det	J_{bare}	J_{Hint2}
bisOH			
CAS(6,4)	16	44.9	-1090.7
CAS(6,4)+ $d \rightarrow d^*$	176	8.39	-304.3
CAS(6,4)+ $d \rightarrow d^* + 1h \text{ Cu}3d$	240	7.6	-311.9
CAS(6,4)+ $d \rightarrow d^* + 1h \text{ N}$	208	-11.6	-220.3
CAS(6,4)+ $d \rightarrow d^* + 1h \text{ N} + 1h \text{ Cu}3d$	272	-12.0	-229.1
CAS(6,4)+DDC2 (reference)	1794393	-231.6	-
$\text{Cu}_2(\text{OH})_2$			
CAS(6,4)	16	-64.5	-1725.5
CAS(6,4)+ $d \rightarrow d^*$	176	-199.4	-516.7
CAS(6,4)+ $d \rightarrow d^* + 1h \text{ Cu}3d$	240	-199.4	-516.7
CAS(6,4)+ $d \rightarrow d^* + 1h \text{ N}$	208	-201.6	-515.9
CAS(6,4)+ $d \rightarrow d^* + 1h \text{ N} + 1h \text{ Cu}3d$	272	-201.6	-515.7
CAS(6,4)+DDC2 (reference)	792324	-522.2	-

gible, in good agreement with the entanglement measures. These excitations introduces the ligand-to-metal delocalization, and the origin of their differential role on these systems can be found in the distinct weight of the N lone pairs on the L_s and L_p orbitals. In other words, these $1h \text{ N}$ excitations correct the defective ligand-to-metal delocalization of the L_s orbital in bisOH. Notice that the quantitative evaluation of J in bisOH requires both an orbital with a large weight on the OH bridge and a correct description of the delocalization of the N lone pair orbitals. Finally, if both the $1h \text{ Cu}3d$ and $1h \text{ N}$ are included in the model space, together with the $d \rightarrow d^*$ excitations, the J values for both systems are nicely close to the fully variational values.

Regarding the performance of the method, it is worth noticing that a reduced number of determinants (272) provides estimates of the magnetic coupling that match the variational values obtained from a space containing 1-2 millions of determinants. This strategy based on the perturbative dressing of a rationally selected model space and the subsequent diagonalization can be envisaged as a promising approach to deal with more complex systems, containing several magnetic centers with several active electrons, and as an alternative to pure variational approaches, usually too demanding for polynuclear compounds, and to DFT approaches, showing the well-known dependence on the chosen functional.

A few (relevant) elements of the dressed matrices for this selected model space are shown in Table 7.7. Comparing these values with those of the bare CAS(6,4), the largest changes occur on the relative energies of the neutral, ionic and CT forms, the modifications of the interaction parameters being less significant. There is a large stabilization of the ionic structures with respect to the neutral ones, resulting in a lowering of the U parameter. Also the LMCT forms show a large lowering in the energy. In both cases the magnitude of this effect is less extreme than that observed with the CAS(6,4) model space. The overall decreasing of the energy of these structures clearly indicates their fundamental role in the description of the splitting. One may say that the effective work of the outer space is to stabilize these determinants in such a way that they can take more importance in the wave function and correctly describes the physics of the system. The outer space consists essentially in single excitations that, when applied to the model space, can be seen as an orbital relaxation effect which lowers the energy of ionic structures. It should be remarked that also in the LMCT structures one of the metallic center bears two electrons, resulting in an "ionic" nature.

In light of these results, it is possible to reconsider the different coupling pathways discussed above. Table 7.9 contains the individual contributions to the $J_{\text{Hint}2}$ value of the described mechanisms previously described in the frame of the two-band model. The evaluation of each contribution follows equations 7.2-7.8, but using the interaction parameters of the dressed, "rationally" selected, model space. It is worth noticing that this small number of contributions provides a significant fraction of the total J value, which means that a reduced number of pathways involving only the CAS(6,4) determinants condensate the main physics effects contained in the CAS(6,4)+DDC2 calculation with almost 2 millions of determinants, and then, much more pathways and of higher order. The results confirm the differential role of the LMCT s in these two systems: the pathways involving the LMCT s have similar impact that those involving the LMCT p for $\text{Cu}_2(\text{OH})_2$, while for bisOH the LMCT s are significantly less important for the coupling than the LMCT p. The large interaction between the ionic and neutral forms in bisOH is also crucial, enhancing all pathways involving this interaction. Such term is almost negligible for $\text{Cu}_2(\text{OH})_2$. Third-order pathways show different signs for L_p and L_s : they almost compensated each other for $\text{Cu}_2(\text{OH})_2$, while they introduce an important ferromagnetic contribution in the case of bisOH. Indeed, neglecting all pathways involving the LMCT s gives a J value of -240 cm^{-1} for bisOH. Finally, as mentioned above, the double ionic forms play a significant role in these two systems, an effect which could be partially ascribed to the use of natural MOs.

Table 7.9: Magnetic pathways and contributions to J_{Hint2} (in cm^{-1}) for the CAS(6,4)+selected model space

pathway	type	bisOH	$\text{Cu}_2(\text{OH})_2$
$2K_{ab}$		82.3	-9.7
N-I-N		-884.4	0.006
N-CT-I-CT-N	p	-610.5	-1684.1
	s	-1.4	-569.2
	s-p	+58.1	+1958.1
N-CT-I-N	p	+1469.6	-6.2
	s	-69.9	+3.6
N-CT-CT-N via t'_{ab}	p	+1695.1	-330.9
	s	-52.0	+225.3
N-CT-CT-N via K_{bt}	p	+345.3	+249.2
	s	-13.0	+420.4
N-CT-DCT-CT-N	p	-2468.7	-7512.0
	s	-4.5	-4044.5
N-CTp-MCT-CTp-N	p	+130.5	+3194.8
N-CTs-MCT-CTs-N	s	+28.6	+2389.0
N-CTs-MCT-CTp-N	s-p	+122.2	+5525.3
Total		-172.7	-190.9

7.4 CONCLUSIONS

In this chapter, we have applied a combined *perturbative+variational* strategy to the evaluation of the magnetic coupling constant in two antiferromagnetic systems. The method makes use of an OVB reading of the wave functions and the Intermediate Hamiltonian theory to select the set of key excitations which need to be treated variationally together to the determinants of an extended active space. These key excitations represent just a very small fraction (less than 0.05%) of the whole CI space, but provide, once dressed, J values that quantitatively reproduce the experimental ones.

The importance of this strategy is then twofold: (i) it is possible to quantitatively estimate the coupling constants at very low-cost, essentially the cost of the diagonalization of a matrix with a few hundred determinants, and (ii) it is possible to isolate and characterize the main excitations contributing to the coupling. Concerning this point, the entanglement maps have proven to be a useful tool to identify the orbitals, and hence the excitations, with a crucial role in the coupling.

The interaction between the LMCT, $1h1p$ and $2h1p$ excitations have been invoked in our previous studies as responsible for the performance of the DDCI approach when dealing with antiferromagnetic systems (99–102). Here, we have demonstrated that among all $1h1p$ and $2h1p$ excitations contained in the rather large DDCI space, those with a key role are the local $d \rightarrow d^*$ excitations, which introduce the relaxation of the 3d shell completely filled in the ionic and charge transfer forms. This result agrees with the recent studies by Giner and Angeli (56, 57) on the impact of these excitations on the correct description of the spin density.

The procedure requires the use of optimized molecular orbitals, which are localized prior to the OVB reading of the wave functions. Besides the satisfactory evaluation of J , the method provides also the values of the interaction parameters among the determinants of the model space, which allow for the identification of the main pathways controlling the coupling.

Regarding the two molecular systems here considered, this study supplies the clues of the difficulties found by Vancoillie et al. (111) in their previous estimation of the coupling in the parent trisOH compound. First, the use of an extended active space, including the bridging OH orbitals is compulsory, the OMs need to be optimized to correctly introduce the metal-ligand delocalization and finally, there exists a non-negligible and surprisingly high effect of the Cu basis functions.

In summary, the work reported here can be considered as a first step towards a general tool to deal with polynuclear systems containing localized spin moments and with the systems where calculations based on a minimal active space fail to quantitatively repro-

duce the magnetic coupling constant, as many ferromagnetic systems (137). Further work need to be done to optimize the molecular orbital sets in a simple and low-cost way. In this regard, the recent proposal by Giner and Angeli (56) for the orbital optimization in open-shell systems seems to be a promising route. Once this issue has been fixed, the here proposed *perturbative+variational* strategy could pave the way for a general and powerful approach to study complex systems and close the gap between the systems proposed by experimentalists and those that are successfully affordable by state-of-the-art quantum chemistry methods.

Entanglement properties and mutual information have been introduced in Section 2.9 of the chapter “Theoretical Methods”. In this chapter, these tools are applied to several molecular systems, focussing on the their dependence on the choice of the orbital set.

Homonuclear dimers such as H_2 , F_2 , N_2 and Cr_2 are analyzed with regard to the internuclear distance, allowing to obtain insights on how different kind of orbitals interact among themselves during the bond formation. Moreover, the use of the entanglement maps combined with different orbital schemes allows to clearly understand how the interpretation of the electronic structure depends on the set of orbitals employed, especially in more complex molecular systems.

8.1 THE HYDROGEN MOLECULE: TWO DIFFERENT APPROACHES

Since the dawn of modern quantum chemistry, the hydrogen molecule has been widely studied, being one of the simplest molecular model to which one may apply and test a new method.

Starting from the $1s_A$ and $1s_B$ atomic orbitals, where A and B indicate the two hydrogen atoms, it is possible to define two different molecular orbitals (MOs), a gerade σ_g and an ungerade σ_u :

$$\sigma_g = \frac{1s_A + 1s_B}{\sqrt{2(1+S)}} \quad (8.1)$$

$$\sigma_u = \frac{1s_A - 1s_B}{\sqrt{2(1-S)}} \quad (8.2)$$

Then, an approximate wave function for the singlet ground state (GS) can be written as a linear combination of the two gerade Slater’s determinants obtained populating the σ_g and σ_u orbitals:

$$\Psi_{GS}^{MO} = \lambda\Phi_g - \mu\Phi_g^* \quad (8.3)$$

where $\lambda, \mu > 0$ and the two determinants are $\Phi_g = \|\sigma_g\bar{\sigma}_g\|$ and $\Phi_g^* = \|\sigma_u\bar{\sigma}_u\|$. This approach may be improved using a larger basis set of atomic orbitals, $\{\chi_r\}$, to define two more flexible symmetry adapted molecular orbitals:

$$\sigma_g = \sum_r c_r \chi_r \quad (8.4)$$

$$\sigma_u = \sum_r c_r^* \chi_r \quad (8.5)$$

The energy of the two-electron in two-orbitals wave function $\Psi_{\text{GS}}^{\text{MO}}$ is then variationally minimized with respect to both the coefficients λ , μ and c_r, c_r^* . This is the well known (2 electrons, 2 orbitals) complete active space self-consistent field method, CASSCF, that produces the best minimal valence description for H_2 and represents a routinely used method in the field of molecular orbitals theory.

Starting from these molecular orbitals, it is possible to return to the local description given by the minimal basis set $\{1s_A, 1s_B\}$ defining two new orthogonal atomic orbitals, OAO, as

$$\mathbf{a} = \frac{\sigma_g + \sigma_u}{\sqrt{2}} \quad (8.6)$$

$$\mathbf{b} = \frac{\sigma_g - \sigma_u}{\sqrt{2}} \quad (8.7)$$

and re-writing the wave function $\Psi_{\text{GS}}^{\text{MO}}$ as:

$$\Psi_{\text{GS}}^{\text{OVB}} = \frac{\lambda + \mu}{2} [\|\mathbf{a}\bar{\mathbf{b}}\| + \|\mathbf{b}\bar{\mathbf{a}}\|] + \frac{\lambda - \mu}{2} [\|\mathbf{a}\bar{\mathbf{a}}\| + \|\mathbf{b}\bar{\mathbf{b}}\|] \quad (8.8)$$

which is equivalent (in terms of energy and properties) to Equation 8.3, due to the invariance of a CASSCF wave function with respect to an arbitrary rotation of the active orbitals.

This approach is usually referred to as orthogonal Valence Bond, OVB, and allows a Valence Bond reading of a CASSCF wave function, that establishes a direct link between the MO and VB theories. Indeed, due to their different nature, the Slater's determinant in Equation 8.8 may be labelled, in a VB-like fashion, as *neutral* and *ionic*, allowing a more transparent interpretation of the wave function.

For instance, in the case of H_2 , from Equation 8.8 (where $\lambda, \mu > 0$) it is clear that the neutral determinants are more important than the ionic ones for the description of the system, *i.e.* the two electrons prefer to occupy different orbitals rather than staying in the same one.

This technique has been firstly explored by the seminal works of Malrieu et al. (51, 52) and subsequently received attention in several fields: from a demonstration of the diabatic nature of the OVB structures of H_2 (23) to the study of the electronic structure of biradicals (138) and the evaluation of magnetic coupling constants (20).

8.2 ANALYTIC ENTANGLEMENT IN H_2

Given the simplicity of the H_2 molecular system, it is straightforward to write an analytic expression for the one- and two-orbital reduced density matrices and, therefore, for the entanglement. In the following, these analytic expressions are obtained and analyzed both in a molecular orbitals and in an orthogonal valence-bond scheme.

8.2.1 Entanglement in the MO scheme

Starting from Equation 8.3 and given that the coefficients λ and μ are normalized, one may write the ground state wave function as:

$$\Psi_{GS}^{MO} = \lambda \|\sigma_g \bar{\sigma}_g\| - \sqrt{1 - \lambda^2} \|\sigma_u \bar{\sigma}_u\| \quad (8.9)$$

Here, λ^2 represents the probability to find the two electrons in orbital σ_g , and $1 - \lambda^2$ is the equivalent for orbital σ_u . In this wave function, there are no terms corresponding to singly occupied orbitals. It is then straightforward to obtain the one-orbital RDM, whose diagonal elements (the eigenvalues) are reported in Table 8.1, the off-diagonal elements being zero by definition, due to the need of preserve the spin and the number of particles.

Table 8.1: Diagonal elements (eigenvalues) of the one-orbital Reduced Density Matrix for H₂ using MOs.

	σ_g	σ_u
$ \bar{-}\rangle$	$1 - \lambda^2$	λ^2
$ \bar{\#}\rangle$	0	0
$ \# \bar{-}\rangle$	0	0
$ \# \bar{\#}\rangle$	λ^2	$1 - \lambda^2$

Then, the one-orbital entropy is trivially obtained by applying Equation 2.123, that gives the same results for the two orbitals: $s(1)_{\sigma_g} = s(1)_{\sigma_u} = -\lambda^2 \ln(\lambda^2) - (1 - \lambda^2) \ln(1 - \lambda^2)$.

Considering the two-orbital RDM, among the 16^2 elements only 4 are not vanishing. Indeed, the elements concerning singly occupied orbitals are vanishing due to the vanishing coefficient, and the element concerning more than two electrons are not relevant for H₂. Moreover, also in this case the spin and the number of the particles must be preserved, that is, all the off-diagonal element between states with a different number of electrons, or a different value of S_z , are zero. One may write the resulting matrix as:

$$\text{RDM}(2) = \begin{array}{cc} \begin{array}{c} |\bar{-}\rangle \\ |\bar{\#}\rangle \end{array} & \begin{array}{c} |\# \bar{-}\rangle \\ |\# \bar{\#}\rangle \end{array} \\ \left[\begin{array}{cc} 1 - \lambda^2 & -\lambda\sqrt{1 - \lambda^2} \\ -\lambda\sqrt{1 - \lambda^2} & \lambda^2 \end{array} \right] & \begin{array}{c} |\bar{-}\rangle \\ |\bar{\#}\rangle \end{array} \end{array} \quad (8.10)$$

where, in the kets indicating the different states, orbital σ_g is on the left and orbital σ_u is on the right. The diagonalization of this matrix provides eigenvalues $\omega_{1,\sigma_g,\sigma_u} = 0$ and $\omega_{2,\sigma_g,\sigma_u} = 1$ for any value of λ , resulting in a two-orbital entropy (according to Equation 2.124) of:

$$s(2)_{\sigma_g,\sigma_u} = 0 \quad (8.11)$$

This result is not surprising, given that any orbital occupation is totally determined at each internuclear distance: when σ_g is doubly occupied, σ_u is empty; when σ_u is doubly occupied, σ_g is empty. There are no possible intermediate situations.

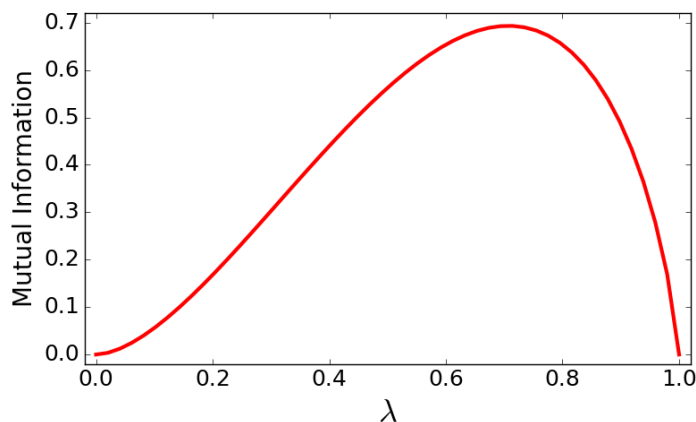


Figure 8.1: Dependence of the mutual information on the coefficient λ .

At this point, the mutual information, I_{σ_g, σ_u} , between the two orbitals can be calculated according to Equation 2.125:

$$I_{\sigma_g, \sigma_u} = - [\lambda^2 \ln(\lambda^2) + (1 - \lambda^2) \ln(1 - \lambda^2)] \quad (8.12)$$

and it turns out to be equal to the one-orbital entropies $s(1)_{\sigma_g} = s(1)_{\sigma_u}$. In Figure 8.1, the dependence of the mutual information on the coefficient λ is reported, and one may see (either from the graphic or from a simple derivation) that the function shows a maximum for $\lambda = 1/\sqrt{2}$ ($\simeq 0.7$). This value of the coefficient is achieved when the internuclear distance approaches infinity, that is, when the Φ_g and Φ_g^* determinants have the same weight, and the corresponding maximum entanglement is $I_{\sigma_g, \sigma_u}^{+\infty} = \ln(2)$.

The dependence of the mutual information with respect to the internuclear distance is reported in Figure 8.2. The wave function is obtained at the CASSCF(2, 2) level using an ANO-L basis set with contraction (8s4p3d)/[3s2p1d]. All the CASSCF calculations in this work has been performed using the MOLCAS program package, version 7.8 (48). As one can see, the entanglement is small when the two atoms are close to each others, and increases when bond is stretched, until it reaches the limit of $1/\sqrt{2}$ at dissociation. At the equilibrium geometry, marked in the Figure with a black dashed line, the mutual information is rather small. This is an indicator of the fact that the wave function is compact, that is, the weight of one determinant (Φ_g) is much larger than the weight of the other.

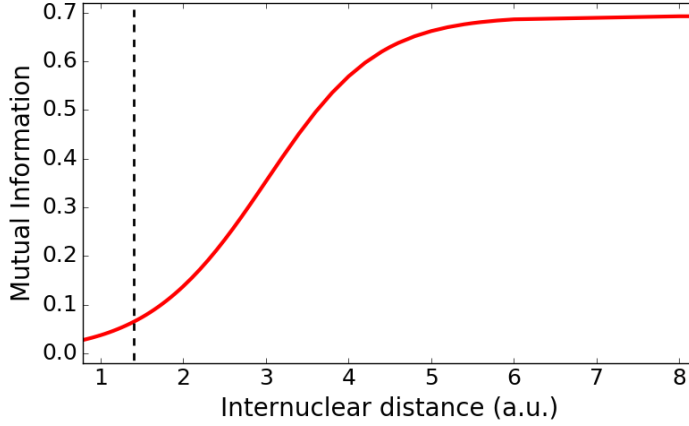


Figure 8.2: Dependence of the mutual information on the internuclear distance using MOs. The black dashed line indicates the equilibrium geometry.

8.2.2 Entanglement in the OVB scheme

Similarly to what done for the MO scheme, the wave function of H₂ may be rewritten, in OVB, as:

$$\Psi_{\text{GS}}^{\text{OVB}} = \lambda \frac{\|\mathbf{a}\bar{\mathbf{b}}\| + \|\mathbf{b}\bar{\mathbf{a}}\|}{\sqrt{2}} + \sqrt{1-\lambda^2} \frac{\|\mathbf{a}\bar{\mathbf{a}}\| + \|\mathbf{b}\bar{\mathbf{b}}\|}{\sqrt{2}} \quad (8.13)$$

In this way there is only one coefficient to be taken into account, but it should be noted that this λ is different from the one used in the MO scheme.

The diagonal elements (eigenvalues) of the one-orbital RDM are reported in Table 8.2. In this case, all the diagonal elements are non-vanishing because all possible orbital occupations are represented in the wave function. Moreover, due to the molecular symmetry, the values are the same for the two orbitals.

Table 8.2: Diagonal elements (eigenvalues) of the one-orbital Reduced Density Matrix for H₂ using OAOs.

	a	b
$ \bar{\downarrow}\rangle$	$(1-\lambda^2)/2$	$(1-\lambda^2)/2$
$ \uparrow\rangle$	$\lambda^2/2$	$\lambda^2/2$
$ \bar{\uparrow}\rangle$	$\lambda^2/2$	$\lambda^2/2$
$ \uparrow\bar{\downarrow}\rangle$	$(1-\lambda^2)/2$	$(1-\lambda^2)/2$

As in the case of MOs, it is trivial to obtain the one-orbital entropies:

$$s(1)_a = s(1)_b = -\lambda^2 \ln\left(\frac{\lambda^2}{2}\right) - (1-\lambda^2) \ln\left(\frac{1-\lambda^2}{2}\right) \quad (8.14)$$

For what concerns the two-orbital RDM, the same considerations made for the MO case still hold, with the only difference that there are more non-vanishing elements involving singly occupied orbitals:

$$\text{RDM}(2) = \frac{1}{2} \begin{bmatrix} |-\uparrow\uparrow\rangle & |\uparrow\uparrow\rangle & |\uparrow\downarrow\rangle & |\downarrow\downarrow\rangle \\ 1-\lambda^2 & \lambda\sqrt{1-\lambda^2} & -\lambda\sqrt{1-\lambda^2} & 1-\lambda^2 \\ \lambda\sqrt{1-\lambda^2} & \lambda^2 & -\lambda^2 & \lambda\sqrt{1-\lambda^2} \\ -\lambda\sqrt{1-\lambda^2} & -\lambda^2 & \lambda^2 & -\lambda\sqrt{1-\lambda^2} \\ 1-\lambda^2 & \lambda\sqrt{1-\lambda^2} & -\lambda\sqrt{1-\lambda^2} & 1-\lambda^2 \end{bmatrix} \begin{matrix} |-\uparrow\uparrow\rangle \\ |\uparrow\uparrow\rangle \\ |\uparrow\downarrow\rangle \\ |-\downarrow\downarrow\rangle \end{matrix} \quad (8.15)$$

Diagonalizing this matrix, one obtains the eigenvalues $\omega_{1,a,b} = \omega_{3,a,b} = 0$ and $\omega_{4,a,b} = 1$, that, according to Equation 2.124, give a two-orbital entropy of:

$$s(2)_{a,b} = 0 \quad (8.16)$$

exactly as in the Molecular Orbital scheme. Even in this case, the result is not surprising: any orbital occupation is totally determined at each internuclear distance, depending only on the value of the coefficient λ . The mutual information, $I_{a,b}$, is then easily obtained as:

$$I_{a,b} = -[\lambda^2 \ln(\lambda^2) + (1-\lambda^2) \ln(1-\lambda^2)] + \ln(2) \quad (8.17)$$

It is interesting to note that the value of the entanglement between orbitals a and b is the same as the one between orbitals σ_g and σ_u (Equation 8.12), shifted by $\ln(2)$. This shift ensure that at dissociation, when the coefficient λ is equal to 1, the entanglement is $I_{a,b} = \ln(2)$, as in the case of the MO scheme.

The dependence of the mutual information on the internuclear distance is reported in Figure 8.3, both for MOs and OAOs. As one can see, the OAOs shows a monotonically decreasing behavior when increasing the nuclear distance, while for the MOs the function is increasing. Both curves converge at dissociation to the limit of $\ln(2)$, but at the equilibrium geometry the entanglement patterns are completely different. Indeed, using localized orbitals, at the equilibrium the mutual information is almost at its maximum, while for delocalized orbitals it is at its minimum. This behavior highlights the differences between the two wave functions: using MOs, at the equilibrium the system is well described even with the sole $\|\sigma_g \bar{\sigma}_g\|$ determinant; using OAOs, instead, the bond is well described only if both the neutral and ionic determinants are taken into account and the wave function results less compact. At dissociation, the situation is reversed: with MOs, one needs both determinants to describe the separating atoms, while with OAOs the wave function is represented only by the two neutral determinants.

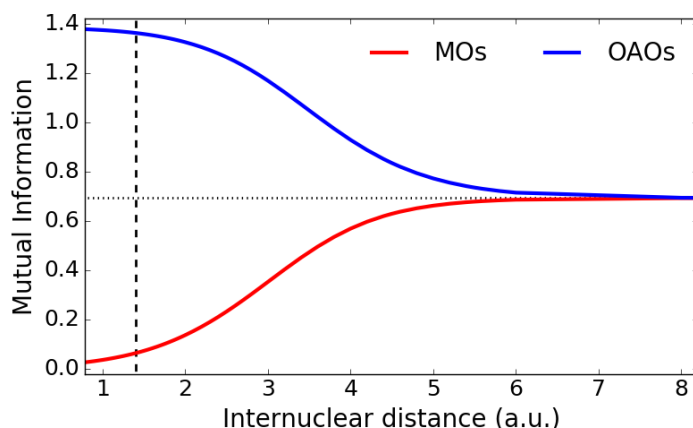


Figure 8.3: Dependence of the mutual information on the internuclear distance using MOs and OAOs for H_2 at the CASSCF(2, 2) level. The black dashed vertical line indicates the equilibrium geometry, the black pointed horizontal line indicates the limit value $\ln(2)$.

8.3 ENTANGLEMENT FOR MORE COMPLEX WAVE FUNCTIONS

For the minimal valence description of H_2 the entanglement properties can be calculated by hand starting from the coefficients of the various wave functions, thus leading to analytical expressions for the mutual information such as Equations 8.12 and 8.17. For larger systems and more complex wave functions, it is not straightforward to obtain analytical expressions, but it is possible to extend this approach and numerically calculate the mutual information between two orbitals. This is done estimating the contribution of each determinant of the wave function to the elements of the one- and two-orbital RDM. For each orbital/pair of orbitals, the diagonal elements are obtained as a sum of the squared coefficients (the weights) of all the determinants which present a certain occupation for that specific orbital/pair of orbitals. For the off-diagonal elements, instead, one simply takes the sum of the product of the coefficients of the two determinants involved.

To automatize this task, a new code has been developed during this PhD thesis, and it has been interfaced both with the CASDI program package (113, 114) and the Quantum Package (139). In the following the entanglement analysis of H_2 in a Full-CI scheme and other more complex systems such as F_2 , N_2 , Cr_2 and decapentene is discussed.

8.3.1 Entanglement in H_2 using Full-CI

Using a full configuration interaction scheme (Full-CI) for the study of the H_2 molecule, the numbers of orbitals, in the chosen basis set, becomes 28, and the number of determinants increases from 4 to 784.

The most important determinants, however, remain the same as in the CASSCF(2, 2), which covers, for both MOs and OAOs, more than the 99% of the wave function for any internuclear distance.

The MOs used in the Full-CI calculation are the same obtained at the CASSCF(2, 2) level, while the OAOs are obtained with a localization method that maximize the overlap with the basis functions, with the exception of orbitals a and b, which are maintained as the ones used in the CASSCF(2, 2) calculation.

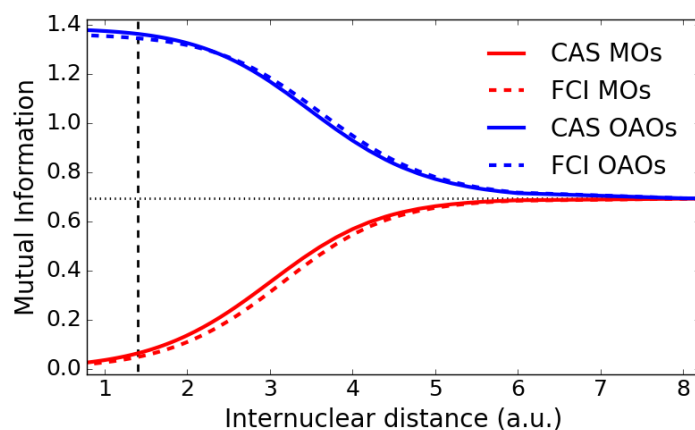


Figure 8.4: Dependence of the mutual information on the internuclear distance using MOs and OAOs for H_2 : comparison between CASSCF(2, 2) and Full-CI (between the most important orbitals, see text). The black dashed vertical line indicates the equilibrium geometry, the black pointed horizontal line indicates the limit $\ln(2)$.

The mutual information between the most important orbitals (σ_g and σ_u for MOs; a and b for OAOs) is reported in Figure 8.4 as a function of the internuclear distance. As one can see, the results obtained using Full-CI and CASSCF(2, 2) are almost the same. This confirms the fact that the physics of the system is already well described at the CASSCF level and the dynamic correlation introduced with the Full-CI does not affect the wave function and the orbital occupation in a qualitative way. The mutual information between the other orbitals is very small and not relevant for this analysis.

8.3.2 Entanglement in F_2

The electronic configuration of fluorine is $1s^2 2s^2 2p^5$ and the bond of the F_2 dimer can be described by a minimal valence CASSCF(2, 2), in which the two unpaired electrons occupy the two p_z orbitals facing each others (OVB scheme) or combinations of them such as σ and σ^* (MOs scheme). The wave functions obtained with these approaches closely resemble those of H_2 and one may refer to Equa-

tions 8.9 and 8.13. For the CASSCF calculation, an ANO-L basis set with contraction (14s9p4d3f)/[4s3p2d] has been used.

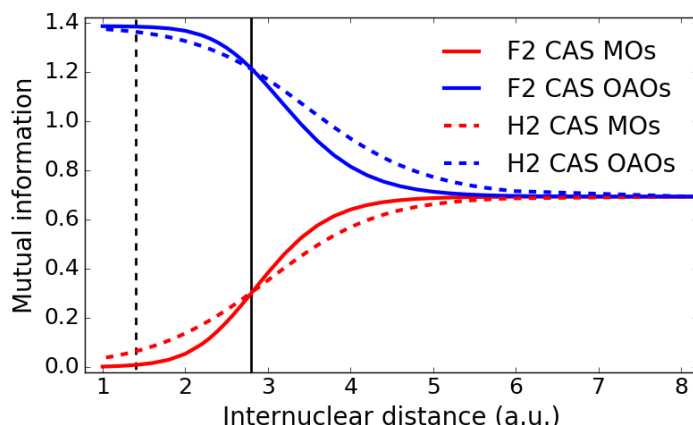


Figure 8.5: Dependence of the mutual information on the internuclear distance using MOs and OAOs for both F_2 and H_2 dimers. CASSCF(2, 2). The black solid and dashed vertical lines indicate the equilibrium geometry for F_2 and H_2 , respectively.

The mutual information between the active orbitals, both for MOs and OAOs, is reported in Figure 8.5 as a function of the internuclear distance. For the sake of comparison, the same properties are reported also for H_2 . As one may see, the entanglement behavior of F_2 is really similar to that of H_2 , reflecting the similarities in the wave functions. However, the equilibrium distance of F_2 is much greater than in H_2 (2.8 vs 1.4 a.u.), and it appears clearly that at the equilibrium the two systems present a different neutral/ionic (and therefore bonding/anti-bonding) coefficients ratio. For instance, in the MOs scheme, the mutual information between σ and σ^* at the equilibrium distance is higher than the corresponding entanglement between the two MOs of H_2 (at its equilibrium geometry). This is due to the fact that the F_2 wave function is less compact at the equilibrium, that is, the determinant involving the anti-bonding orbital has a higher coefficient, while for H_2 the wave function is dominated by the $\|\sigma_g \bar{\sigma}_g\|$ determinant. In other words, at the CASSCF(2, 2) level of calculation, F_2 has a more neutral nature than H_2 . This is evident from the OAOs scheme, where the mutual information for F_2 is lower than for H_2 (at the corresponding equilibrium geometries) because of the lowering of the coefficient of the ionic determinant with respect to the neutral (one should remember that, at the dissociation limit, only the neutral determinant has a non-vanishing weight while at closer distances, the weights of the neutral and the ionic determinants tend to be the same).

8.3.3 Entanglement in N_2

The N_2 dimer consists in a triple bond formed by the three unpaired p electrons owned by each atom. A CASSCF(6, 6) treatment furnishes a good approximation for the study of this system. An ANO-L basis set with contraction (14s9p4d3f)/[4s3p2d] has been used.

In a OVB scheme, the σ bond is formed between the two electrons occupying the two p_z atomic orbitals, aligned with the internuclear axis of the dimer. The other two are π bonds formed between the equivalent p_x and p_y atomic orbitals, orthogonal to the internuclear axis. In a MOs scheme, the p atomic orbitals are instead combined in-phase or out-of-phase to obtain a bonding and anti-bonding pair of σ and two bonding and anti-bonding pairs of π orbitals.

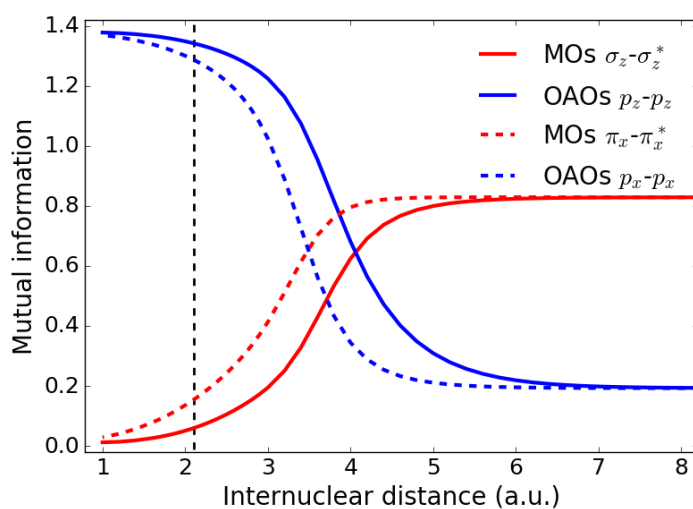


Figure 8.6: Dependence of the mutual information on the internuclear distance using MOs and OAOs for N_2 . CASSCF(6, 6). The black dashed vertical line indicates the equilibrium geometry. y orbitals are not reported but have the very same behavior of x.

The mutual information between the two orbitals expanded on the same atomic orbitals is reported in Figure 8.6 as a function of the internuclear distance. The general behavior is similar to H_2 and F_2 : the entanglement between OAOs decreases when the bond is stretched and the one between MOs increases. The main difference lays in the fact that at infinite distance the two functions does not converge to the same value of $\ln 2$ but to about 0.8 for MOs and 0.2 for OAOs.

For the OAOs case, this can be easily related to the nature of the ground state of the N atoms (4S). At $R = \infty$, the wave function describing the singlet coupling of two spins with $S = 3/2$ has for each OAO $S(1) = \ln 2$, while for a couple of OAOs on different atoms, one may demonstrate that $s(2)_{a,b} = -[(3/9) \ln (1/9) + (2/3) \ln (2/3)]$, thus

$I_{ab} = \ln 2 - s(2)_{a,b}/2 = 0.191788$. A similar derivation for two OAOs on the same atom leads to $s(2)_{a,a'} = \ln 3$ and $I_{aa'} = 0.143841$.

It should be noted that the curves corresponding to the σ bond (solid lines) are shifted with respect to the ones corresponding to the π bonds (dotted lines). This is due to the different spatial extent of the orbitals involved in the bond. Indeed, starting at $R = \infty$ and approaching the two atoms, the orbitals contributing to the π bonds start interacting (overlapping) at shorter internuclear distances than those describing the σ bond.

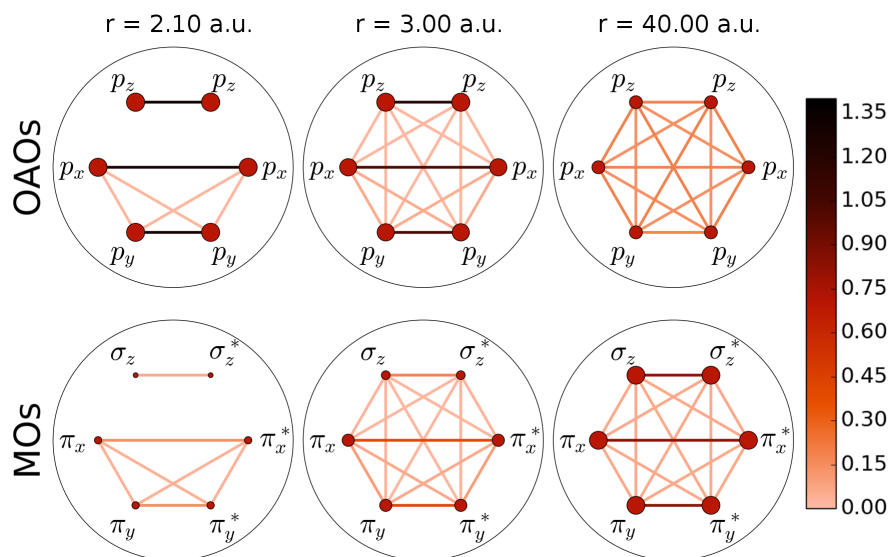


Figure 8.7: Entanglement maps for N_2 , CASSCF(6, 6), at different internuclear distances, both for MOs and OAOs. The color of the lines between the orbitals indicates the amplitude of the mutual information, the size of the red circles is proportional to the one-orbital entropy.

The use of “entanglement maps” represents an alternative way to visualize the mutual information between different orbitals, in addition to their respective one-orbital entropy. Figure 8.7 represents some entanglement maps for N_2 at different internuclear distances, both for MOs than for OAOs. The color of the lines connecting two orbitals indicates the amplitude of the mutual information and the size of the circles around each orbital is proportional to its one-orbital entropy.

For what concerns the OAOs, one may see that at the equilibrium geometry (2.10 a.u.) there is a strong entanglement between the p atomic orbitals of the same symmetry, corresponding to the three bonds. Moreover, the p_x and p_y localized on both atoms are weakly entangled with each others. Stretching the bonds (3.00 a.u.), also the p_z starts to be weakly entangled with the p_x and p_y . At a very large distance (40.00 a.u.), all orbitals present weak entanglement with each others, and the one-orbital entropy is decreased with respect to the equilibrium geometry.

Looking at the MOs, the behavior is reversed. At the equilibrium geometry there is a small entanglement between corresponding pairs of bonding/anti-bonding orbitals, that gradually increases with the distance. Even the one-orbital entropy shows the same pattern, small at the equilibrium and large when the bond is stretched.

8.3.4 Entanglement in Cr_2

The chromium molecule is one of the most challenging dimers in quantum chemistry, being formed by two atoms with 6 unpaired electrons each (the chromium electronic configuration is $[\text{Ar}]3d^54s^1$). The minimal valence CASSCF(12, 12) is not sufficient to well describe its bond and a more sophisticated method is required, such as multireference perturbation theory or DMRG with a large active space. However, the potential energy curve obtained with the CASSCF(12, 12), although not being a binding curve, shows a *shoulder* around the area where the real minimum is expected. Therefore, some hints on how the bond is formed can be obtained from the entanglement maps even at this low level of calculation.

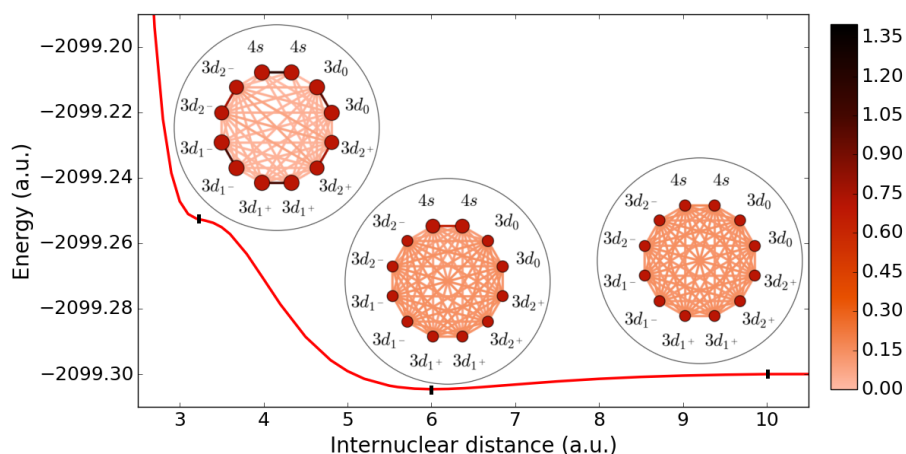


Figure 8.8: Entanglement maps for Cr_2 using orthogonal atomic orbitals at different internuclear distances. CASSCF(12, 12).

The entanglement maps for Cr_2 using orthogonal atomic orbitals and molecular orbitals are reported in Figures 8.8 and 8.9, respectively. An ANO-RCC basis set with contraction $(21s15p10d6f4g2h)/[10s10p8d6f4g2h]$ has been employed and the Douglas-Kroll Hamiltonian has been used for the integral calculation. The maps correspond to three different positions in the potential energy curves: 3.2 a.u., corresponding to the shoulder; 6.0 a.u., corresponding to a small minimum; and 10.0 a.u.

Using orthogonal atomic orbitals, at 10.0 a.u., all orbitals are slightly entangled with each others and the one-orbital entropy is the same, and equally small, for all the orbitals. At 6.0 a.u. it appears clear that the minimum is due to the approaching of the 4s orbitals forming

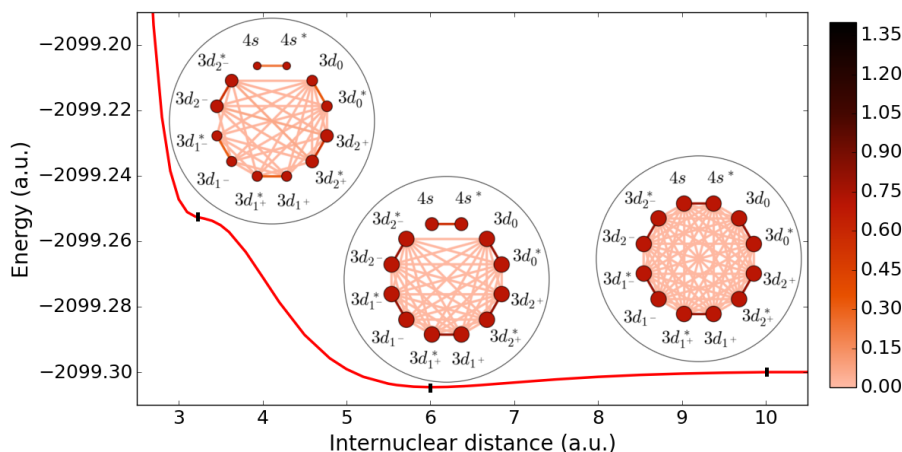


Figure 8.9: Entanglement maps for Cr_2 using delocalized orbitals at different internuclear distances. CASSCF(12, 12).

a σ bond, given that their mutual entanglement and the one-orbital entropies increase. This is not unexpected considering the wider spatial extent of the 4s orbitals with respect to the 3d ones. At 3.2 a.u., finally, even the entanglement between the corresponding pairs of 3d orbitals becomes noticeable, giving an hint of the expected sextuple bond (140).

Using molecular orbitals, the picture is not as clear as with orthogonal atomic orbitals, due to the presence of lots of small entanglements without a recognizable and significant pattern.

8.3.5 Entanglement in decapentaene

Finally, the entanglement maps for decapentaene with three different orbital sets has been analyzed, as an example of the insights that can be extrapolated from entanglement for more complex and large molecules. Decapentaene, $\text{C}_{10}\text{H}_{12}$, belongs to the series of all-trans conjugated linear polyenes that has received lot of attention since the dawn of Quantum Chemistry, being a model for the study of more complex delocalized system. The same simplified geometry used in Chapter 4 has been used, with all the 5 π bonds considered to be equal, at a distance of 1.35 a.u., and the single bonds at 1.45 a.u. The angles, both C-H than C-C, are all of 120 degrees. The calculations have been performed at the full-valence CASSCF(10, 10) level, using an ANO-L basis set with contraction (14s9p4d3f)/[4s3p1d] for the Carbon atoms and (8s4p3d)/[2s1p] for the hydrogen.

Three orbitals sets have been considered: the symmetry adapted delocalized molecular orbitals (DMOs); the orthogonal atomic orbitals (OAOs), obtained localizing the DMOs on the p_z atomic functions; and the localized bond molecular orbitals (LMOs), obtained combining the OAOs, in-phase and out-of-phase, for each π bond (see Chapter 4 for more details).

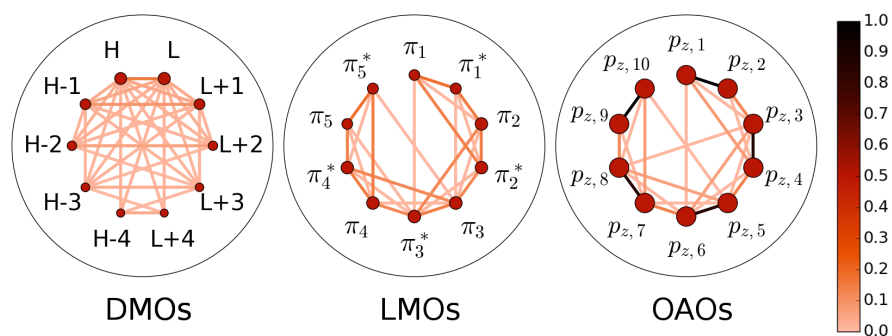


Figure 8.10: Entanglement maps for decapentaene using three different orbital sets: delocalized molecular orbitals (DMOs), localized molecular orbitals (LMOs) and orthogonal atomic orbitals (OAOs). CASSCF(6, 6).

Figure 8.10 shows the entanglement maps obtained with the three different orbital sets. In the DMOs scheme, the entanglement maps consists of a lot of small contributions. It is clear that the more important orbitals are the HOMO and the LUMO (marked with H and L, respectively), which have a larger one-orbital entropy and shows a larger entanglement between each others, as expected. The LMOs scheme is more intuitive from a chemists point of view: there is a strong entanglement between $\pi - \pi^*$ pairs of orbitals, that stands for the electron correlation internal to each double bond. In addition, each π orbital is strongly entangled with the adjacent π^* orbital, representing the charge delocalization between conjugated pairs of double bonds. Finally, with OAOs, all the atomic orbitals show a large one-orbital entropy and a strong entanglement is present between orbitals involved in a double bond. These results are in complete agreement with the OVB analysis of the wave function reported in Chapter 4, where the most important OVB structures, besides the Lewis structure, are the IC determinants (double excitations on a given double bond) and the CT determinants (single excitations from a given π orbital to the neighbor π^* orbitals). One should note that, both for LMOs and OAOs, the entanglement maps are more compact than for DMOs and allow one to get an immediate qualitative idea about the wave function.

IMPROVING THE DMRG EFFICIENCY WITH ORBITAL LOCALIZATION

In this chapter, the dependence of the efficiency of the density matrix renormalization group (DMRG) approach on the nature of the orbitals is reported for the case of the full valence description of linear polyenes. The standard (delocalized) molecular orbitals and two sets of localized orbitals are considered: orthogonal atomic orbitals (OAOs) and localized molecular orbitals (LMOs). It is shown that using localized orbitals improves considerably both the convergence rate of the energy together with the ability of the DMRG algorithm to reach the correct target value. More precisely, it is found here that the use of LMOs, which follows the chemical description of a conjugated π system, makes DMRG particularly efficient.

9.1 INTRODUCTION

As already stated in several chapters of this work, an important property of a FCI eigenfunction is its invariance under a unitary transformation of the one-electron basis (often identified with the molecular orbitals, MOs) with which it is computed. It is worth stressing that such an invariance concerns the wave function and, therefore, all its properties, such as, for instance, the energy. Obviously, the representation of a FCI eigenfunction depends on the chosen basis for the Hilbert space, but the eigenfunction itself does not.

The CASCI (possibly CASSCF) approach, being a FCI strategy in a restricted set of MOs, benefits from a similar invariance property, provided that the unitary transformation is restricted to the active orbitals. Actually, one can show that these wave functions are invariant also for unitary transformations among the doubly occupied MOs, but this aspect is not relevant for the present study.

The use of orthogonal localized orbitals obtained by a unitary transformation of the standard delocalized orbitals in the framework of the wave function approaches has been exploited in details in the above chapters, in a strategy aiming at providing an analysis of the wave function in terms of Valence Bond-like (VB) structures recalling the Lewis description of the molecular architecture. Moreover, it is well known that the use of localized MOs in a wave function frame allows for a more compact description of the wave function, for an increased computational efficiency, and for the possibility to take advantage of the locality of the MOs for a rational selection of the Slater determi-

nants to be considered in calculations trying to approach the linear scaling limit.

The aim of this paper is to investigate how the choice of the starting MOs affects the convergence rate of the DMRG approach and to verify if one can take benefit from the flexibility offered by the starting MO basis to improve the computational efficiency. In particular, it is interesting to check how the use of localized orbitals, which are able to reconcile quantum chemistry with the chemical description of a molecule, can improve the efficiency of the DMRG algorithm.

9.2 THE DENSITY MATRIX RENORMALIZATION GROUP

Density matrix renormalization group (DMRG) has been developed by S. White in 1992 (14) in the field of condensed matter physics, where nowadays it is considered one of the most efficient techniques. Later it has been applied to quantum chemistry problems (15) and since then it has received an increasing attention from the chemistry community, due to its ability to treat very large systems at a very high level of accuracy. It is indeed often compared to an approximate CASSCF treatment able to considerably extend the dimension of the active space.

In this chapter, the efficiency of DMRG is analyzed with respect to the use of different sets of localized orbitals and the technique is used almost as a *black box*. Thus, for these purposes it is not necessary to dive into the complexity of this theory and the curious reader is referred to other sources (such as the comprehensive review of U. Schollwöck, (16)). Therefore, only a very short introduction to this techniques is reported hereafter.

In the DMRG formalism, the wave function may be written as a linear combination of Slater determinants using matrix product states (MPS):

$$|\Psi\rangle = \sum_{\sigma} M^{\sigma_1} M^{\sigma_2} \dots M^{\sigma_L} |\sigma\rangle \quad (9.1)$$

where the coefficients of the linear combination are encoded in the matrix product. Here, L is the number of orbitals and $|\sigma\rangle$ is the occupation number vector which refers to all the possible orbital occupations. For each orbital there is a set of four possible matrix corresponding to its four possible occupations (empty, with an α or β electron, and doubly occupied) and the CI coefficients are obtained from the contraction of the matrices via matrix-matrix product. In the DMRG jargon, an orbitals is referred to as a *site*.

Then, the DMRG consists in an iterative procedure where the matrices of orbital sites are variationally optimized with respect to the energy. The particularity of this scheme is that not all the sites (their

matrices) are optimized at the same time, but only the *active sites* (here corresponding to two sites at a time). Then, the matrices of these two sites are updated in accordance to the variational procedure and other two sites are taken into account as active sites. This task is repeated for all the sites, from left to right and vice-versa (the so-called *sweeping*) until convergence is reached.

Several parameters affect the result of a DMRG calculation, for instance, the ordering of the sites, the starting orbitals and so on. A central parameter is surely the maximum dimension m that a matrix may assume, which basically controls the precision of the results. Indeed, if m is large enough, that is, if it is equal to the Hilbert space dimension of the system, DMRG becomes equal to the Full CI technique. Anyway, usually very low values of m are sufficient in order to get very accurate energies and wave functions. It must be reported that the m parameter is often referred to as the number of renormalized basis states or as the number of the block states and that the number of variational parameters corresponds to $16m^2$.

In the following, the accuracy of DMRG is analyzed using different sets of molecular orbitals and different values of the m parameter.

9.3 COMPUTATIONAL DETAILS

The geometrical parameters of the *all-trans* polyenes studied in this work are chosen to be fixed at standard values. Indeed, the purpose is here to compare different strategies to perform a given calculation rather than to have results comparable with the experimental findings. For this reason, reasonable standard geometries are adequate to describe our systems. Accordingly, as done in the preceding chapters, all single C-C bond lengths are fixed to 1.45 Å, the double C-C bonds to 1.35 Å, the C-H bond lengths to 1.08 Å and all CCH and CCC angles to 120°. The molecule lies in the xy plane.

For all calculations, the Atomic Natural Orbital (ANO) basis sets (141) is used. The carbon atoms are represented by the ANO-L basis set with the contraction (14s9p4d)/[4s3p1d], while the contraction (8s4p)/[2s1p] is used for the hydrogen atoms.

The CASSCF calculations are performed using the MOLCAS 7.8 program package. DMRG results are obtained using the development version (year 2014) of the QCMAquis program package (142). The active space contains all π orbitals and electrons (full π active space). The localized orbitals are obtained from the CASSCF delocalized orbitals using a procedure developed and implemented in the Theoretical Chemistry group of the University of Ferrara. The details of this procedure are described in the section 9.4.

9.4 ORBITAL LOCALIZATION

With the aim of analyzing the effect of the orbital localization on the computational performances of the DMRG procedure, we explore two different kinds of localized orbitals, namely the localized molecular orbitals and the orthogonal atomic orbitals. In both cases they are obtained by a unitary transformation of the full valence delocalized CASSCF active orbitals. Indeed, as said, the CASSCF wave function and its properties are invariant with respect to an arbitrary orbital rotation within each orbital class (doubly occupied, active, and virtual). Hereafter, only the active orbitals are localized and this transformation is achieved maximizing, with the constraint of orthogonality on the final orbitals, the overlap of the transformed orbitals with a set of reference strongly localized orbitals (possibly not orthogonal).

In the present case (conjugated *all-trans* polyenes) the LMOs consist of pairs of bonding and anti-bonding π -orbitals localized on the double bonds of the chain. Their reference functions in the localization procedure are the in-phase and out-of-phase combinations of the $2p_z$ basis functions centered on the carbon atoms involved in the double bond. The OAOs, instead, consist in orthogonal p_z orbitals localized on the carbon atoms and their references are simply the p_z basis functions of the corresponding atoms.

For both the LMOs and the OAOs, it is worth stressing that, even if they are local, they are of CASSCF quality and they are optimized in the molecular reality. In this regard they are of higher quality than, for instance, OAOs obtained by a simple orthogonalization of the strictly atomic orbitals.

9.5 RESULTS AND DISCUSSION

In what follows, the DMOs, LMOs, and OAOs are used as the MO basis for a DMRG calculation in which a Full CI is performed within the full- π active space. As the LMOs and OAOs are obtained from the CASSCF DMOs by a unitary transformation within the active space, the DMRG algorithm should formally provide the CASSCF wave function and therefore the CASSCF energy.

The analysis of the calculations performed here on the all-trans conjugated polyenes of increasing size has shown that the effect of the MOs used is meaningful only for the largest systems. Indeed, indicating with n the number of double bonds in the chain, for values of n lower or equal to five the convergence rate of the DMRG energy is very fast and the DMRG procedure reaches the CASSCF energy both with localized and delocalized orbitals. This behaviour was also observed for small values of the m parameter, which clearly indicates that the localization of the MOs does not affect the DMRG convergence rate for small polyenes.

For values of n larger than five, instead, the differences between the use of localized and of delocalized orbitals become more significant, in particular for what concerns the dependence of convergence rate of the energy on the m parameter.

Nevertheless, the request to perform the CASSCF step (required to compute the delocalized orbitals) forces n to be not too large, the limiting value being 8-9. It is worth noticing that this limitation comes from the computational scheme here conceived (use of MO sets of CASSCF quality) and it is not inherent to the DMRG step, for which much larger active spaces are assailable.

In the following we focus on the polyene with 7 double bonds ($C_{14}H_{16}$). The other systems of the conjugate polyenes series give very similar results. The delocalized orbitals are obtained from a CASSCF(14,14) calculation. If the molecular symmetry is not considered, the CAS space contains more than 11 million determinants. Using the CASSCF canonical delocalized molecular orbitals (DMOs), the DMRG method requires quite a large number of preserved states (the m parameter) to achieve the target energy. Indeed, in order to reach the CASSCF energy up to the 6th digit, m must be equal to or larger than 7168, which, for the system under study, implies a rather expensive computational effort. The convergence of the DMRG energy using the three types of MOs here considered and a value of the m parameter set to 7168 is reported in Figure 9.1.

In this calculation, a DMRG *sweep* (back and forth) consists in 26 microiterations. As it is apparent from Figure 9.1, in the first microiterations the energy is lower using the DMOs (ordered following an energy criterion), while with the localized ones (both LMOs and OAOs) the energy is much higher. This behavior has been observed with all values of m and it indicates that the delocalized nature of the orbitals ("sites" in the DMRG language) allows a better representation of the system at the very beginning of the DMRG procedure. In the contrary, with LMOs and OAOs, the sites are obviously localized and only a portion of the molecule is correctly taken into account during the first microiterations, thus requiring a complete sweep to lower the energy. However, already after the first sweep, the DMRG energy is lower with the localized orbitals (with the LMOs giving values lower than the OAOs) than with the DMOs. Eventually, with the delocalized orbitals the energy achieves the CASSCF value after almost two sweeps, while with localized orbitals, especially with LMOs, the convergence is faster and it occurs just after a single sweep.

It is important to point out that the use of localized orbitals, besides reducing the number of microiterations required to reach the convergence, is also cheaper from a computational point of view. Indeed, using LMOs and OAOs the average DMRG single sweep is more than ten times faster than in the case of DMOs.

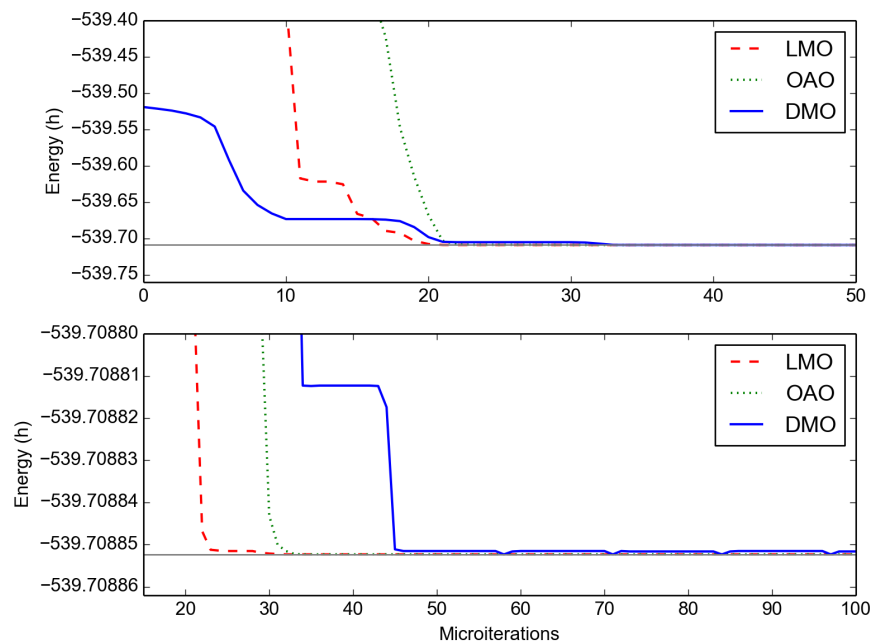


Figure 9.1: Polyene with $n = 7$, convergence of the DMRG method ($m = 7168$) with different orbital sets (DMOs, LMOs, and OAOs) as a function of the number of microiterations. The upper panel reports the full convergence trend, while the lower panel shows a zoom in the energy axis close to the convergence value. The horizontal line indicates the CASSCF energy.

Moreover, the better performances of LMOs and OAOs with such a large value of m (7168) do not fully account for the benefits one can have with a localized MO basis. Indeed, the number of preserved states required to converge to the CASSCF energy (up to the 6th digit) is different for the various MO sets. Using LMOs, the smallest value of m for which one obtains the CASSCF energy is 128, while for OAOs it is 64. For instance, in the case of OAOs the calculation with m equal to 64 is again ten times faster than the one with 7168 and the same set of orbitals. Therefore, one may say that, at least for the system under analysis, using a set of localized MOs is more than 100 times faster than using canonical orbitals. In the context of optimization of the computational efficiency of the DMRG algorithm, such results appear to be important.

The convergence behaviors for the three sets of orbitals with $m = 128$ and $m = 64$ are shown in Figures 9.2 and 9.3, respectively. In the former case, the lowest energy achieved with DMOs shows an error on the second decimal digit compared to the CASSCF value, while with both OAOs and LMOs the DMRG energy converges to the right value. With $m = 64$, the DMOs behaves even worse, with the energy reaching a value $\simeq 0.03$ a.u. far from the CASSCF reference. On the contrary, with LMOs and OAOs the error is on the sixth digit.

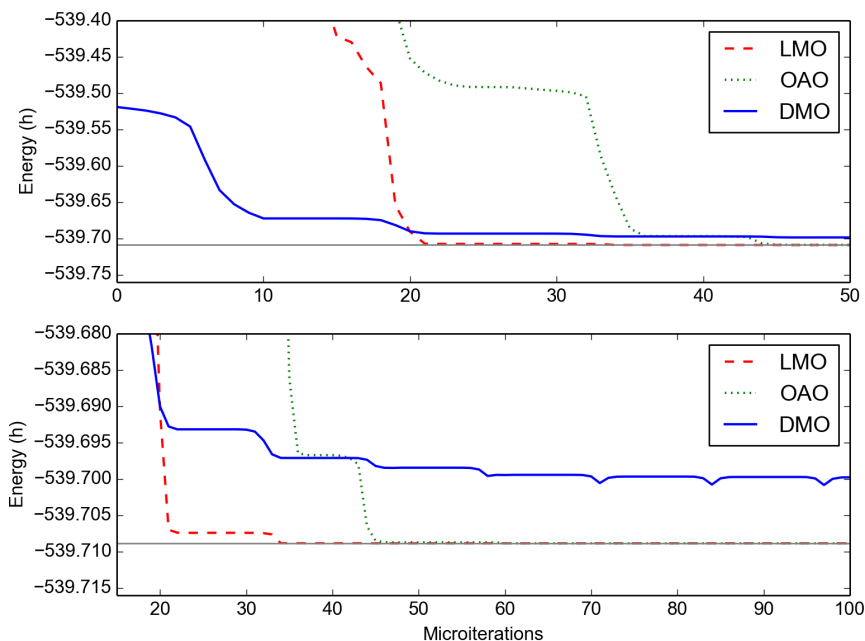


Figure 9.2: Polyene with $n = 7$, convergence of the DMRG method ($m = 128$) with different orbital sets (DMOs, LMOs, and OAOs; see text) as a function of the number of microiterations. The upper panel reports the full convergence trend, while the lower panel shows a zoom in the energy axis close to the convergence value. The horizontal line indicates the CASSCF energy.

It is worth noticing that in all cases the convergence of the DMRG energy with delocalized orbitals shows a “saw-tooth” shape, with the lowest energy reached only for a few iterations, while in the other iterations a higher value is computed. This effect, which appears with a well defined frequency (twice a sweep), is due to the inadequacy of the m states to represent the system in most of the microiterations. Even if it is rather weak, this effect is observable also with m equal to 7168, and it can be removed only considering larger values for m .

In order to summarize the results commented above, Figure 9.4 shows the convergence behaviors of the DMRG energy for the lowest value of m for which the CASSCF energy is achieved (up to the 6th digit) for each set of orbitals. As one can see, the LMOs and OAOs orbitals also manifest some kind of instability in the convergence trend of the DMRG energy, but this happens with very low values of m . As in the case of delocalized orbitals, this problem is solved using larger values of m . In all cases, however, the magnitude of this oscillation in the energy is very low given that in hartrees it concerns the sixth/seventh decimal digits.

As a final comment on the convergence trend of the DMRG energy, we want to remark that from Figure 9.4 one could think that the behaviors of the OAOs and LMOs is worse than that of the DMOs,

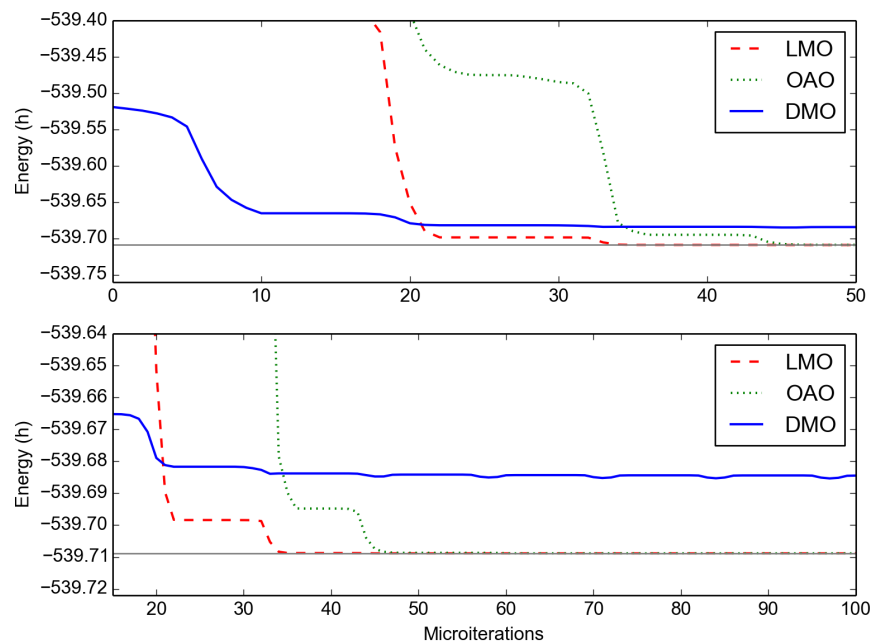


Figure 9.3: Polyene with $n = 7$, convergence of the DMRG method ($m = 64$) with different orbital sets (DMOs, LMOs, and OAOs) as a function of the number of microiterations. The upper panel reports the full convergence trend, while the lower panel shows a zoom in the energy axis close to the convergence value. The horizontal line indicates the CASSCF energy.

because with localized orbitals the target CASSCF energy is obtained with a larger number of microiterations. Actually, it is important recalling that, due to the much smaller m value, the CPU time per microiteration is much shorter when using localized orbitals.

Given the complexity of the DMRG method, it is not trivial to fully understand why with the localized orbitals such an improved convergence is observed if compared with the delocalized orbitals. One can, however, note that the *all-trans* conjugated polyenes are substantially 1D systems, and the use of localized orbitals brings back the DMRG approach to a framework similar to the solid-state physics lattices, for which this method has been initially developed.

To better clarify the consequences of the use of different orbital sets (let us stress again that they are different but fully equivalent for what concerns the final wave function) in the DMRG approach, an important information can be deduced from the entanglement measures, namely the single-orbital entropy and the mutual information (13, 17). The entanglement measures for the polyene with seven double bonds ($n = 7$) described with the DMO is reported in Figure 9.5. The single-orbital entropy is proportional to the dimension of the red circles indicating the orbitals. The (canonical) orbitals are ordered according to their energy (orbital 1 has the lowest energy, orbital 14 the

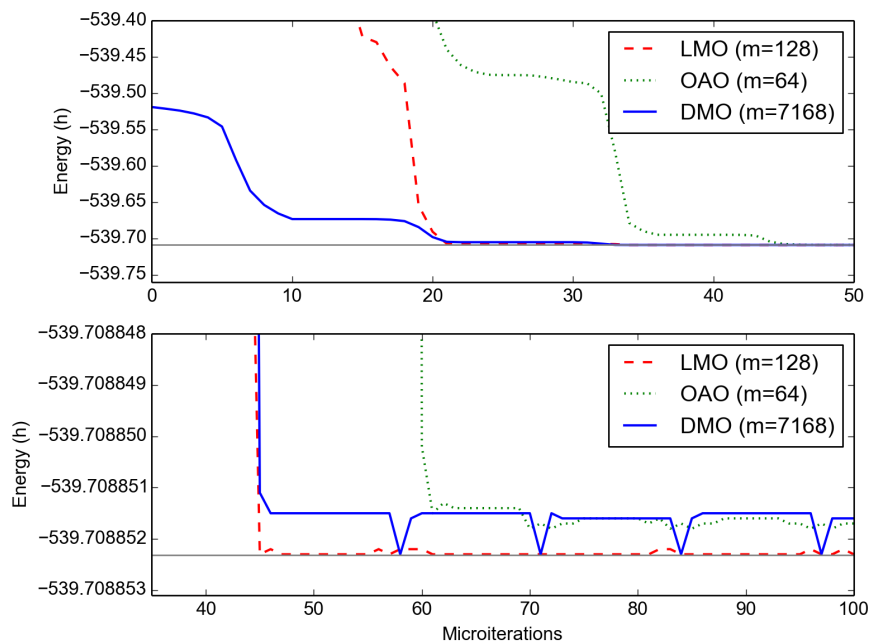


Figure 9.4: Polyene with $n = 7$, convergence of the DMRG method with the lowest m giving the CASSCF energy (up to the 6th digit) with different orbital sets (DMOs, LMOs, and OAOs) as a function of the number of microiterations. The upper panel reports the full convergence trend, while the lower panel shows a zoom in the energy axis close to the convergence value. The horizontal line indicates the CASSCF energy.

highest). In a single reference description of the system and following the *aufbau* principle (the first seven orbitals are doubly occupied, the others are empty), the single-orbital entropy is vanishing for all orbitals (the orbitals are either doubly occupied or empty). Actually, at the DMRG level it is in all cases small, with the highest values found for the HOMO and LUMO (number 7 and 8, respectively), for which a sizeable modification of the occupation numbers is expected when passing from the single determinant description to more refined wave functions. Overall, one can observe a bell shape described by the values of the single-orbital entropy, going from orbital 1 to 14. The mutual information (represented by the lines connecting two orbitals in Figure 9.5, the nature of the line is related to the value of the mutual information), instead, is quite chaotic. Indeed, it is clear that the mutual information has a medium-weak value for all couple of orbitals, with the only exception of the HOMO-LUMO couple, for which a large value is found.

Using LMOs, the entanglement measures are strongly modified, as is apparent from Figure 9.6. In this case the orbitals are ordered following a space criterion, from the left to the right side of the molecule: the orbitals with odd numbers are bonding orbitals, while

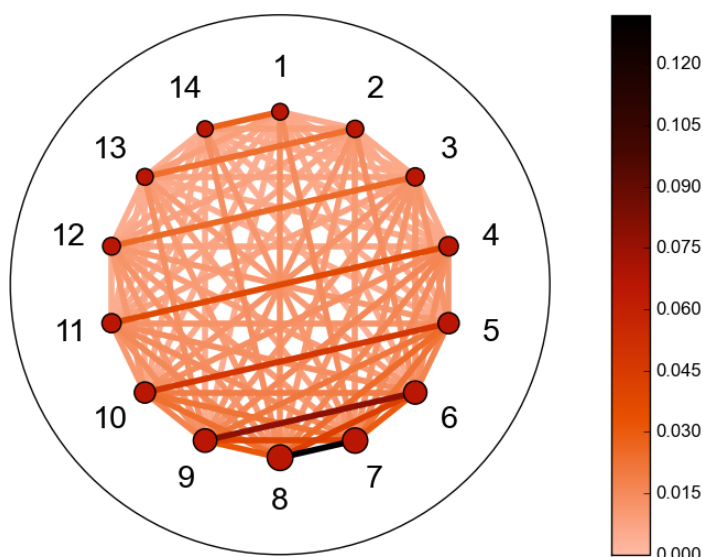


Figure 9.5: Entanglement measures for the polyene with $n = 7$ using the DMO set: the dimension of the red circles is proportional to the single-orbital entropy, while the lines connecting two orbitals indicate the mutual information (see text).

those with even numbers are the corresponding anti-bonding orbitals. The single-orbital entropies are overall larger than in the DMOs case and they have approximately the same value for each orbital. The mutual information measures show a regular pattern: each bonding orbital has a strong mutual information with the anti-bonding centered on the same double bond (like the couples 1-2, 3-4, and so forth) and with the anti-bonding orbitals localized on the adjacent bonds (like 3 with 2 and 6, 5 with 4 and 8, and so forth). These patterns give an indication of the fact that these couples are strongly involved in the electronic correlation. Indeed, in a wave function treatment based on the LMOs, one finds that the most important Slater determinants, beyond the pseudo HF one, are those obtained from it by a double excitation from a π to the π^* orbital on the same bond and by a single excitation from a π orbital to the π^* orbitals of the neighbour bonds.

The use of the OAOs, similarly to what found with the LMOs, leads to regular patterns in the entanglement measures, as apparent from Figure 9.7. The atomic orbitals are spatially ordered from the left (orbital 1) to the right (orbital 14) of the molecule. The single-orbital entropy measures are almost constant along the conjugate chain (this is also an indication of the quasi equivalence of the different carbon atoms) and their value is the largest observed in this study (even larger than that observed with the LMOs). Concerning the mutual information measures, there are more strong values and less medium-

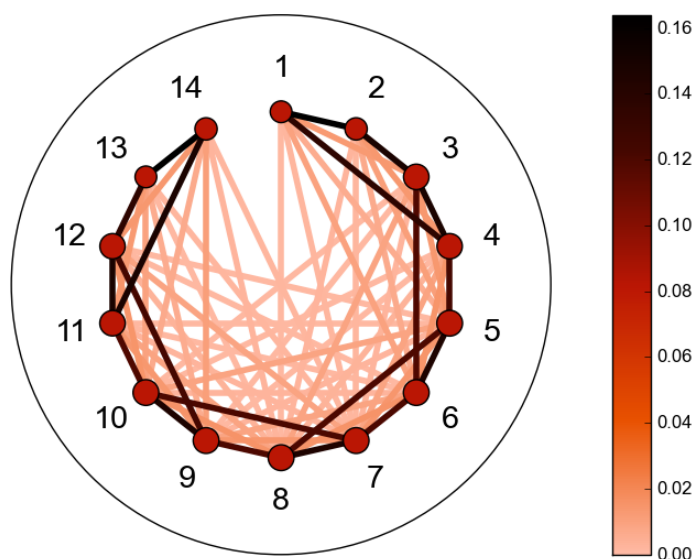


Figure 9.6: Entanglement measures for the polyene with $n = 7$ using the LMO set: the dimension of the red circles is proportional to the single-orbital entropy, while the lines connecting two orbitals indicate the mutual information (see text).

weak ones compared to what have been observed with the LMOs or the DMOs. As found with the LMOs, it is easy to give a physical interpretation to the presence of the large values of the mutual information measure: indeed, a very large value is found between a given OAO and the adjacent one when they are involved in a double bond. Orbitals involved in a single bond, instead, shows “medium” values of interaction. One should note, however, that this medium interaction can be considered as strong if compared with the mutual information plots obtained with DMOs and LMOs. Generally speaking, indeed, the mutual information values are larger when one makes use of OAOs.

In conclusion, it is straightforward to understand why the orthogonal atomic orbitals requires a lower value of m to achieve the CAS-CI energy, compared to the other localization schemes. Indeed, the description of only a portion of the molecule, implicit in the DMRG algorithm in which the system is partitioned in the active part and the environment, is more independent from the rest of the system than in a more delocalized picture, as happens with DMOs (and partially also with LMOs). The information of the system is, in a sense, more “additive” or “transferable”, that is the properties of a group of “sites” (orbitals) are less dependent on a detailed knowledge of the properties of the other sites. Obviously, when the “sites” are delocalized orbitals such a result is not expected. Moreover, using OAOs in

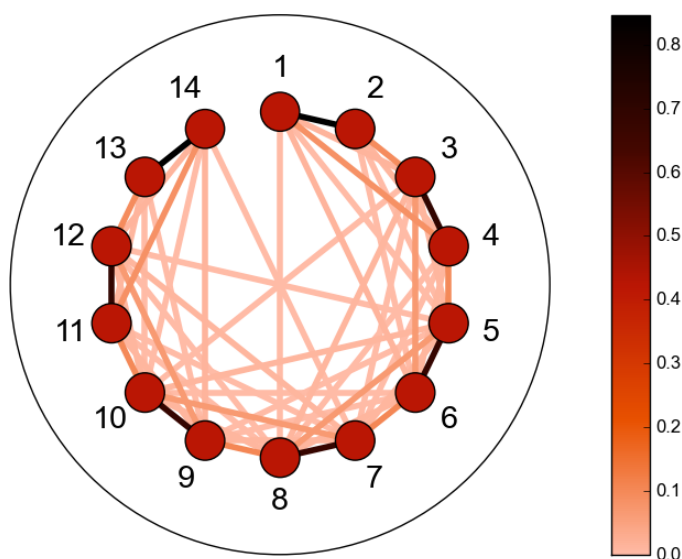


Figure 9.7: Entanglement measures for the polyene with $n = 7$ using the OAO set: the dimension of the red circles is proportional to the single-orbital entropy, while the lines connecting two orbitals indicate the mutual information (see text).

the DMRG sweep, each time a site is added to the active subsystem one is sure that this site has a strong interaction with the subsystem.

The general behavior here reported for the case $n = 7$ has been observed also for the other polyenes. A critical comparison of the polyene series confirms the superiority of the localized OAOs and LMOs (in particular the OAOs) for what concerns the convergence properties of the DMRG approach. Indeed, one can reach the correct CASSCF energy with less sweep steps and using a lower value for m (a parameter which has a marked impact on the computational cost of a single sweep step).

Moreover, a very important difference between the localized MOs and DMO case is that in the former the mutual information follows a regular pattern which is transferable from one polyene to another, while with the DMOs it is much harder to anticipate its behavior.

9.6 CONCLUSIONS

The dependence of the DMRG approach on the choice of the MO basis has been studied, focusing on the effect of the number of preserved states (the m parameter) and on the convergence speed. Among the three sets of MOs, the LMOs and OAOs have shown to be much more effective than the DMOs, both for the number of sweeps required to reach the exact energy and for the minimal value of the m

parameter for which this energy is obtained at convergence. More precisely, it has been found that the use of OAOs allows one to strongly lower the critical value of the m parameter for which the correct CAS-CI energy is recovered. These results suggest that the building of the CAS-CI wave function with the DMRG formalism is much more compact using strictly localized orbitals rather than delocalized ones. Such idea contrasts with what is found using the standard CAS-CI approaches, as in such case the wave function is much more compact using the DMOs or LMOs rather than using OAOs.

These results highlight the crucial role played by the nature of the MO basis set in the DMRG calculations and indicate strategies to further improve the efficiency of this approach.

BIBLIOGRAPHY

1. J. C. Slater, *Quantum Theory of Matter* (McGraw Hill, 1951).
2. L. Brillouin, *Actualites Scientifiques et Industrielles* **159** (1934).
3. T. Koopmans, *Physica* **1**, 104 (1933).
4. B. Levy, G. Berthier, *Int. J. Quant. Chem.* **2**, 307 (1968).
5. B. O. Roos, P. Linse, P. E. Siegbahn, M. R. Blomberg, *Chemical Physics* **66**, 197–207 (1982).
6. K. Andersson, P. A. Malmqvist, B. O. Roos, A. J. Sadlej, K. Wolinski, *The Journal of Physical Chemistry* **94**, 5483–5488 (1990).
7. K. Andersson, P.-Å. Malmqvist, B. O. Roos, *J. Chem. Phys.* **96**, 1218 (1992).
8. C. Angeli, R. Cimiraglia, S. Evangelisti, T. Leininger, J.-P. Malrieu, *J. Chem. Phys.* **114**, 10252 (2001).
9. C. Angeli, R. Cimiraglia, J.-P. Malrieu, *Chem. Phys. Lett.* **350**, 297 (2001).
10. C. Angeli, R. Cimiraglia, J.-P. Malrieu, *J. Chem. Phys.* **117**, 9138 (2002).
11. C. Angeli, S. Borini, M. Cestari, R. Cimiraglia, *J. Chem. Phys.* **121**, 4043–4049 (2004).
12. C. Bloch, *Nuclear Physics* **6**, 329–347 (1958).
13. J. Rissler, R. M. Noack, S. R. White, *Chem. Phys.* **323**, 519–531, ISSN: 0301-0104 (2006).
14. S. R. White, *Phys. Rev. Lett.* **69**, 2863–2866 (19 1992).
15. S. R. White, R. L. Martin, *The Journal of Chemical Physics* **110**, 4127–4130 (1999).
16. U. Schollwöck, *Annals of Physics* **326**, January 2011 Special Issue, 96–192, ISSN: 0003-4916 (2011).
17. K. Boguslawski, P. Tecmer, O. Legeza, M. Reiher, *J. Phys. Chem. Lett.* **3**, 3129–3135 (2012).
18. K. Boguslawski, P. Tecmer, G. Barcza, O. Legeza, M. Reiher, *J. Chem. Theory Comp.* **9**, 2959–2973 (2013).
19. C. J. Stein, M. Reiher, *Journal of Chemical Theory and Computation* **12**, PMID: 26959891, 1760–1771 (2016).
20. L. Tenti, D. Maynau, C. Angeli, C. J. Calzado, *Physical Chemistry Chemical Physics* **18**, 18365–18380 (2016).
21. Lewis, Gilbert N., *J. Am. Chem. Soc.* **38**, 762 (1916).

22. E. Majorana, *Rend. Acc. Lincei* **13**, 58 (1931).
23. C. Angeli, R. Cimiraglia, J.-P. Malrieu, *Molecular Physics* **111**, 1069–1077 (2013).
24. R. Pariser, R. G. Parr, *The Journal of Chemical Physics* **21**, 767–776 (1953).
25. R. Pariser, R. G. Parr, *The Journal of Chemical Physics* **21**, 466–471 (1953).
26. J. A. Pople, *Transactions of the Faraday Society* **49**, 1375 (1953).
27. J. Hubbard, *Proceedings of the Royal Society of London A: Mathematical, Physical and Engineering Sciences* **276**, 238–257 (1963).
28. R. K. Nesbet, in *Advances in Chemical Physics* (John Wiley & Sons, Inc., 1965), pp. 321–363.
29. C. Angeli, *Journal of Chemical Education* **75**, 1494 (1998).
30. J. Lennard-Jones, *Proceedings of the Royal Society A* **198**, 1–13 (1949).
31. J. Lennard-Jones, *Proceedings of the Royal Society A* **198**, 14–13 (1949).
32. G. Hall, J. Lennard-Jones, *Proceedings of the Royal Society A* **202**, 155–165 (1950).
33. J. Lennard-Jones, J. A. Pople, *Proceedings of the Royal Society A* **202**, 166–180 (1950).
34. L. Brillouin, *Actualites Scientifiques et Industrielles* **71** (1933).
35. G. E. Scuseria, P. Y. Ayala, *The Journal of Chemical Physics* **111**, 8330–8343 (1999).
36. N. Flocke, R. J. Bartlett, *The Journal of Chemical Physics* **121**, 10935–10944 (2004).
37. J. E. Subotnik, A. Sodt, M. Head-Gordon, *The Journal of Chemical Physics* **125**, 074116 (2006).
38. M. Kobayashi, Y. Imamura, H. Nakai, *The Journal of Chemical Physics* **127**, 074103 (2007).
39. P. Pinski, C. Riplinger, E. F. Valeev, F. Neese, *The Journal of Chemical Physics* **143**, 034108 (2015).
40. Y. Guo, K. Sivalingam, E. F. Valeev, F. Neese, *The Journal of Chemical Physics* **144**, 094111 (2016).
41. A. C. Hurley, J. Lennard-Jones, J. A. Pople, *Proceedings of the Royal Society of London A: Mathematical, Physical and Engineering Sciences* **220**, 446–455 (1953).
42. J. M. Parks, R. G. Parr, *The Journal of Chemical Physics* **28**, 335–345 (1958).
43. R. McWeeny, *Proceedings of the Royal Society of London A: Mathematical, Physical and Engineering Sciences* **253**, 242–259 (1959).

44. S. Diner, J. P. Malrieu, P. Claverie, *Theoretica chimica acta* **13**, 1–17 (1969).
45. J. P. Malrieu, P. Claverie, S. Diner, *Theoretica chimica acta* **13**, 18–45 (1969).
46. S. Diner, J. P. Malrieu, F. Jordan, M. Gilbert, *Theoretica chimica acta* **15**, 100–110 (1969).
47. J.-P. Malrieu, P. Durand, J.-P. Daudey, *Journal of Physics A: Mathematical and General* **18**, 809 (1985).
48. F. Aquilante *et al.*, *J. Comput. Chem.* **31**, 224 (2010).
49. J. M. Foster, S. F. Boys, *Rev. Mod. Phys.* **32**, 303–304 (1960).
50. C. Edmiston, K. Ruedenberg, *Rev. Mod. Phys.* **35**, 457–464 (1963).
51. J.-P. Malrieu, N. Guihéry, C. J. Calzado, C. Angeli, *Journal of Computational Chemistry* **28**, 35–50 (2007).
52. C. Angeli, R. Cimiraglia, Jean-Paul Malrieu, *Journal of Chemical Education* **85**, 150–158 (2008).
53. C. Angeli, *Journal of Computational Chemistry* **30**, 1319–1333 (2009).
54. C. Angeli, *International Journal of Quantum Chemistry* **110**, 2436–2447 (2010).
55. C. Angeli, C. J. Calzado, C. de Graaf, R. Caballol, *Physical Chemistry Chemical Physics* **13**, 14617–14628 (2011).
56. E. Giner, C. Angeli, *The Journal of Chemical Physics* **143**, 124305 (2015).
57. E. Giner, C. Angeli, *The Journal of Chemical Physics* **144**, 104104 (2016).
58. D. Maynau, S. Evangelisti, N. Guihéry, C. J. Calzado, J.-P. Malrieu, *The Journal of Chemical Physics* **116**, 10060–10068 (2002).
59. J.-P. Malrieu, D. Maynau, *Journal de Chimie Physique* **75**, 31 (1978).
60. P. Reinhardt, J.-P. Malrieu, *The Journal of Chemical Physics* **109**, 7632–7643 (1998).
61. J.-P. Daudey, J.-L. Heully, J.-P. Malrieu, *The Journal of Chemical Physics* **99**, 1240–1254 (1993).
62. L. E. Nitzsche, E. R. Davidson, *The Journal of Chemical Physics* **68**, 3103–3109 (1978).
63. L. E. Nitzsche, E. R. Davidson, *Journal of the American Chemical Society* **100**, 7201–7204 (1978).
64. E. R. Davidson, L. E. McMurchie, S. J. Day, *The Journal of Chemical Physics* **74**, 5491–5496 (1981).
65. N. B. Amor, D. Maynau, *Chemical Physics Letters* **286**, 211–220 (1998).

66. B. Pradines, N. Suaud, J.-P. Malrieu, *The Journal of Physical Chemistry A* **119**, 5207–5217 (2015).
67. P. G. Szalay, A. Karpfen, H. Lischka, *The Journal of Chemical Physics* **87**, 3530–3538 (1987).
68. H. Guo, M. Karplus, *The Journal of Chemical Physics* **94**, 3679–3699 (1991).
69. J. Y. Lee, O. Hahn, S. J. Lee, H. S. Choi, H. Shim, B. J. Mhin, K. S. Kim, *The Journal of Physical Chemistry* **99**, 1913–1918 (1995).
70. J. Y. Lee, O. Hahn, S. J. Lee, B. J. Mhin, M. S. Lee, K. S. Kim, *The Journal of Physical Chemistry* **99**, 2262–2266 (1995).
71. S. Hirata, H. Yoshida, H. Torii, M. Tasumi, *The Journal of Chemical Physics* **103**, 8955–8963 (1995).
72. C. S. Page, M. Olivucci, *Journal of Computational Chemistry* **24** (2003).
73. A. J. A. Aquino, M. Barbatti, H. Lischka, *ChemPhysChem* **7**, 2089–2096 (2006).
74. N. Suaud, R. Ruamps, J.-P. Malrieu, N. Guihéry, *The Journal of Physical Chemistry A* **118**, 5876–5884 (2014).
75. O. Valsson, C. Angeli, C. Filippi, *Phys. Chem. Chem. Phys.* **14**, 11015–11020 (31 2012).
76. C. Angeli, M. Pastore, *The Journal of Chemical Physics* **134**, 184302 (2011).
77. Said, Moncef and Maynau, Daniel and Malrieu, Jean Paul, *Journal of the American Chemical Society* **106**, 580–587 (1984).
78. J.P. Malrieu, I. Nebot-Gil and J.Sánchez Marín, *Pure & Appl. Chem* **56**, 1241–1254 (1984).
79. K. Hirao, H. Nakano, K. Nakayama, M. Dupuis, *J. Chem. Phys.* **105**, 9227 (1996).
80. T. H. Dunning, *The Journal of Chemical Physics* **90**, 1007–1023 (1989).
81. G. A. Gallup, *Valence Bond Methods. Theory and Applications* (Cambridge University Press, 2002), pp. 16–17.
82. W. Kolos, L. Wolniewicz, *J. Chem. Phys.* **43**, 2429–2441 (1965).
83. P. W. Anderson, *Phys. Rev.* **79**, 350 (1950).
84. O. Kahn, B. Briat, *J. Chem. Soc., Faraday Trans. 2* **72**, 268 (1976).
85. P. J. Hay, J. C. Thibeault, R. J. Hoffmann, *J. Am. Chem. Soc.* **97**, 4884 (1975).
86. P. de Loth, P. Cassoux, J.-P. Daudey, J.-P. Malrieu, *J. Am. Chem. Soc.* **103**, 4007 (1981).
87. M. Charlot, M. Verdaguer, Y. Journaux, P. de Loth, J. Daudey, *Inorg. Chem.* **23**, 3802 (1984).

88. P. de Loth, J. Daudey, H. Astheimer, L. Walz, W. Haase, *J. Chem. Phys.* **82**, 5048 (1985).
89. P. de Loth, P. Karafiloglou, J. Daudey, O. Kahn, *J. Am. Chem. Soc.* **110**, 5676 (1988).
90. C. J. Calzado, J. M. Clemente-Juan, E. Coronado, A. Gaita-Ariño, N. Suaud, *Inorg. Chem.* **47**, 5889 (2008).
91. C. de Graaf, F. Illas, *Phys. Rev. B* **63**, 014404 (2001).
92. C. de Graaf, I. de P. R. Moreira, F. Illas, Ò Iglesias, A. Labarta, *Phys. Rev. B* **66**, 014448 (2002).
93. F. Nepveu, W. Haase, H. Astheimer, *J. Chem. Soc. Faraday II* **82**, 551 (1986).
94. H. Astheimer, W. Haase, *J. Chem. Phys.* **85**, 1424 (1986).
95. J. Miralles, J.-P. Daudey, R. Caballol, *Chem. Phys. Lett.* **198**, 555 (1992).
96. J. Miralles, O. Castell, R. Caballol, J.-P. Malrieu, *Chem. Phys.* **172**, 33 (1993).
97. R. Broer, W. J. A. Maaskant, *Chem. Phys.* **102**, 103 (1986).
98. J. Malrieu, R. Caballol, C. J. Calzado, F. de Graaf, N. Guihery, *Chem. Rev* **114**, 429–492 (2014).
99. C. J. Calzado, J. Cabrero, J.-P. Malrieu, R. Caballol, *J. Chem. Phys.* **116**, 2728 (2002).
100. C. J. Calzado, J. Cabrero, J.-P. Malrieu, R. Caballol, *J. Chem. Phys.* **116**, 3985 (2002).
101. C. J. Calzado, C. Angeli, D. Taratiel, R. Caballol, J.-P. Malrieu, *J. Chem. Phys.* **131**, 044327 (2009).
102. J. Cabrero, C. J. Calzado, D. Maynau, R. Caballol, J.-P. Malrieu, *J. Phys. Chem. A* **106**, 8146 (2002).
103. T. Mitchell, W. Bernard, J. Wasson, *Acta Crystallogr. Sect. B* **26**, 2096 (1970).
104. L. M. Mirica, D. P. Stack, *Inorg. Chem.* **44**, 2132–2133 (2005).
105. J. Yoon, L. M. Mirica, D. P. Stack, E. I. Solomon, *J. Am. Chem. Soc.* **126**, 12586–12595 (2004).
106. J. Yoon, E. I. Solomon, *Inorganic Chemistry* **44**, 8076–8086 (2005).
107. J. Yoon, L. M. Mirica, T. D. P. Stack, E. I. Solomon, *Journal of the American Chemical Society* **127**, 13680–13693 (2005).
108. P. A. M. Dirac, *Proc. Roy. Soc. London Ser. A* **112**, 661 (1926).
109. W. Heisenberg, *Z. Phys.* **49**, 619 (1928).
110. J. H. van Vleck, *Electric and Magnetic Susceptibilities* (Clarendon Press, Oxford, 1932).

111. S. Vancoillie, J. Chalupský, U. Ryde, E. I. Solomon, K. Pierloot, F. Neese, L. Rulíšek, *The Journal of Physical Chemistry B* **114**, PMID: 20469875, 7692–7702 (2010).
112. *OVB-Ferrara package developed at the Department of Chemical and Pharmaceutical Sciences, University of Ferrara, Italy.*
113. *CASDI package developed at the Laboratoire de Physique Quantique, Université Paul Sabatier, Toulouse, France.*
114. N. Ben Amor, D. Maynau, *Chem. Phys. Lett.* **286**, 211 (1998).
115. J. Pipek, P. G. Mezey, *The Journal of Chemical Physics* **90**, 4916–4926 (1989).
116. C. Angeli, S. Evangelisti, R. Cimiraglia, D. Maynau, *J. Chem. Phys.* **117**, 10525–10533 (2002).
117. C. J. Calzado, S. Evangelisti, D. Maynau, *J. Phys. Chem. A* **107**, 7581 (2003).
118. C. J. Calzado, C. Angeli, R. Caballol, J.-P. Malrieu, *Theor. Chem. Acc.* **126**, 185 (2010).
119. D. Munoz, C. De Graaf, F. Illas, *Journal of Computational Chemistry* **25**, 1234–1241, ISSN: 1096-987X (2004).
120. C. Angeli, C. J. Calzado, *J. Chem. Phys.* **137**, 034104 (2012).
121. N. Suaud, R. Ruamps, N. Guihéry, J.-P. Malrieu, *J. Chem. Theory Comput.* **8**, 4127–4137 (2012).
122. W. T. Borden, E. R. Davidson, D. Feller, *Tetrahedron* **38**, 737 (1982).
123. B. H. Botch, T. H. Dunning Jr., J. F. Harrison, *J. Chem. Phys.* **75**, 3466 (1981).
124. K. Pierloot, *Int. J. Quantum Chem.* **111**, 3291 (2011).
125. M. Spivak, C. Angeli, C. Calzado, C. de Graaf, *J. Comp. Chem.* **35**, 1665–1671 (2014).
126. C. J. Calzado, J.-P. Malrieu, *Phys. Rev. B* **63**, 214520 (2001).
127. A. Gellé, M. Munzarová, M. B. Lepetit, F. Illas, *Phys. Rev. B* **68**, 125103 (2003).
128. R. Broer, W. C. Nieuwpoort, *Theor. Chim. Acta* **73**, 405 (1988).
129. R. Broer, A. Van Oosten, W. C. Nieuwpoort, *Rev. Solid State. Sci.* **5**, 79 (1991).
130. R. Broer, L. Hozoi, W. C. Nieuwpoort, *Mol. Phys.* **101**, 233 (2003).
131. A. B. van Oosten, R. Broer, W. C. Nieuwpoort, *Int. J. Quantum Chem. Symp.* **29**, 241 (1995).
132. A. B. van Oosten, R. Broer, W. C. Nieuwpoort, *Chem. Phys. Lett.* **257**, 207 (1996).

133. E. Bordas, R. Caballol, C. de Graaf, J.-P. Malrieu, *Chem. Phys.* **309**, 259 (2005).
134. W. Geertsma, *Physica B* **241**, 164 (1990).
135. H. Eskers, H. Jefferson, *Phys. Rev. B* **9788**, 48 (1993).
136. B. Huron, J. P. Malrieu, P. Rancurel, *The Journal of Chemical Physics* **58**, 5745–5759 (1973).
137. A. Ozarowski, C. J. Calzado, R. P. Sharma, S. Kumar, J. Jezierska, C. Angeli, F. Spizzo, V. Ferretti, *Inorganic Chemistry* **54**, 11916–11934 (2015).
138. C. Angeli, C. J. Calzado, C. de Graaf, R. Caballol, *Phys. Chem. Chem. Phys.* **13**, 14617 (2011).
139. A. Scemama, E. Giner, T. Applencourt, G. David, M. Caffarel, *Quantum Package* vo.6, Sept. 2015.
140. B. O. Roos, A. C. Borin, L. Gagliardi, *Angewandte Chemie International Edition* **46**, 1469–1472 (2007).
141. P.-O. Widmark, P.-Å. Malmqvist, B. Roos, English, *Theoretica Chimica Acta* **77**, 291–306, ISSN: 0040-5744 (1990).
142. S. Keller, M. Dolfi, M. Troyer, M. Reiher, *The Journal of Chemical Physics* **143**, 244118 (2015).

COLOPHON

This document was typeset using the typographical look-and-feel classicthesis developed by André Miede. The style was inspired by Robert Bringhurst's seminal book on typography "*The Elements of Typographic Style*". classicthesis is available for both L^AT_EX and L^YX:

<https://bitbucket.org/amiede/classicthesis/>

Happy users of classicthesis usually send a real postcard to the author, a collection of postcards received so far is featured here:

<http://postcards.miede.de/>